INFORMATION TO USERS

This manuscript has been reproduced from the microfilm master. UMI films the text directly from the original or copy submitted. Thus, some thesis and dissertation copies are in typewriter face, while others may be from any type of computer printer.

The quality of this reproduction is dependent upon the quality of the copy submitted. Broken or indistinct print, colored or poor quality illustrations and photographs, print bleedthrough, substandard margins, and improper alignment can adversely affect reproduction.

In the unlikely event that the author did not send UMI a complete manuscript and there are missing pages, these will be noted. Also, if unauthorized copyright material had to be removed, a note will indicate the deletion.

Oversize materials (e.g., maps, drawings, charts) are reproduced by sectioning the original, beginning at the upper left-hand corner and continuing from left to right in equal sections with small overlaps.

Photographs included in the original manuscript have been reproduced xerographically in this copy. Higher quality 6" x 9" black and white photographic prints are available for any photographs or illustrations appearing in this copy for an additional charge. Contact UMI directly to order.

Bell & Howell Information and Learning
300 North Zeeb Road, Ann Arbor, MI 48106-1346 USA

UMI®
800-521-0600

DISSERTATION

ONCOSTATIC MECHANISMS OF MELATONIN and
ANALYSIS OF 8-OXOGUANINE BY GAS CHROMATOGRAPHY MASS SPECTROMETRY

Submitted by

Aaron Scott

Department of Environmental Health

In partial fulfillment of the requirements

For the Degree of Doctor of Philosophy

Colorado State University

Fort Collins Colorado

Fall 1999

COLORADO STATE UNIVERSITY

August 17, 1999

WE HEREBY RECOMMEND THE DISSERTATION PREPARED UNDER OUR SUPERVISION BY AARON SCOTT ENTITLED ONCOSTATIC MECHANISMS OF MELATONIN and ANALYSIS OF 8-OXOGUANINE BY GAS CHROMATOGRAPHY MASS SPECTROMETRY BE ACCEPTED AS FULFILLING IN PART REQUIREMENTS FOR THE DEGREE OF DOCTOR OF PHILOSOPHY

Committee on Graduate Work:

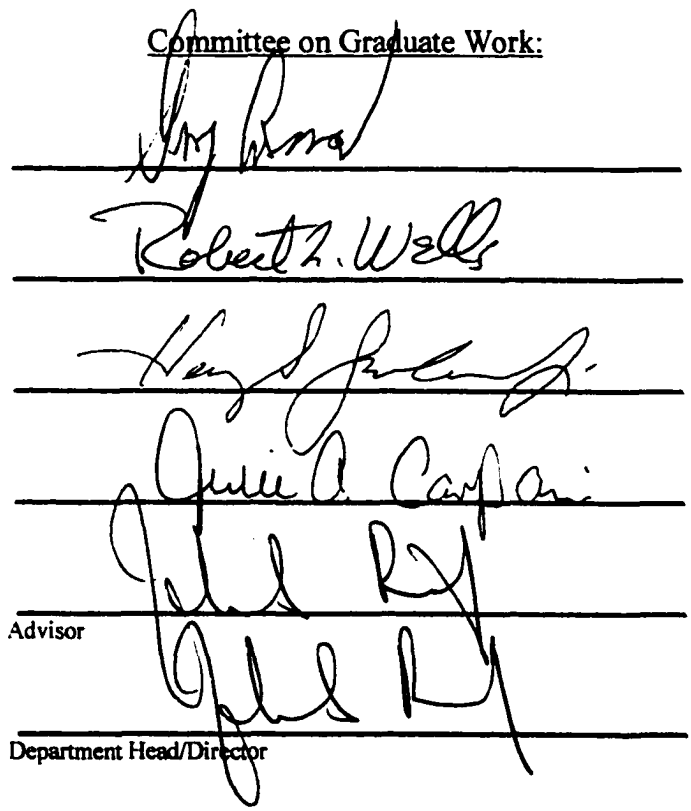

Advisor

Department Head/Director

ABSTRACT OF DISSERTATION

ONCOSTATIC MECHANISMS OF MELATONIN and ANALYSIS OF 8-OXOGUANINE BY GAS CHROMATOGRAPHY MASS SPECTROMETRY

Melatonin studies have previously demonstrated the hormone to inhibit growth of estrogen receptor positive breast cancer cells after *in vitro* treatment through mechanisms not clearly understood. Chapter 1 experiments herein described a novel mechanism of cytotoxicity in MCF-7 human breast carcinoma cells through a mechanism disrupting mitochondrial bioenergetic pathways after less than 24 hours of treatment in estrogen extracted medium. Cell numbers were decreased to 40% of controls with morphologic and biochemical studies demonstrating acute cell death and increased electron transport activity accompanied by decreased cellular ATP levels. Estradiol rescued cells from the melatonin toxicity. Chapter 2 presented experimental evidence of differentiation in MCF-7 cells following melatonin treatment. Specifically, morphologic changes such as single nucleoli, decreased pseudopodia, and increased numbers and size of intermediate filament bundles were present as well as significantly increased numbers of cornified envelopes. Chapter 3 described laboratory bioassay methodology for clinical aspirates of gross fibrocystic breast disease fluid treatment of MCF-7 cells. The studies presented a novel finding of melatonin in the cyst fluids and explored the correlation of the hormone concentration to cell growth in a bioassay as well as biochemical endpoints. Interestingly, the results of this preliminary study suggested that melatonin concentration in breast cysts directly modulated MCF-7 cell growth. Finally, TGFβ levels in the culture medium from treated cells was also significantly related to MCF-7 cell number.

Section II studies evaluated an internal standard method for the analysis of 8-oxoguanine by gas chromatography mass spectrometry. Additionally, an isotope dilution method with modifications and improvements over previously published procedures was described with the addition of quality control and quality assurance (QC/QA) data. In brief, the isotope dilution analysis demonstrated a sensitivity of 20 femptomoles, precision of 6.9%, and recovery accuracy of 99.7%. Chromatograms from the studies described column degeneration along with QC/QA recommendations to avoid error from this problem. Oxidation artifact was quantified and found as high as 1.1% of total guanine. Finally, room temperature derivatization was shown to be effective and precise with a 50% decrease in oxidation artifact. Surprisingly, addition of the antioxidant, ethane thiol, resulted in increased oxidation artifact.

Aaron E. Scott DVM
Department of Environmental Health
Colorado State University
Fort Collins Colorado 80523
Fall semester 1999

ACKNOWLEDGEMENTS:

Graduate committee:

Dr. Greg Cosma
Dr. Bob Wells
Dr. John Reif
Dr. Hank Gardner
Dr. Julie Campain
Dr. Dan Gustafson

Others advising or participating in research:

Dr. Tony Frank
Dr. Lun Yi Zang
Dr. Cary Jackson
Brian Cranmer M.S.

Students and friends in the Cosma laboratory:

Mr. Dave Ufferfilge
Ms. Cheryl Dowell .
Mr. Tony Martinez

Laboratories, facilities and equipment:

CSU Department of Environmental Health Cosma Laboratory
CSU Department of Environmental Health Billings Laboratory
CSU Department of Environmental Health Analytic Laboratory
CSU Department of Radiological Health Sciences Elkind Laboratory
U.S. Army Center for Environmental Health Research

TABLE OF CONTENTS:

LIST OF TABLES:

LIST OF FIGURES:

GENERAL INTRODUCTION.

There are two philosophical approaches to the study of disease. The first and most common approach is to examine the factors that cause malfunction of organs, tissues, or cells. A second and more humble approach relies heavily on a Darwinian belief that life evolved for several million years, and that every disease necessarily has extant mechanisms of "anti-disease". This scientific philosophy dictates that the biomedical researcher first understand and then expand upon the natural design of health preserving pathways that have been biologically tested and improved over millions of years. For example, historically smallpox was a devastating disease resulting in death unless circulating anti-bodies were pre-formed against it [1]. By understanding and exploiting mechanisms of "anti-disease", Louis Pasteur was able to augment the natural response with a vaccine, which ultimately led to the eradication of the disease.

On a more contemporary note, breast cancer is a disease, which has been intensely studied and associated with many causal risk factors [2]. In fact, dozens of gene mutations have been defined throughout the stages of cancer progression and mapped to specific chromosomes [3]. Never the less, and in spite of advances in understanding of the disease pathology, it remains a grim specter to approximately 180,000 women each year in this country [2]. Thus the question, "what is the disease?" may not be as important as Pasteur's converse question, "what is the anti-disease?"

The first section of this dissertation presents three sets of MCF-7 human breast carcinoma cell studies, which explore the thesis that melatonin is an endogenous oncostatic hormone; in other words, a mechanism of anti-disease. Chapter 1 data shows that melatonin in low estrogen medium is cytotoxic to the cancer cells. Other published reports cited in this dissertation (and confirmed by cell studies in the Cosma laboratory at

Colorado State University) describe an anti-estrogenic role for melatonin in MCF-7 proliferation experiments. Chapter 2 suggests a role for the hormone to induce terminal differentiation characteristics in the breast cancer cells. Finally, Chapter 3 applies this intriguing information to bioassay studies using clinical gross fibrocystic breast disease aspirate fluid to modulate MCF-7 cell growth. In Chapter 3, preliminary data further correlates cell growth to melatonin concentrations within the fluid. Hence, the findings of studies presented herein substantiate the possibility that melatonin is an endogenous anti-breast cancer hormone. More importantly, the findings suggest the question, "Could the oncostatic mechanisms of melatonin effect on MCF-7 cells be expanded or exploited pharmacologically in the treatment or prevention of breast cancer?"

Section II evaluates analytic methods for quantification of the DNA base adduct, 8-oxoguanine (8-OHG), by gas chromatography mass spectrometry (GC-MS). Although many studies are cited using GC-MS techniques, little or no published data is available defining quality control parameters of the methods. Unfortunately, population studies utilizing 8-OHG as a biomarker are reliant on the quality of analytic data. For this reason, the studies in Chapter 4 were undertaken. First, experiments were conducted to evaluate an internal standard method for precision, accuracy, and stability of the standard. Chapter 4 data secondly details an isotopic dilution method of analysis with modifications and improvements of previously published work, including quality control and assurance criteria. Finally, studies were designed to address and characterize GC-MS analytic error due to column degeneration and guanine oxidation artifact.

SECTION I: CHAPTER 1

CYTOTOXICY ASSOCIATED WITH MITOCHONDRIAL BIOENERGETIC DISRUPTION IN MCF-7 HUMAN BREAST CARCINOMA CELLS 15 TO 20 HOURS AFTER MELATONIN TREATMENT

INTRODUCTION.

Experiments in the early 1980's defined a role for melatonin as a potential anti-carcinogenic agent in chemical induced rodent mammary cancer (review [4;5]). In these studies, both size and numbers of tumors were increased in pinealectomized rats while melatonin replacement prevented carcinogenesis and/or significantly increased the latency period (review [4-6]). Unfortunately, subsequent studies have demonstrated a variety of factors that modulate its anti-tumor effects and define them as interactions of multiple complex pathways (review [4-9]). In other words, the dose, the timing of administration, interactions with other hormones, intra-cellular targets, and status of downstream signaling pathways change the cellular responses produced by melatonin.

Melatonin modulation of cell function occurs in less than twenty-four hours.

Melatonin is an endocrine hormone of most vertebrate species and acts to modulate diurnal cycles through mechanisms not completely understood [4-6]. Data from numerous studies demonstrate that timing of exposure is related to cell effects and, additionally, that cyclic dosing of the hormone is more effective than continuous exposure [4;6;10]. The diurnal cycle is also associated with oncostatic effects in both rodent and *in vitro* mammary cancer models [4;6;10]. This suggests that general pathways of melatonin activity involve mechanisms that switch cell functions on and off within hours of treatment.

A likely candidate for such a mechanism in melatonin treated MCF-7 breast carcinoma cells was described by Molis et al [11]. Receptor mediated signal transduction with increases of c-*fos*, c-*myc*, *tgf*-β, and *tgf*-α RNA (<4 hr) was followed by rapid declines after one hour for c-*fos*, and twelve hours for *tgf*-α. Both c-*myc* and *tgf*-β remained elevated for over 48 hours. These rapid gene transcription effects from a

diurnally secreted hormone intuitively suggest that understanding the early mechanisms of melatonin action is critical to understanding its physiological activity.

In addition to effects on early responsive gene transcription, melatonin has been well established as a hormone inhibiting estrogenic growth in a number of estrogen receptor positive (ER+) cell lines but not in ER- lines [12;13]. The most probable mechanism of this activity is mediated through estrogen receptor down regulation [12;14]. Interestingly, this inhibition of growth is not evident until near confluence of cultures (4-7 days), while the effects on ER transcription result within six hours of melatonin exposure [14]. Thus, it appears that melatonin must have multiple downstream targets to prevent ER+ cell line growth in addition and in combination with ER down regulation and early gene transcription effects.

Does melatonin have a role in regulation of bioenergetics?

Melatonin levels are highly correlated with the induction and arousal of vertebrate species from hibernation, and heat production by brown fat metabolism (thermogenesis) (review [15]). In addition, the hormone has been closely linked to the nighttime drop in human sleep associated core body temperature [15]. Cellular pathways responsible for these relationships have not been defined, but clearly suggest a role for the hormone in the body temperature regulation and therefore, in cellular bioenergetics.

Bioenergetic disturbances in the oxidative phosphorylation pathway of MCF-7 energy production are suggested by morphologic alterations in mitochondria following treatment with melatonin [16]. Interestingly, the authors found these changes associated with other ultra-structural features reminiscent of a more differentiated phenotype such as less prevalent pseudopodia, smaller nuclear size, cytokeratin bundles, and more

prominent Golgi bodies. Although causality from bioenergetic disturbance was not postulated, the researchers also reported evidence of nuclear degeneration with cell lysis in the cultures showing mitochondrial morphologic changes. A more recent investigation described an increasingly differentiated phenotype in MCF-7 cells depleted of mitochondria by continuous passage in presence of ethidium bromide [17]. Together these studies suggest that melatonin treatment results in modulation of cellular bioenergetics and that disruption of oxidative respiration may alter the malignant phenotype of the MCF-7 cells.

Melatonin binds multiple receptors and exhibits a "U" shaped dose response curve in MCF-7 cell proliferation studies.

The melatonin dose-response growth curve in ER+ breast carcinoma cell models is typically a "U" shaped curve with maximal inhibition of growth in the concentration range of 10 pM to 100 nM [16;18]. At higher concentrations, the growth inhibitory effect is lost and the rate of cell proliferation begins to increase [14;16]. Although yet unexplained, the answer to this probably lies in the hormone's ability to bind multiple receptors and to function as an *in vitro* antioxidant. Complex signal transduction pathways for melatonin involve at least two cell surface receptors and one putative nuclear orphan receptor, each with different binding affinities [19-21]. The dose response curve predicted for the hormone would therefore be dependent upon the dose, the k_d of each receptor, and the expression level of the receptors. For example, a high affinity receptor might dominate the response curve at picomolar doses of melatonin while a low affinity but highly expressed receptor could overwhelm its effect at nanomolar dose levels. Furthermore, at pharmacological doses (uM and mM), non-receptor mediated effects could be possible [4;9].

There are two important implications for this type of dose response. First, the concentration of melatonin in the study is critical to the definition of its effect. That is, high physiological and pharmacological doses of the hormone are likely to exert effects through different pathways than the physiological dose ranges. A second less obvious implication is that other hormones and growth factors with the ability to modulate expression of melatonin receptors could dramatically alter its dose response. Two important considerations, therefore, in the design of melatonin experiments are the dose response relationship and the definition or control of other hormones that could influence melatonin response pathways.

Melatonin has direct antioxidant effects as well as receptor mediated pathways.

Melatonin is a direct *in vitro* scavenger of singlet oxygen, hydrogen peroxide, and indirectly of hydroxyl radical [22-24]. There is dual significance to the reduction of reactive oxygen species in cultured cancer cell models. First, pro-oxidant agents provide the potential for cancer induction and promotion as well as being a source of cellular macromolecular damage associated with aging [24;25]. Thus, from an evolutionary viewpoint, melatonin's antioxidant role is highly compatible with its oncostatic effects. A second consideration of pro-oxidant agents is the role of cytoplasmic redox status as a transcriptional modifier and growth gene inducer [26-28]. As an antioxidant, therefore, high concentrations of melatonin may play an indirect role in increasing cell growth and proliferation. Hence, caution must be used when interpreting proliferation data from experiments with pharmacological doses of melatonin that could alter cytoplasmic redox potential.

What is the significance of data from ER+ MCF-7 cell studies performed in estrogen extracted medium?

Ovarian estrogens in the adult human female reach low extremes of concentration at two distinct times. First, during the normal menstrual cycle (figure 1.1), serum estrogen levels drop to low picomolar concentration for about five days and then, prior to ovulation, peak at approximately one-half to one nanomole per liter [29]. A second more profound drop in serum estrogen levels occurs at the time of menopause with ovarian estrogen ceasing [29].

The maximal and minimal levels of estrogen that breast cells are exposed to *in vivo* are unknown, but it is apparent that the cells are affected by estrogen cyclic activity and show monthly mitotic and apoptotic activity [30]. In spite of *in vivo* cyclic effects, most *in vitro* studies have been conducted with static one to ten nM estrogen concentrations in the culture medium, and are thus above the maximal serum levels of human patients. The experiments in Chapter 1 of this dissertation were completed in medium supplemented with fetal bovine serum that had been charcoal dextran depleted of estrogen to a final concentration of approximately 1.1 pM. Parallel experiments to test the effects of melatonin in the presence of estrogen were performed in medium supplemented with either 10% fetal bovine serum or charcoal dextran extracted FBS with additional amounts of 17β-estradiol.

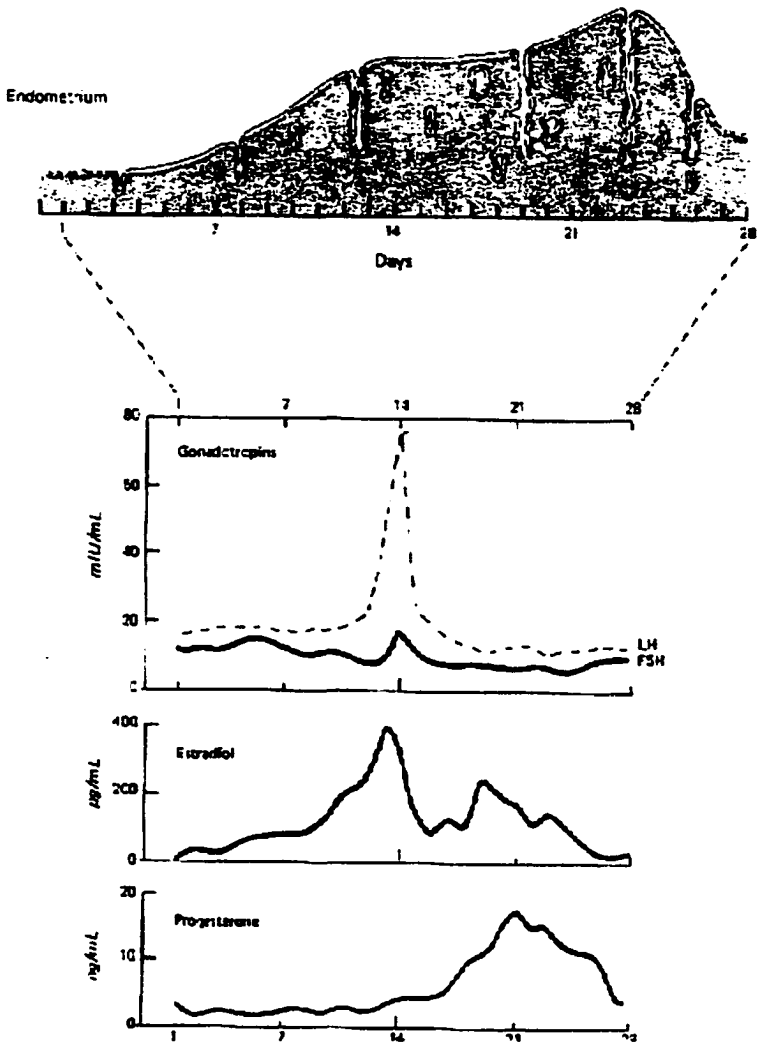

Figure 1. 1 Chart of normal menstrual cycle hormone changes.

The menstrual cycle showing pituitary and ovarian hormone levels and associated histologic changes of the endometrium. Serum estradiol levels reach low picomolar levels at the end of the cycle in association with quiescent endometrial proliferation (and endometrial cell death). (Reproduced with permission from Meyers FH, Jawetz, E, Goldfien A: Review of Medical Pharmacology, 7th ed. Lange, 1980)

The hypothesis of the study...

It is postulated that physiological melatonin concentrations have an acute, early, cytotoxic effect on MCF-7 human breast carcinoma cells cultured in estrogen depleted medium, and that the mechanism of the cytotoxicity is due to mitochondrial bioenergetic disruption.

MATERIALS AND METHODS:

Cell Culture.

MCF-7 human breast adenocarcinoma cells were obtained from American Type Culture Collection (ATCC, Rockville MD) at passage 154. The MCF-7 cell line was initially isolated from the pleural effusion of a metastatic breast cancer, and expresses both estrogen and progesterone receptors. Cell cultures were grown in a humidified incubator at 5% CO_2 and 37^{0}C. All reagents and supplies were purchased from Sigma, (St. Louis, MO) unless otherwise specified. Cells were maintained in Dulbecco's Modified Eagle's Medium (DMEM) supplemented with fetal bovine serum (FBS) 10% v/v), MEM non-essential amino acids (1% v/v), penicillin-streptomycin (1% v/v), hydrocortisone (200 nM), sodium pyruvate (1 mM), and insulin (0.003 unit/ml). For experiments, cells were grown in phenol red free medium supplemented with charcoal-dextran extracted FBS to reduce exogenous hormone levels. Melatonin concentration in the extracted serum was below the detection limit of 1.9 picomole per liter as measured by radioimmunoassay [31]. Cells were maintained in the estrogen-depleted medium (concentration of estradiol at 0.114 pM) for two to four days and were in mid to late log phase growth at the time of experimental treatments. Cells were enumerated by

hemocytometer count using Trypan Blue dye viability assay or by Coulter cell counter (Particle Data Inc., model EL Zone 180).

Preparation of charcoal dextran extracted serum.

Fetal bovine serum from Summit laboratory (Fort Collins, CO) of lot number 43036 was used throughout the studies. Charcoal (0.625 g) was washed twice with 15 ml of cold milipore water then combined with 0.0625 g dextran and 50 ml TEG buffer (10 mM Tris-HCL pH 7.4, 1.5 mM EDTA, 10% glycerol v/v). After vortexing, the suspension was split into four 12.5 ml aliquots and centrifuged at 10,000 x g for ten minutes. The supernatant was discarded and 12.5 ml of cold serum added to the resulting pellet. Serum was rocked at 4^0C for one hour, then centrifuged twice at 10,000 x g for ten minutes to remove charcoal. The serum was sterilized by passage through a 0.2 um filter and stored at -20^0C until use. Analysis of aliquots gave final concentrations of 1.14 pM for estradiol and less than the detection limit of 1.9 pM melatonin.

Tritiated thymidine uptake.

MCF-7 cells were seeded at a density of $8*10^5$ cells per 60 mm petri dish and maintained in experiment medium until late log phase growth. After 16 hours of exposure to melatonin, vehicle, or estradiol, cultures were pulsed with [^{3}H]thymidine (1Ci/ml) for 30 minutes. After rinsing with 4^0C PBS, ice cold trichloroacetic acid was added for 10 minutes, and followed with ice cold 70% ethanol. Cells were lysed with Toplayer II (18.15 g NaOH, 29.3 g NaCl, 3.81g tetra-sodium EDTA, 5.23 g Brij-58, in one liter of double deionized water). A scintillation cocktail prepared with 75 ul HCl, 300 ul H20, and 10 ml of Ready Safe (Beckman Coulter, Miami, FL) was analyzed on a Beckman LS 5801 liquid scintillation system using counts per minute (CPM) from the

tritium window. CPMs were standardized to mean cell counts from cultures grown in parallel to each group.

Comet Assays.

Comet assays were performed essentially as described previously [32;33]. Briefly, 0.5 ml of cells at an approximate concentration of 10,000 cell/ml were added to 1.5 ml of low melting point 1% agarose gel, vortexed, rapidly layered on a microscope slide, and allowed to gel on a cold surface. The cells were lysed (0.03M NaOH, 1 M NaCl, 0.1% sarcosyl) for one hour in the dark at room temperature. The slides were then rinsed (0.03M NaOH, 3mM EDTA) twice for 20 to 30 minutes and electrophoresed in fresh 0.03M NaOH / 3mM EDTA at 0.5 volt/cm for 25 minutes. Current was set at 34 milliampere. After rinsing with DDI water for 10 minutes, slides were stained with 2.5 ug/ml propidium iodide for an additional 10 minutes, rinsed and stored in light and airtight boxes until read the following day. Comets were analyzed using a Zeiss fluorescent microscope with an attached ITT intensified solid state camera and image analyzing system. Approximately 200 to 400 comets were captured per slide. The parameters of "tail moment", DNA concentration, and comet number were analyzed as previously described [32]. DNA stand breakage was express in terms of "tail moment", which is a mathematical product of the length of DNA migration and quantity of DNA in the comet tail. This parameter of DNA damage is a more sensitive measure of DNA strand breakage than either tail migration or DNA amount [33;34]. Data from the imaging system was processed by an interfaced personal computer and analyzed graphically by SigmaPlot graphing software.

Flow cytometry.

Cells were prepared by standard ethanol fixation and propidium iodide staining. Briefly, cells were harvested by trypsin digest, washed in cold PBS, and re-suspended to a volume of 2 ml in cold PBS. Two ml of cold 100% ethanol was added dropwise while vortexing the cells. An additional 3 ml of 100% ethanol was added to give a final concentration of 70%. The cells were centrifuged out of the ethanol fixative and re-suspended in 1 ml of 10 ug/ml propidium iodide containing 40 KU/ml of RNAase. Analysis was done on an EPIC V (Coulter) flow cytometer with excitation by a 488 nm argon laser with a 515 nm blocking filter in tandem with a 630 nm long pass filter. Cicero software on an interfaced personal computer was used for analysis of 30,000 events per sample with integral signal amplification. Data was plotted on single parameter histograms with modal analysis of peaks as indicated.

Fluorescence microscopy examination of cells with ethidium bromide and acridine orange staining.

MCF-7 cells were seeded in 60 mm petri dishes at a density of approximately $1*10^6$ cells per dish and treated with either 0.00005% ethanol (vehicle) or 100 nM melatonin for 16 hours. The procedure for analysis was minimally modified from that in Methods in Cell Biology: Cell Death [34]. Briefly, dishes were stained with 1 ml of acridine orange and ethidium bromide (100 ug/ml each) for 10 minutes and examined with fluorescence microscopy using a FITC green filter. Acridine orange is an intercalating nucleic acid stain actively taken up by vital cells, and emits at a peak of 530 nm when bound to double stranded DNA. Ethidium bromide enters the cell through damaged plasma membranes and in combination with AO emits orange colored light (600-700 nm). Together, the two dyes allow visualization of nuclear structure as well as identification of

cells with degenerating nuclei. Photographs were taken with Kodak 135-100 and 135-200 gold film with exposure time preset at 5 seconds.

Glutathione (GSH) and glutathione peroxidase (Gpox) assays.

Cells were scraped into 250-500 ul of 10 mM HCl for GSH analysis, and into phosphate buffered saline (PBS) or Hank's Balanced Salt Solution (HBSS) for Gpox. The cell suspension was placed in Eppendorf tubes, flash frozen in liquid nitrogen, and stored at -80^{0}C until the assays were performed one week later.

The principle of the assay involves the non-enzymatic reduction of DTNB (5,5'-dithio bis-2-nitrobenzoic acid) by two molecules of GSH to produce oxidized glutathione (GSSG). When reduced, DTNB is a yellow chromophore that absorbs at λ= 405 nm and may be followed spectrophotometrically. NADPH and glutathione reductase are added in excess to ensure that GSSH is reduced to GSH providing a concentration consistent with the original sample. The kinetic rate of absorbency change at 405 nm is proportional to the molar amount of reduced DTNB in the reaction.

The GSH assay procedure generally follows the method of Vandeputte et al. [35]. Briefly, cell suspensions were freeze-thawed 3 times in alcohol-dry ice and a 37^{0}C water bath. The resultant suspension was diluted 4X with 10 mM HCl and 1.3% SSA. For analysis, 20 ul of blanks, standards, and samples were pipetted into a 96 well MTP followed by 20 ul of phosphate buffer (143 mM sodium phosphate with 6.3 mM EDTA pH 7.4) to neutralize the pH. Next, 200 ul of assay reagent mix (5 ml 10 mM DTNB, 8.5 ml of 2 mM NADPH, 36.5 ml of 143 mM sodium phosphate buffer with 6.3 mM EDTA pH 7.4) was added to each well and incubated 5 minutes at room temperature. To initiate the reaction, 40 ul of glutathione reductase (8.5 IU/ml) was added and the kinetic rate

then monitored at 405 nm on a Beckman DU65 spectrophotometer. Quantification was done from a standard curve prepared with known concentrations of GSH. An aliquot of each sample was used for standardization of protein concentration with the BCA protein analysis kit (Pierce, Rockford, IL). Results are reported as nMole GSH/mg protein.

Hydrogen peroxide was used as a substrate for the Gpox enzyme assay. The principle of the assay is as follows. Two moles of GSH are oxidized to GSSG and act as cofactors for each mole of peroxide substrate reduced by Gpox. The GSSG product is reduced by glutathione reductase, which is added in excess in the presence of the cofactor, NADPH. The reaction rate is followed spectrophotometrically as NADPH is consumed in the reduction of GSSG (λ=340nM = O.D. of NADPH). The molar quantity of GSSG formed is proportional to the amount of glutathione peroxidase originally present. Vinylpyridine is added to remove excess GSH accumulation. Rates are standardized to protein quantified by the BCA assay, and data reported as 1 unit Gpox activity = 1nMol NADPH oxidized/ min/100ug protein @ 25^{0}C.

Briefly, the procedure was as follows. First, 2.8 ml of assay mix (on ice; 50 mM potassium phosphate buffer pH 7.0, 1 mM EDTA, 1.25 M sodium azide, 150 mM GSH, 8.4 nM NADPH, glutathione reductase 5 ul / 3 ml assay mix) was added to 0.1 ml H_2O_2 (30% = 9.8 M). A background rate was monitored at 340 nm before adding sample (100 ul). The rate of NADPH consumption was then followed for 2 minutes at 340 nm. The reaction kinetic rate (slope) was recorded for each sample.

Electron Microscopy.

MCF-7 cultures were grown for 18 hours in the presence of 1 nM or 100 nM melatonin, 0.00005% ethanol, or 1 nM 17β-estradiol. The flasks were harvested by

trypsin digest, rinsed once in PBS, and immediately fixed in glutaraldehyde. Slides were prepared by osmium tetraoxide post-fixation, sequential dehydration, infiltration, and plastic imbedding prior to staining and examination.

Polarography/oxygen consumption.

MCF-7 cells were harvested and re-suspended in medium to provide a concentration of $1*10^6$ cell per analysis. Samples were incubated for 30 minutes at 37^0C and 5% CO_2 immediately prior to polarographic measurements. Oxygen uptake was measured with an Instech Laboratories (Horsham, PA) micro-chamber instrument with a Clark type oxygen electrode and circulating water jacket maintained at 35^0 C. Oxygen levels were quantified using a Yellow Springs Instruments (Yellow Springs, OH) model 53 oxygen monitor calibrated from 100 to 0% oxygen saturation by the addition of sodium sulfite to air saturated deionized water. Data measurements were taken over a linear range of oxygen consumption (R^2>0.99) for 20 minutes.

Isolation of rat liver mitochondria.

Fresh rat livers were obtained from untreated control animals sacrificed at completion of an unrelated neurobiology study. Mitochondrial isolation was done with little modification from the procedures previously described (Methods in Toxicology; Mitochondrial Dysfunction [36]. All steps of the procedure were completed in ice-cold buffer and/or refrigeration. Livers were removed immediately following carbon dioxide narcosis and immersed in ice cold isolation buffer (225 mM sucrose, 10 mM potassium phosphate, 5 mM magnesium chloride, 20 mM triethanolamine hydrochloride pH 7.4, 0.1 mM phenylmethylsulfonyl fluoride, and 2 mM ethylene glycol bis(b-aminoethyl ether)-N,N,N',N',-tetraacetic acid). The tissue was minced with scissors and rinsed in buffer

three times to remove blood. Approximately 1 square centimeter of minced liver was added to a hand held Dounce homogenizer in 30 ml ice cold isolation buffer. Homogenization required ten strokes with care taken to not traumatize the mitochondria or create foaming. The homogenate was centrifuged at 600 x g for 10 minutes in a Sorval RC-5B (Du Pont, Wilmington Delaware) centrifuge (4^0C) to remove tissue remnants. The supernatant was then centrifuged for 5 minutes at 15,000 x g and the pellet washed and re-centrifuged at 15,000 x g for 5 minutes. The final pellet was re-suspended in buffer giving an estimated final concentration of approximately 4 mg protein per ml (25 ml/10g liver). Protein was measured by BCA protein analysis kit (Pierce, Rockford IL).

Preparation of submitochondrial particles (SMPs).

Isolated mitochondria were stored at -80^0C, thawed, and maintained on ice for use. SMPs were prepared by subjecting the thawed mitochondria to 10 five-second bursts of a Tekmar Sonic disrupter on medium setting.

Measurement of respiratory complex activity I in submitochondrial particles.

NADH:ubiquinone oxidoreductase enzymatic activity was measured by following the decrease in 340 nm absorbance due to NADH oxidation on a Beckman DU640 spectrophotometer. Protein concentration of previously prepared rat liver sub-mitochondrial particles (SMP) was determined using the Pierce BCA assay. The assay buffer used was potassium phosphate (pH2 @ 20^0C) 25 mM, and magnesium chloride 5 mM. An NADH substrate was prepared in assay buffer at five final concentrations of [0uM], [1uM], [10uM], [100uM], and [250uM]. Melatonin was prepared at final concentrations for five sets of experiments with [0uM], [10nM], [100nM], [1uM], and [10uM]. Substrate, melatonin, and SMP were incubated for 60 seconds and then

followed on a Beckman DU600 spectrophotometer at λ= 340 nm for a background reading. Ubiquinone-2 was added to initiate the reaction mixture and serve as an electron acceptor "shuttle". Kinetic readings were taken for 3 minutes and all reactions were carried out at 37°C in 1 milliliter final volume.

Measurement of respiratory complex II in sub-mitochondrial particles.

The method generally follows that described in Methods in Toxicology Mitochondrial Dysfunction [36]. Rotenone, antimycin A, and potassium cyanide (KCN) were used to isolate complex II from either backward or forward movement of electrons. Ubiquinone acts as an electron acceptor and "shuttle system" for the complex while succinate is the electron donor and enzymatic substrate. Dichlorophenolindophenol is the final electron acceptor and, when reduced, is a chromophore followed at λ=600 nm. Protein content of previously prepared sub-mitochondrial particles was determined using the Pierce BCA assay. The assay buffer was composed of 25 mM potassium phosphate pH2 @ 20^{0}C, 5mM magnesium chloride, and succinate at five final concentrations of [6.25], [12.5], [25], [50], and [100] mM. The addition solution contained 2 ug/ml antimycin A, 2 ug/ml rotenone, 2 mM potassium cyanide, and 50 uM dichlorophenol-indophenol. Melatonin was first dissolved in ethanol (215 mM) and then diluted with assay buffer to [0], [1 uM], [100 nM], [10 nM], and [1 nM]. Each sample was prepared with 790 ul of assay buffer with succinate, 300 ug SMP protein, and 100 ul of melatonin solution. This was incubated for 60 seconds, then used as a blank for the spectrophotometer. The reaction was initiated by adding ubiquinone (to final concentration of 65 uM), and read for 45 seconds on a Beckman DU600 spectrophotometer in kinetic mode.

Cytochrome C oxidase assays.

The cytochrome C oxidase microtiter plate assay was performed with minimal modification from the method of Chrzanowska-Lightowlers [37]. Briefly, MCF-7 cell membranes were permeabilized with 0.25% saponin for ten minutes prior to adding substrate mix containing reduced cytochrome C and 3,3'-diaminobenzidine-tetrachloride (DAB). The oxidation of DAB maintains a constant substrate pool of reduced cytochrome C and forms a polymer that absorbs at 450 nm. Enzyme assays were standardized to cell number in 96 well microtiter plates with approximately $1.5*10^6$ cells required per assay well for optimal detection of enzyme activity. Kinetic readings taken on a Bio-tek EL_x 800 plate reader were linear for at least fifteen minutes in all samples. Background absorption was measured in wells with culture medium but no cells (assay blank) and subtracted from cell samples. The addition of 3 mM potassium cyanide to control wells inhibited 100% of enzyme activity, thus verifying that the reaction was catalyzed by cytochrome C oxidase. Data is reported as mean velocity of enzyme activity (linear slope of DAB oxidation = Δabsorbance/minute) per 10^6 cells.

In addition, the AlamarBlue™ dye assay (AccuMed International, Inc. Westlake OH) was used to detect changes in electron transport complex IV activity. AlamarBlue dye is reported by the manufacturer to be a final electron acceptor between the reduction of oxygen and cytochrome C oxidase (cyt.a_3). The dye is reduced by the removal of oxygen and its replacement by hydrogen with the amount of reduced dye (emitting at 590 nm) being proportional to the activity of cyt.a3 [38]. Cells were incubated with AlamarBlue for four hours at 37^0C as described by the manufacturer's protocol. The amount of dye reduced during the incubation was quantified by fluorometric measurements using a Cytofluor 2300 instrument with excitation filter at 530 nm and

emission at 590 nm. Data is reported as reduced dye fluorescent units per cell per four-hour incubation standardized to cell number.

Analysis of succinate dehydrogenase activity.

Mitochondrial complex II activity was measured by the MTT assay with minor modification of the original Mosman method [39]. Briefly, 50,000 MCF-7 cells were seeded in 48 well microtiter plates in 500 ul DMEM supplemented with penstrep, insulin, sodium pyruvate, non-essential amino acids, hydrocortisone and C-D extracted FBS as described previously. After three days growth, the cells were re-fed, then treated two days later with fresh medium containing 0.003% ethanol, melatonin (1 nM, 10 nM, 100 nM), luzindole 1uM, or 1 uM luzindole plus 100 nM melatonin. MTT (3-(4,5-dimethylthiazol-2-yl)-2,5 diphenyl tetrazolium bromide) was dissolved in PBS at 5 mg/ml and filter sterilized. After 17 hours treatment, each well received 75 ul of MTT dye and was incubated for three additional hours. Medium was aspirated with care not to disturb formazan crystals formed by the cell metabolism. DMSO was then added to each well (200 ul) and placed on a plate shaker at low speed. After 5 minutes, 150 ul of the DMSO solubilized dye solution was transferred to a 96 well MTP and 550 nm absorbance read on a Bio-tek EL_x 800 microtiter plate reader. Cells from parallel treatments were counted by hemocytometer and Trypan Blue dye exclusion to standardize MTT results with cell number. Statisical analysis was performed by one way ANOVA with Fisher's comparison of means test.

Luciferin-Luciferase Chemiluminescent ATP Assay.

Quantification of cellular ATP by chemiluminescent measurement was performed as described in Sigma Chemical technical bulletin number BL-100 using luciferase-

luciferin in glycine buffer (cat. no. L0633). Luminometry measurements were recorded using an EG&G Berthold Lumat model LB9501/16 luminometer.

Cell samples were extracted with 0.1% triton X and diluted five-fold in assay buffer containing 100 mg BSA and 10 ml each of 200 mM Tris HCL, 20 mM EDTA, and 100 mM $MgSO_4$ at pH 7.8. Results were standardized to cell protein using the BCA protein assay (Pierce, Rockford, IL) and reported as moles of ATP per mg protein from a standard curve (figure 1.2).

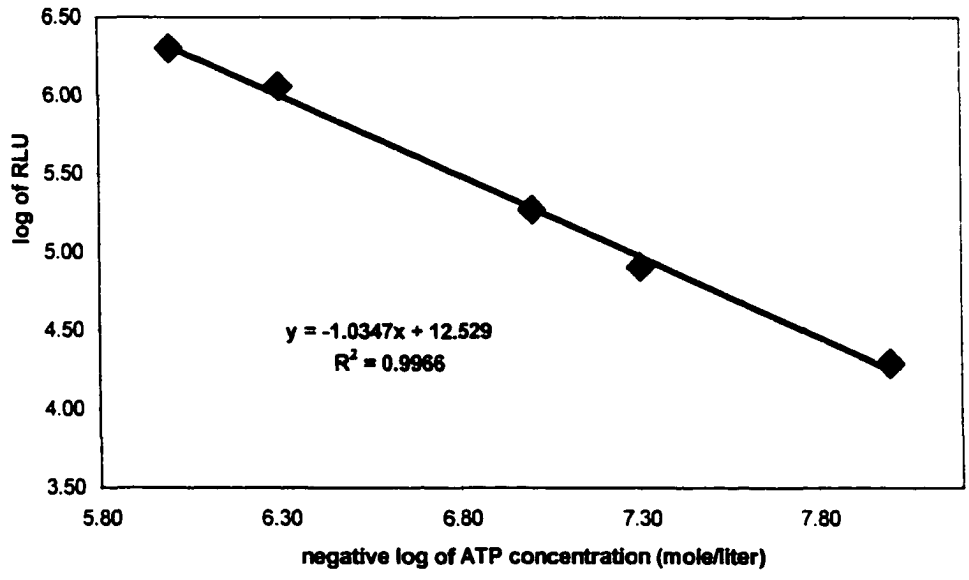

Figure 1. 2 Standard curve for luciferin-luciferase assay.

ATP standards were prepared as described in Sigma technical bulletin BL100. Raw data in the form of relative light units (RLU) was recorded on the Y-axis and regressed against the negative log of ATP molar concentration as shown above. The curve was linear within this range with R^2=0.997.

BCA protein assay.

The principle of the BCA assay involves the reduction of Cu^{++} ions to Cu^{+} when complexed with protein in an alkaline environment. The cuprous ion is detected as a

chelated complex with two molecules of bicinchonic acid that absorbs strongly at 562nm. The chromophore thus produced is measured by spectrophotometry and compared against a standard curve prepared from bovine serum albumin (figure 1.3). The BCA detection limit is 0.5 ug/ml with a broad linear range of at least three magnitudes of ten. The protocol was minimally modified from the manufacturer's recommendations. Briefly, a working reagent was prepared by adding 25 parts of reagent A to 24 parts of B and finally adding 1 part of reagent C. One ml of each standard, sample, or diluent buffer (blank) was added to an appropriate tube followed by one ml of the working reagent. The tubes were incubated for 60 minutes at 37^0C and absorbency read at 562 nm with a Beckman DU640 (Fullerton CA) spectrophotometer.

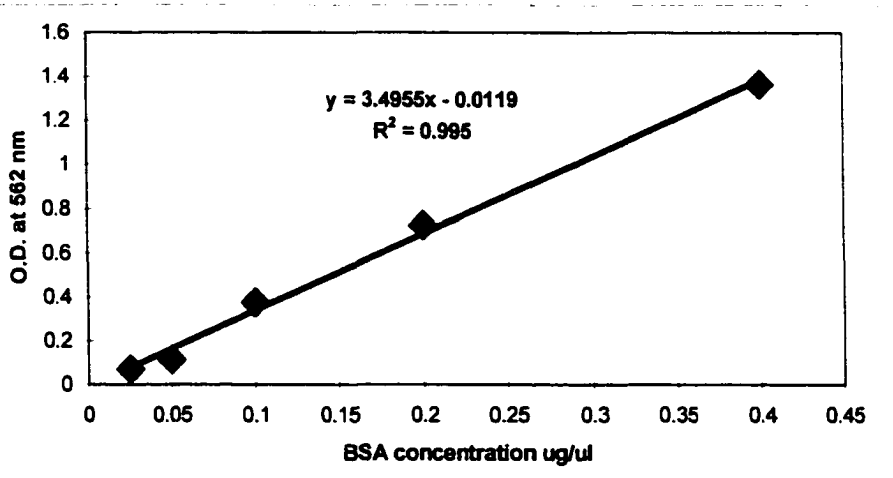

Figure 1. 3 Standard curve for BCA protein assay.

Standards were prepared from bovine serum albumin stock solution (Pierce, Rockford IL). The measured optical density was plotted by linear regression against its corresponding concentration. The curve was linear with R^2=0.995. Sample protein concentrations were calculated from the regression equation (concentration = (O.D.+ 0.119) / 3.4955).

Statistical analysis.

Where applicable, results were analyzed by one way analysis of variance (ANOVA) using Microsoft Excel or Minitab statistical software. Comparisons of sample means and control means were calculated with Minitab software using Fishers, Tukeys, Dunnetts, or Student's T tests with the assumption of equality of variance as indicated for each experiment. Two tailed critical values were used in all experiments with level of significance as noted. Significance of oxygen consumption curves and linear plots of mitochondrial complex I and II activity were done with Minitab software by statistical slope comparison within the context of multiple linear regression [see for example, ch 14, Kleinbaum et al. [40]]. All experiments were conducted in triplicate or quadruplicate fashion.

RESULTS.

Loss of cells at 17 to 20 hours.

Initial proliferation studies of melatonin treated MCF-7 cells confirmed and extended the previous reports of its oncostatic activity in breast tumor cells. After 17 to 20 hour melatonin treatments, the cells were enumerated by directly counting the cells (via coulter and/or hemocytometer). As shown in Figure 1.4, a significant loss of cells was observed following these short-term treatments with melatonin concentrations as low as 1 nM. The cell loss followed a "U" shaped dose-response curve with a maximum 63% decrease in cell number at the 100 nM treatment level compared to control cultures. Considering the abbreviated time-course of these effects, the results suggested a cytolethal mechanism of oncostatic action, rather than an inhibition of cell proliferation. Addition of the melatonin G-protein coupled receptor antagonist, luzindole, to the culture medium prevented the cell loss (figure 1.4) suggesting a partial inhibition of the

melatonin induced cytotoxicity through receptor binding inhibition. Furthermore, when the studies were repeated in the presence of FBS that was not depleted of estrogen, the cell loss was prevented at both 1 nM and 100 nM concentrations of melatonin (figure 1.5). Additionally, estrogen rescue of the early cytotoxicity was observed with the addition of 1 nM 17 β-estradiol to the culture medium concurrently with melatonin (data not shown).

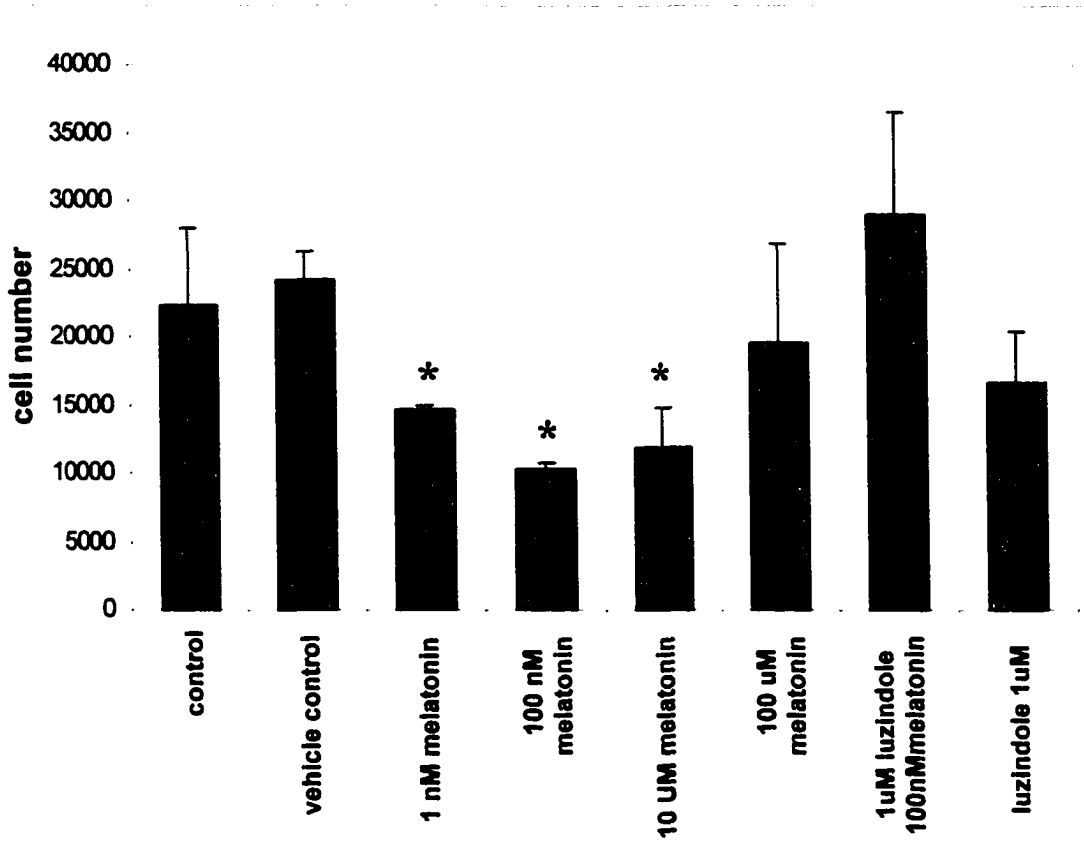

Figure 1. 4 MCF-7 cells treated for 18 hours with vehicle control, melatonin, or luzindole.

Cells were enumerated by Trypan Blue dye exclusion assay and hemocytometer count. Treatments were performed in triplicate in 48 well microtiter plates. Statistically significant differences from control ($p<0.05$ by one way ANOVA and Dunnets comparison of means to control test) are indicated by *.

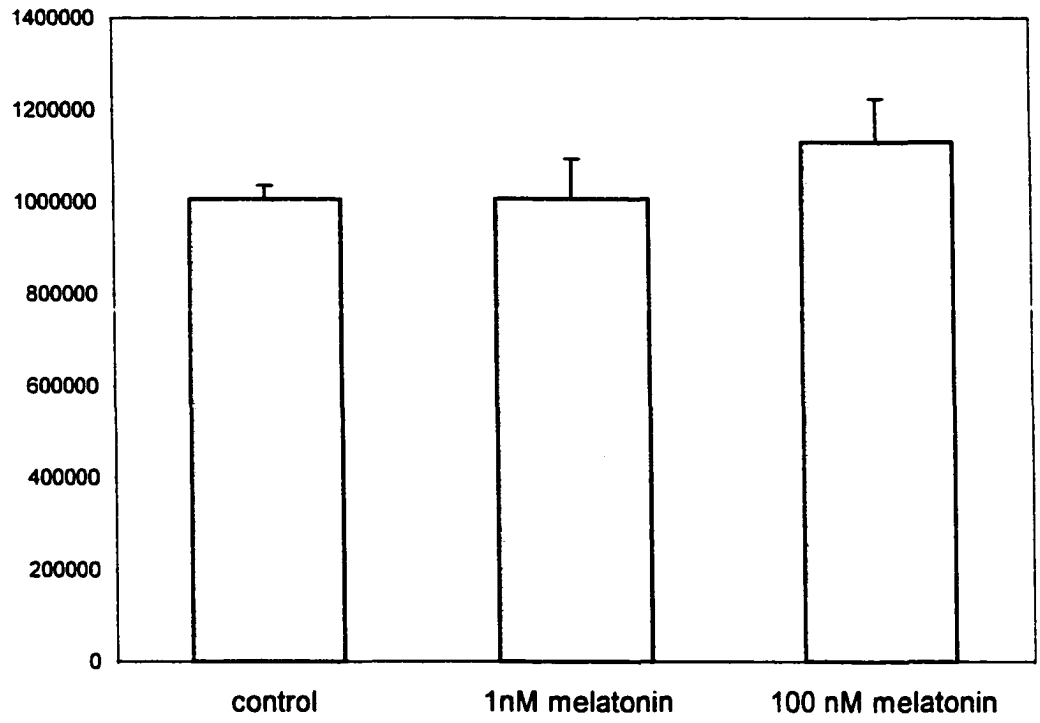

Figure 1. 5 MCF-7 cell number at 16 hours following treatment with 1nM and 100 nM melatonin.

Cells were grown in medium supplemented with 10% FBS that was not charcoal dextran depleted of estrogen. There was no statistical difference in cell number between any of the treatment groups.

Trititiated thymidine did not suggest cell cycle changes.

Tritiated thymidine uptake/nascent DNA synthesis studies provided further evidence for cytolethality due to melatonin treatment. As depicted in Figure 1.6, following the same melatonin treatments described above, there were no significant differences in tritiated thymidine uptake in treated vs. control MCF-7 cell cultures. On the other hand, cells treated with 1 nM 17 β-estradiol demonstrated a significant increase in tritiated

thymidine uptake, thus confirming the positive proliferative response to estrogen in the MCF-7 cells. These results suggested a lack of effect by melatonin on the cell cycle/DNA synthesis, and provided further evidence for a cytolethal mechanism of action.

Flow cytometry.

Flow cytometric analysis further confirmed the lack of cell cycle change between treatment and control cultures. Histograms in figure 1.7 show that cells of both groups were predominantly in the G_0-G_1 phase of the cell cycle. Interestingly, dual parameter analysis of forward angle light scatter vs. I90 light scatter indicated that two different populations of MCF-7cells were present based on cell size (figure 1.8A and 1.8B). Histograms produced by gating on the smaller cell population (figure 1.8C and 1.8D) again indicated no change in cell cycle, but demonstrated a slight but consistently lower DNA content in the smaller compared to the larger population. Additionally, the 9-hour melatonin treatment histograms suggested degenerate cells or nuclear fragments in the sub-G_1 area. However, neither distinct sub-G_1 nor sub-G_2 peaks indicative of classical apoptosis were present.

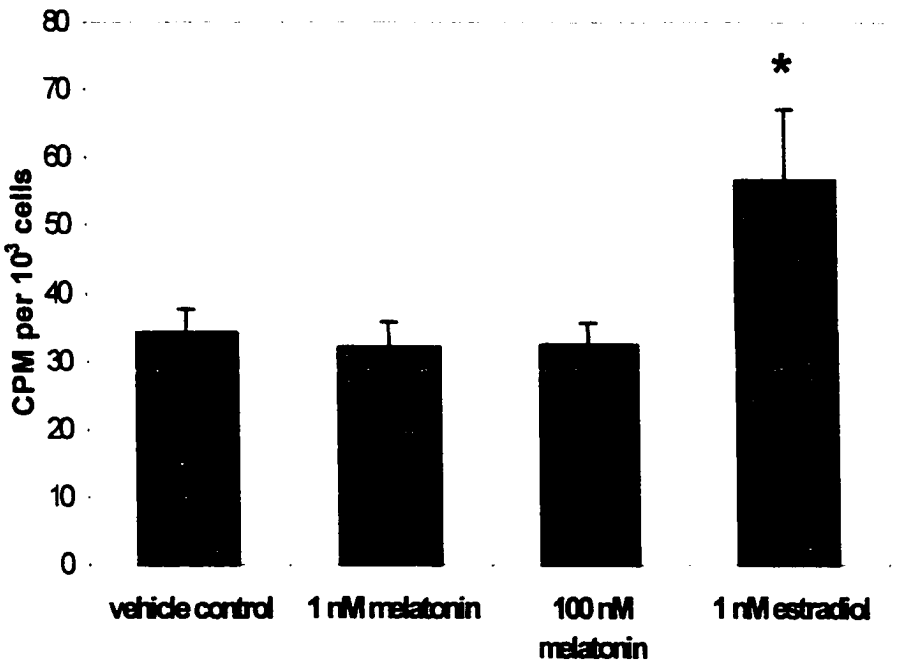

Figure 1. 6 Tritiated thymidine uptake by MCF-7 cells 16 hours following melatonin or 17β-estradiol treatment.

Tritiated thymidine studies were conducted as described in methods. No difference in DNA synthesis was evident after either 1 nM or 100 nM melatonin treatment. Significant difference between estradiol and control groups by Student's T test is indicated by * $p<0.05$. All treatments were done in triplicate.

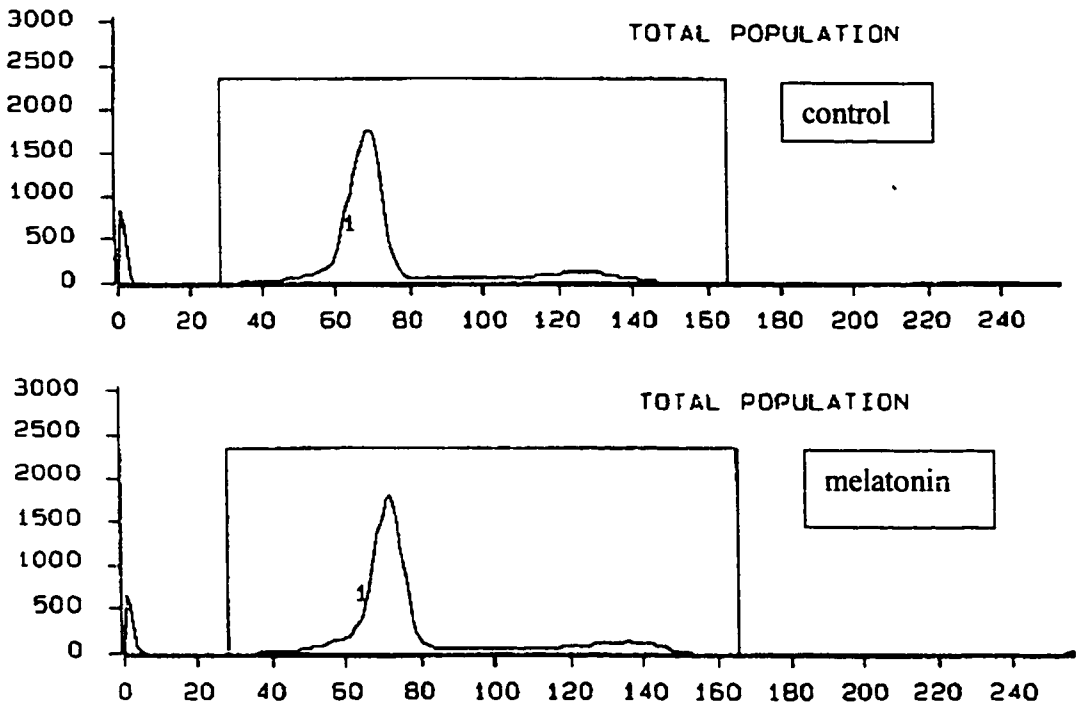

Figure 1. 7. Flow cytometry DNA histograms of MCF-7 cells at 9 hours following treatment with either 0.00005% ethanol (vehicle) or 1 nM melatonin.

Cell cycle distribution was nearly identical for treatment and control groups with most cells in G_1 of the cell cycle. Histograms from 18 hour samples showed similar distributions with no difference between treatment and control cells. X-axis is channel number of propidium iodide DNA stain and Y-axis represents number of events counted.

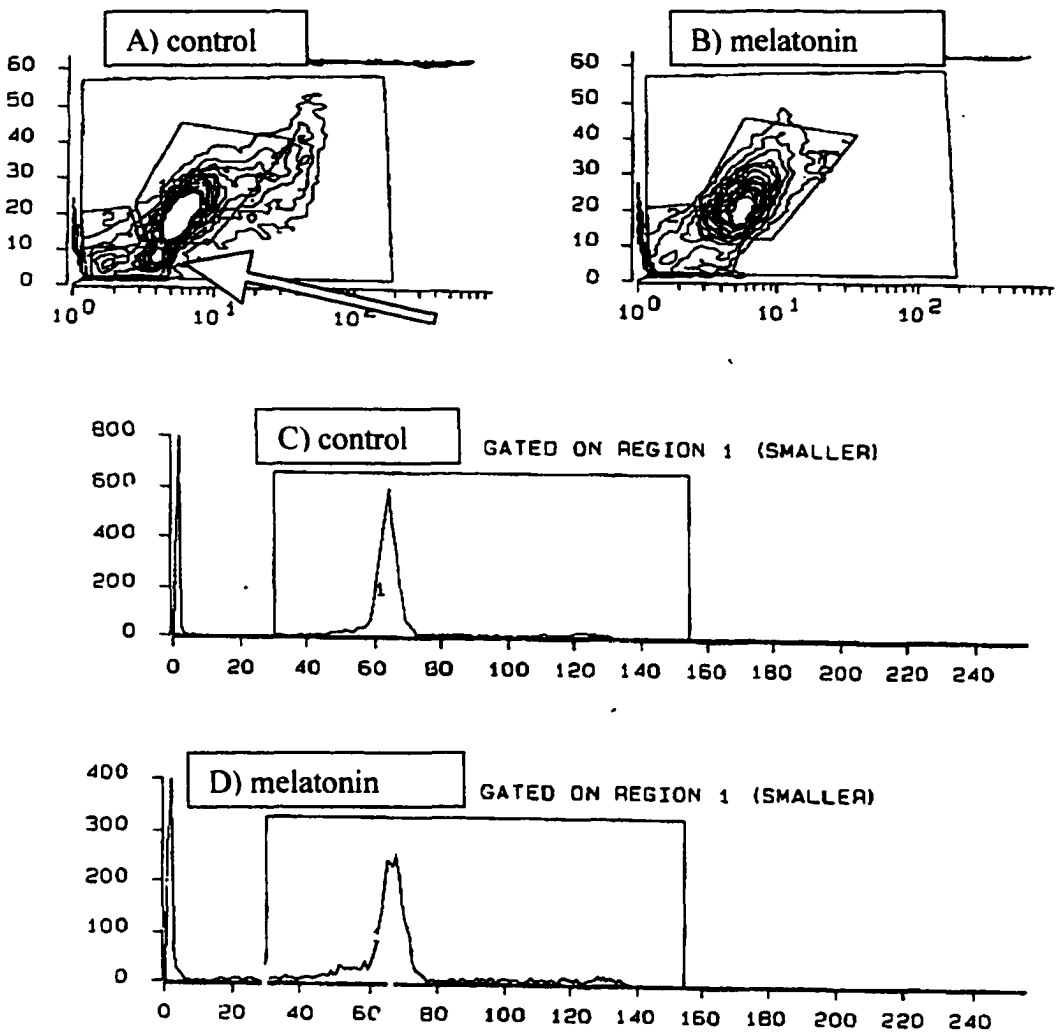

Figure 1. 8. Flow cytometry histograms 9 hours after treating MCF-7 cells with vehicle (0.00005% ethanol) or 1 nM melatonin.

Each histogram was based on a count of 30,000 events. The X-axis of (A) and (B) represents I90 light scatter and the Y-axis parameter represents forward angle light scatter (size of the cells). A cell population of smaller size was observed in the control cells (arrow) but by 18 hours, was not evident in either control or treated groups (not shown). Histograms C) and D) were gated on the region of smaller sized cells with DNA staining (brightness of PI fluorescence) on the X axis. The mode of G_1cells (DNA content) in control (C) was at channel 64 and 1 nM melatonin (D) at 67. The corresponding modes for the population of larger cells were consistently higher at 70 and 71 respectively (not shown). The histogram in (D) shows an increased number of cells in a sub-G1 area (circled) in the smaller sized melatonin treated cells that was suggestive of degenerating nuclei and apoptosis.

Comet assays.

Comet assays were performed to screen for further evidence of programmed cell death following melatonin treatment. Minimal difference was observed in tail moment (a mathematical parameter combining functions of DNA movement within the electrophoretic field and DNA content of the comet [33]) between treatment and control experiments (figures 1.9C and 1.10C). There was, however, a reduced mean DNA content of the comets in melatonin treated cells (figures 1.9A and 1.10A) and a wider range of DNA content values (figures 1.9B and 1.10B). Together these findings suggested that an apoptotic pathway was not present, but that the melatonin treated cell group contained cells with altered amounts and possibly damaged DNA. This again implied the possibility of non-viable and/or degenerate cells with gross fragmentation of DNA.

Dual staining fluorescent phase contrast examination.

Visual examination of cells was performed by fluorescence and phase contrast microscopy with dual acridine orange and ethidium bromide staining [41]. The melatonin treatment, but not vehicle control or estradiol appeared to have increased numbers of non-viable cells indicated by morphology and intra-cellular concentration of EB (figure1.11). While the difference was qualitative, it further suggested the presence of acute necrosis in the MCF-7cells.

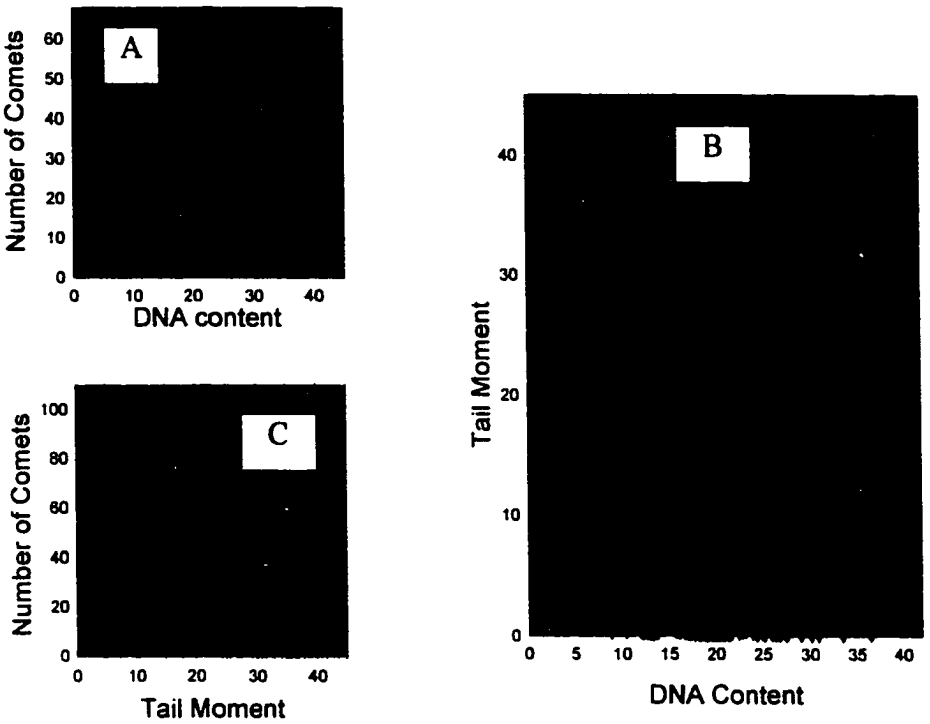

Figure 1. 9. Comet assay of MCF-7 cells 18 hours after treatment with vehicle (0.00005% ethanol)

A) DNA content of comets analyzed B) Tail moment vs. DNA content C) Number of comets at each calculated tail moment

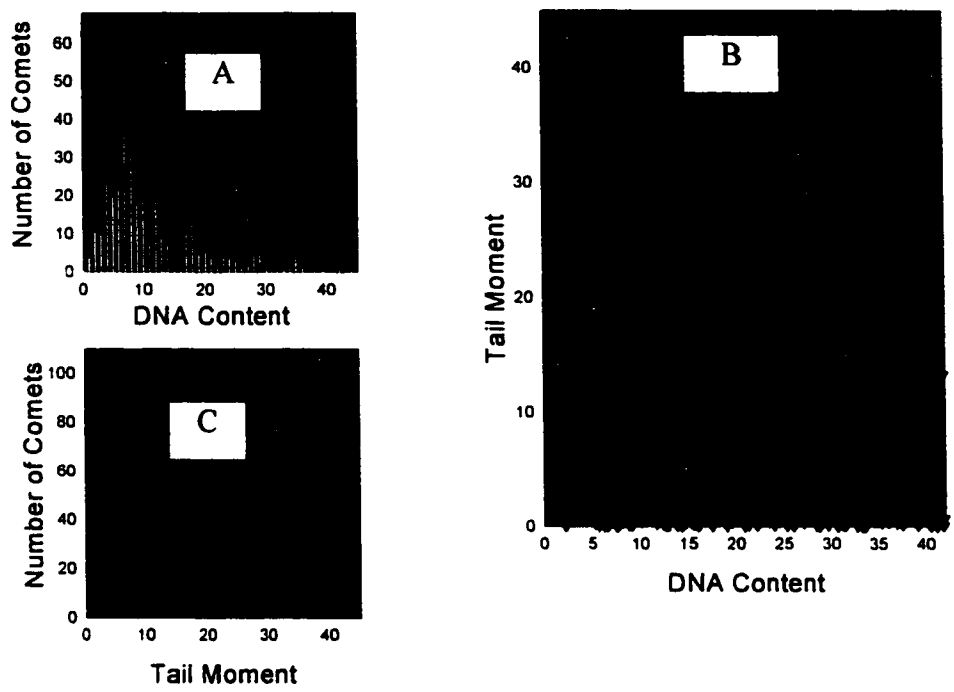

Figure 1. 10 Comet assay of MCF-7 cells 18 hours after treatment with 1 nM melatonin.

A) Mean DNA content of the comets was less than half that of the control cells suggesting either loss of DNA or non-viable cells with comets from fragmenting nuclei. B) There were relatively few comets with large tail moment compared to control but the DNA content of the comets varies widely. C) Overall magnitude of the tail moment parameter was very little different than control cells shown in figure 1.4. These data do not suggest a pathway of programmed cell death.

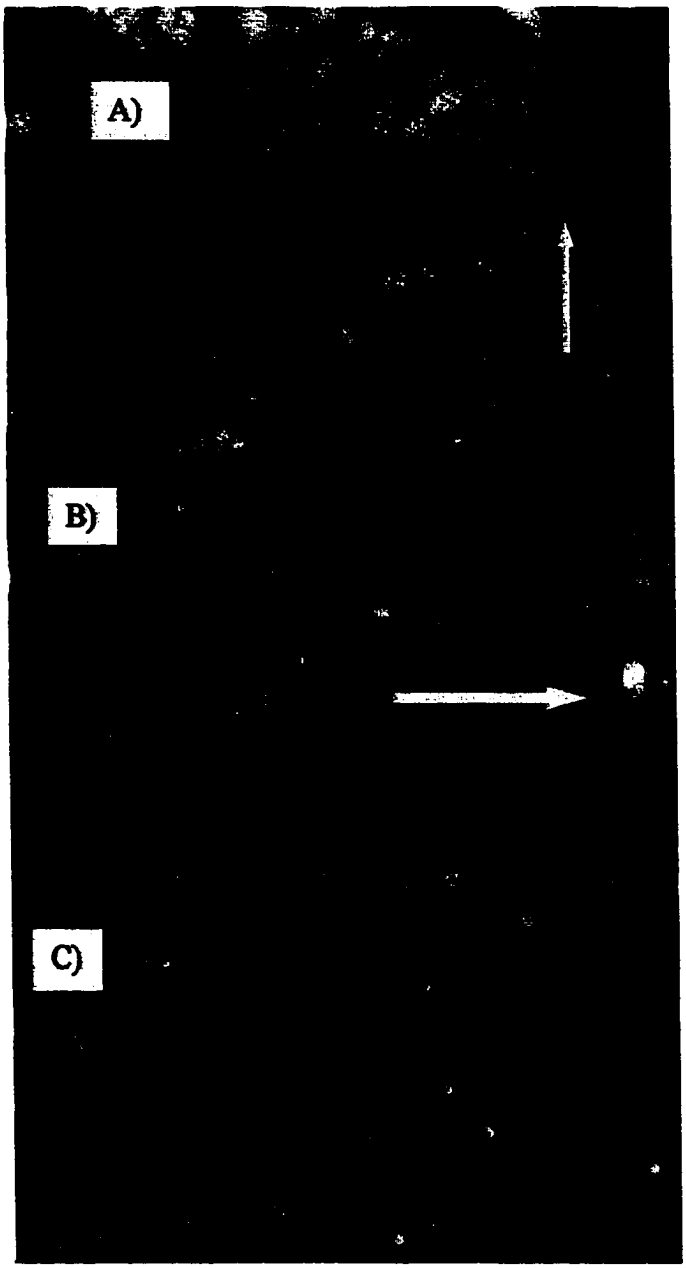

Figure 1. 11. MCF-7 cells stained concurrently with ethidium bromide and acridine orange.

A) Control cells photographed in panel A were treated with the stains and incubated for 4 hours until cytotoxicity became apparent from stain exposure. Arrow indicates cells that have begun taking up EB following degradation of the cytoplasmic membrane. The distinctly orange cell indicated by the arrow (upper right) has taken up a significant amount of EB due to complete loss of membrane integrity. Bright yellow cells are beginning to take up the EB while only a few viable (green) cells remain.

B) MCF-7 cells treated with vehicle control for 16 hours. Cells show green AO staining but no evidence of EB entering the cells. Nucleoli (arrow) stain more intensely than remainder of nucleus and could be confused with apoptotic bodies without careful evaluation of surrounding DNA. (400 X)

C) MCF-7 cells treated with melatonin for 16 hours. Scattered orange staining cells were present as well as an overall increase in the intensity of yellow staining in the nucleus and cytoplasm. Distinct apoptotic bodies were not seen, but chromatin in the brighter yellow cells appeared to be more condensed. (200 X)

Glutathione and glutathione peroxidase assays.

Glutathione and glutathione peroxidase levels were measured to explore melatonin effects on general redox status of the cells (figure 1.12). There was no significant increase of GSH levels or Gpox activity in melatonin treated cells as compared to ethanol controls (data analysis with one way ANOVA and Fisher's pairwise comparison of means). The GSH levels did increase significantly following the addition of fresh medium but then declined over the four-day treatment time to become significantly lower than day one levels. This decrease of GSH with time in culture agrees with the data of Blask et al. [42]. However, GSH did not increase in response to melatonin as was previously shown in Blask's experiments. A possible explanation of this difference was that Blask's culture system contained fetal bovine serum (FBS), while this experiment was performed in estrogen depleted FBS medium. The suggestion then, was that GSH up-regulation by melatonin may require estrogen and/or the estrogen-receptor complex.

Glutathione peroxidase levels were below the assay detection limit in all samples indicating first that the cells were not producing significant amounts of the enzyme, and secondly, that there was no iatrogenic oxidation of the GSH.

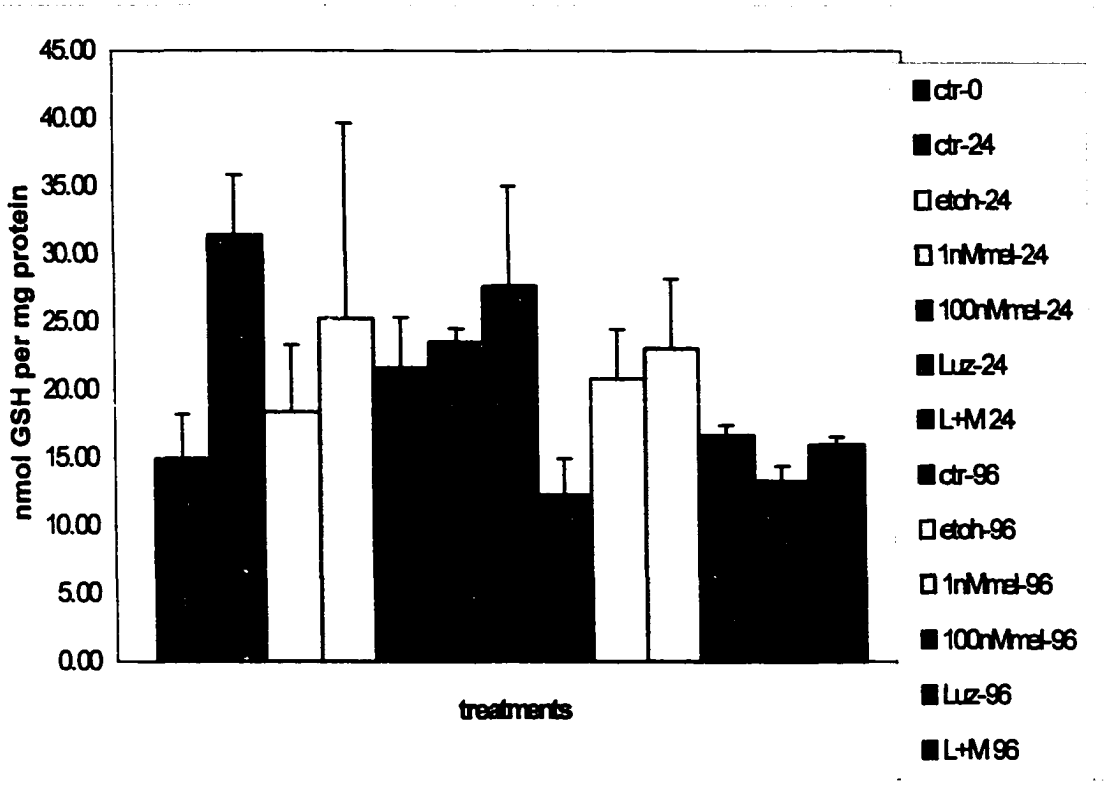

Figure 1. 12. Glutathione concentration in MCF-7 cells at 0, 24, and 96 hours after treatment with vehicle (0.00005% ethanol), 1 nM or 100 nM melatonin, luzindole 1 uM, or luzindole 1 uM plus melatonin 100 nM.

Analysis was performed as described in materials and methods. No significant difference was present between treatment groups (data analysis by one way ANOVA with Fishers pairwise comparison of means α=0.05). Untreated controls but not vehicle controls had significantly higher GSH at 24 hours as compared to day 0 and four. This coincides with the addition of fresh culture medium.

Histology and electron microscopy.

Histologic and electron microscopic evaluation of melatonin treated MCF-7 cells revealed morphologic evidence of acute cytotoxicity. Cells with pale degenerate cytoplasm were present in Hematoxilin and Eosin stained histology slides along with multiple autophagocytic inclusions (figure 1.13) and substantial amounts of intercellular debris. Further examination of fixed grids by electron microscopy confirmed the

identification of the inclusion bodies as phagolysosomes (figure 1.14). Additionally, mitochondrial changes consisting of swollen and degenerate cristae, loss of ultrastructural features of the cristae, and dissolution of the outer mitochondrial membrane were present in treated cells but not in control or estrogen treated cultures (figure 1.15).

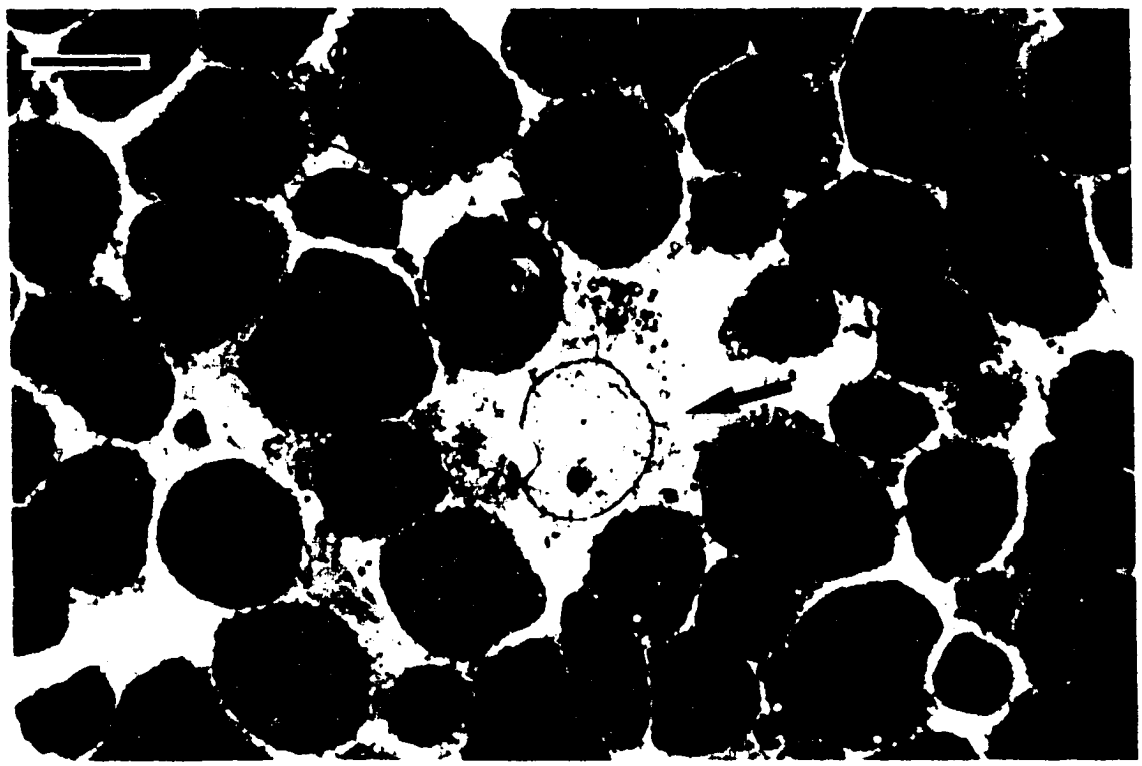

Figure 1. 13. Light micrograph of MCF-7 cells 18 hours after treatment with 100 nM melatonin.

(H and E stain 1000x magnification) Multiple pale staining cells (arrow) were present in slides from melatonin treated cells but absent in both the vehicle control (0.00005% ethanol) and estrogen (1 nM) treated cultures. Many of the treated cells contained cytoplasmic inclusion bodies (arrowhead) that appeared to be degenerating cell bodies.

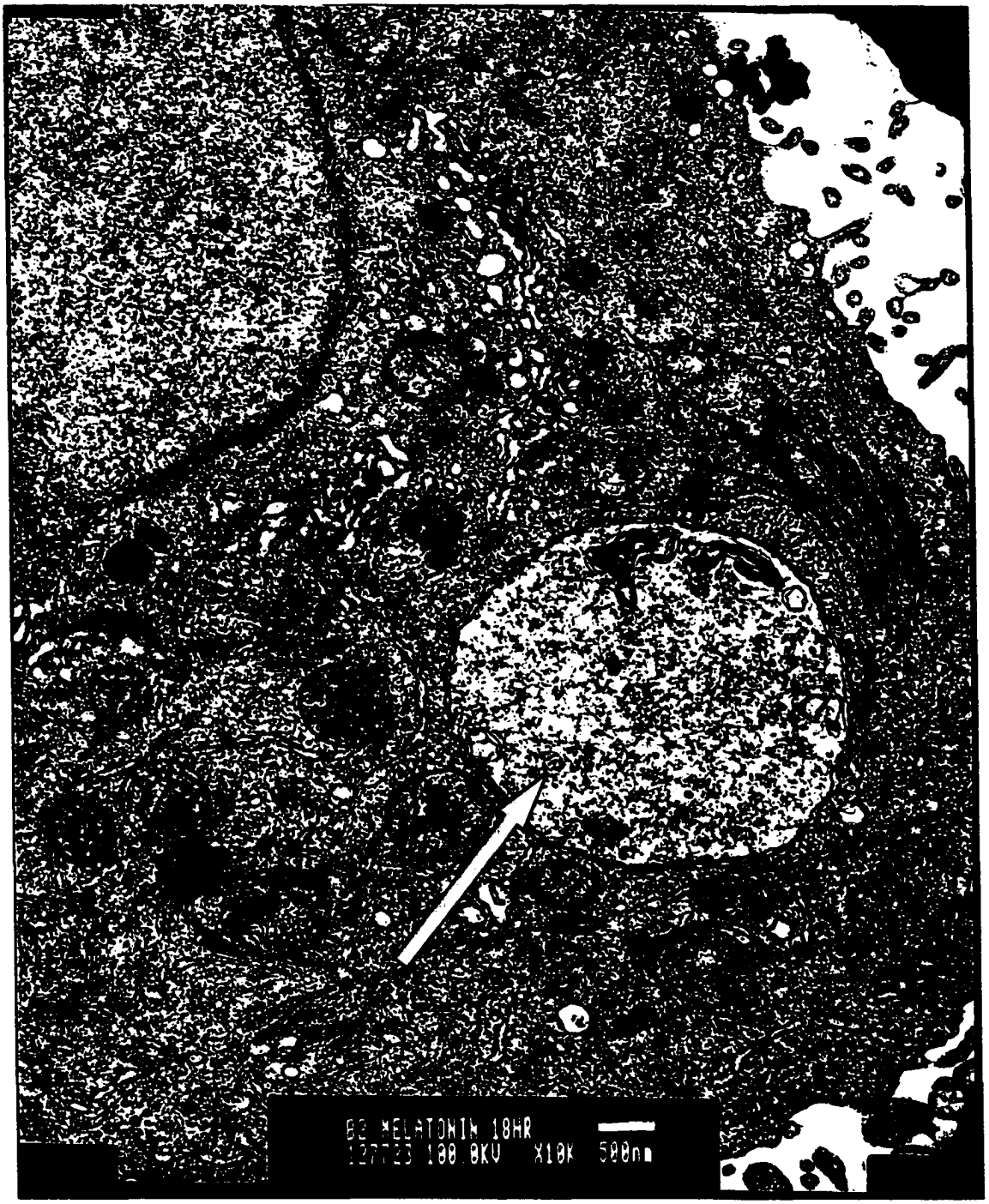

Figure 1. 14. Transmission electron micrograph of MCF-7 cell 18 hours after treatment with 100 nM melatonin. (magnification 10,000x)

The inclusion body (phagolysosome) shown in figure 1.8 is indicated by the arrow. Note the presence of nuclear remnants and degenerating organelles within the phagolysosome.

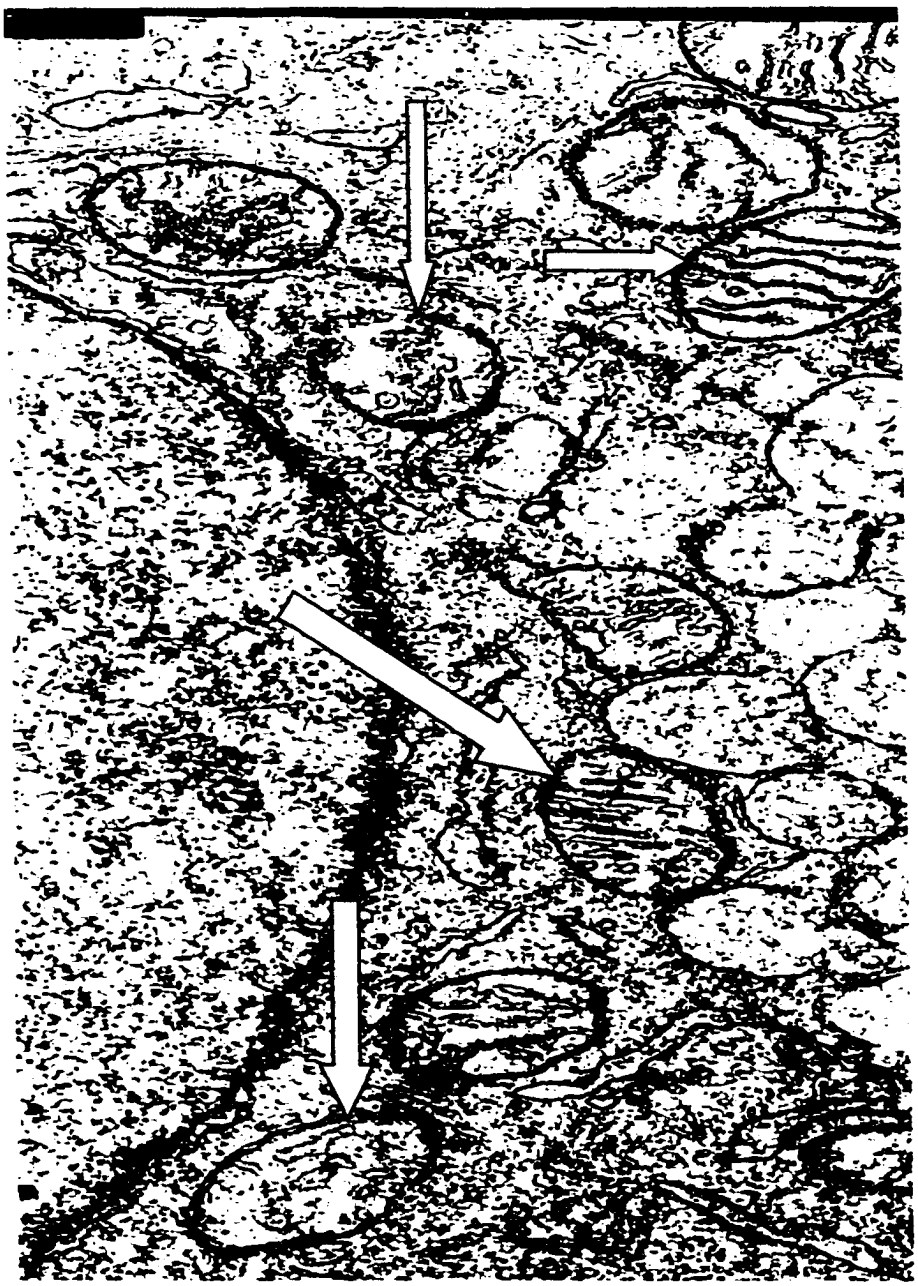

Figure 1. 15. Transmision electron micrograph of MCF-7 cell 18 hours after treatment with 100 nM melatonin. (magnification 15,000 x)

Mitochondria (arrows) were in varying states of degeneration. A normal mitochondrion (upper right) had distinct morphologic ultrastructure and clearly defined cristae. Other mitochondria demonstrated changes that included swelling of cristae, degeneration of cristae, and degeneration of mitochondrial wall.

Mitochondrial respiration- polarography.

Because of the acute toxicity that melatonin appeared to inflict in the MCF-7 cells, as well as morphologic evidence of mitochondrial degradation, mitochondrial activity/respiration in melatonin treated breast tumor cells was further explored. Standard polarography was used to measure oxygen consumption in MCF-7 cells treated with melatonin in similar fashion to the previously described proliferation studies. As shown in Figure 1.16, 100 nM melatonin treatment resulted in a significantly ($p<0.05$) increased oxygen consumption by MCF-7 cells 17 hours after treatment. Furthermore, the oxygen consumption was dose responsive for control, 1 nM, and 100 nM samples. A positive control containing 1 nM estradiol (figure 1.16) also showed a significant increase in oxygen uptake of magnitude comparable to the increase seen in tritiated thymidine uptake shown in figure 1.6. On the other hand, melatonin treated MCF-7 cells that were grown in FBS not C-D extracted of estrogen showed no significant change in oxygen consumption compared to corresponding control cultures (data not shown). Likewise, the addition of luzindole to the 100 nM melatonin treatment eliminated any significant increase in oxygen consumption (figure 1.16).

Succinate dehydrogenase activity- MTT assay.

The identification of elevated levels of oxygen consumption prompted a hypothesis that a specific bioenergetic target was affected by melatonin. Data from the MTT (3-4,5-dimethylthiazol-2-yl)2,5-diphenyltetrazolium bromide) assay (figure 1.17) suggested increased activity of succinate dehydrogenase in MCF-7 cells grown in C-D extracted FBS medium following nineteen hours of treatment with melatonin. This information in

conjunction with increased oxygen consumption suggested that electron transport chain activity was increased by melatonin treatment.

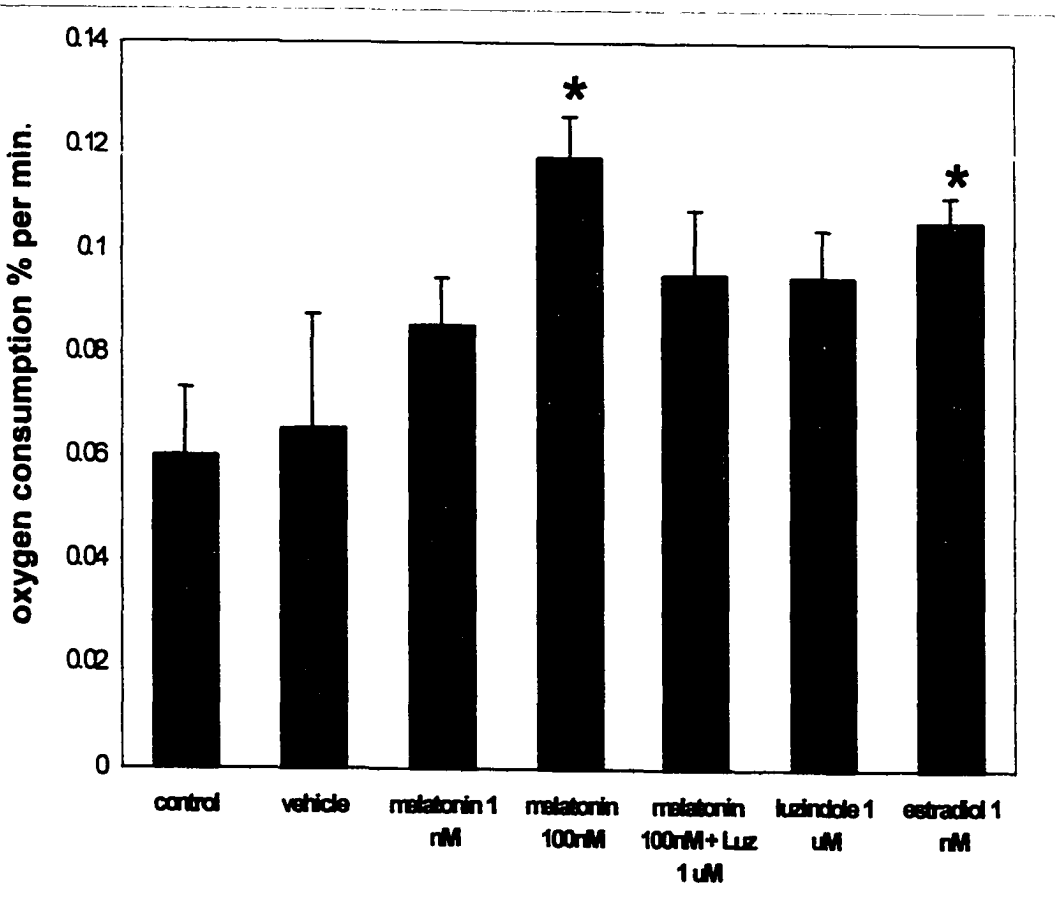

Figure 1. 16. Oxygen uptake by MCF-7 cells (16 to 20 hours) after treatments with vehicle (0.00005% ethanol), melatonin, luzindole, or estrogen.

Slopes for oxygen consumption curves were from a linear range ($R^2 \geq 0.99$) over 20 minutes. Bars represent mean slope of triplicate samples with error bars representing one standard deviation of each set mean. The slope of both estradiol 1nM and melatonin 100 nM were significantly higher than vehicle control by one-way ANOVA and Tukeys comparison of means test ($p<0.05$).

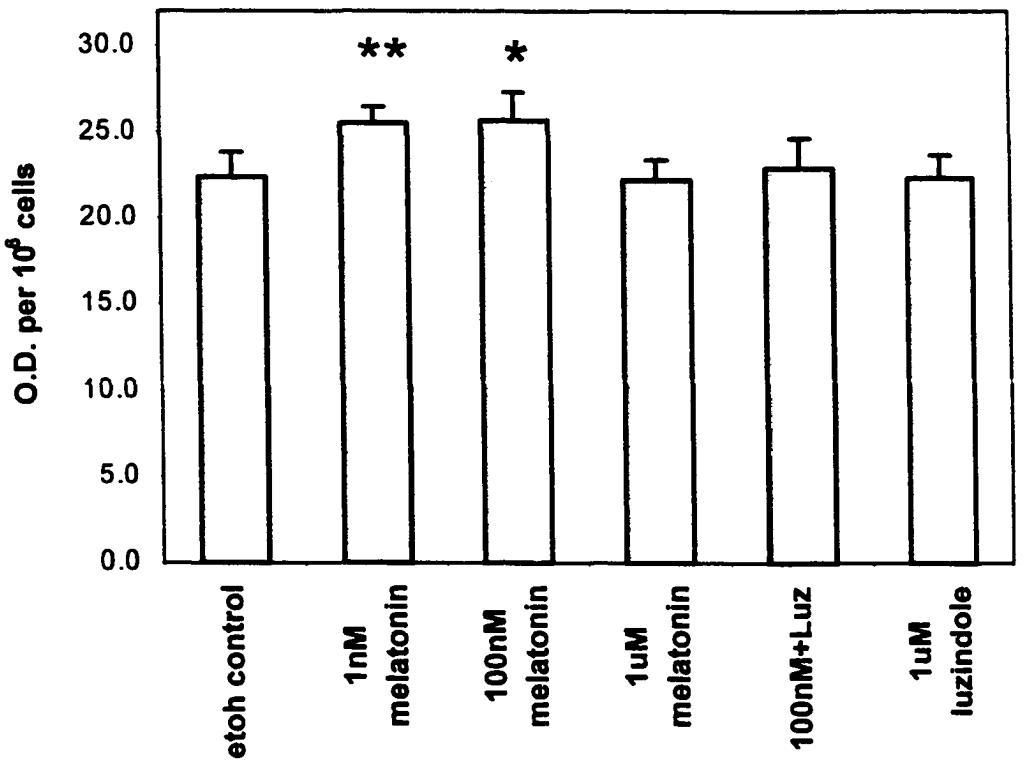

Figure 1. 17. MTT assay.

MCF-7 cells were treated for 19 hours with vehicle (0.003% ethanol), 1 nM melatonin, 100 nM melatonin, 1 uM luzindole, or combination of 100 nM melatonin plus 1 uM luzindole. Optical density of the microtiter plate assay was standardized to cell number and results represent absorbance per million cells. Both 1 nM and 100 nM melatonin treatments were significantly higher than vehicle control ($p<0.01$ and $p<0.05$) by two tailed Students T test.

Cytochrome C oxidase activity.

To further explore the possibility of increased electron transport chain activity, complex IV activity was studied by directly performing enzyme-substrate kinetic analysis in detergent permeabilized MCF-7 cells with the microtiter plate method of Lightowlers et al. [37]. This procedure provides an activity measurement of cytochrome C oxidation by cytochrome C oxidase and represents the acceptance of electrons by the CuA-heme moiety. A significant increase in Cox activity (complex IV) was present 17 hours after treatment of MCF-7 cells with 100 nM melatonin (Figure 1.18). The apparent increase in

complex IV activity was further confirmed by employing the use of a mitochondrial vital dye, AlamarBlue, which undergoes a detectable change in fluorescence following reduction by complex IV (Figure 1.19). These studies again yielded evidence of an increase in cytochrome C oxidase activity in melatonin treated MCF-7 cells compared to controls. Hence, the combined data showing increased activity of succinate dehydrogenase, increased reduction of cytochrome C by Cox, and increased terminal electron transfer from heme a-a3/CuB to AlamarBlue suggested an overall increase in electron transport chain activity in melatonin-treated MCF-7 cells.

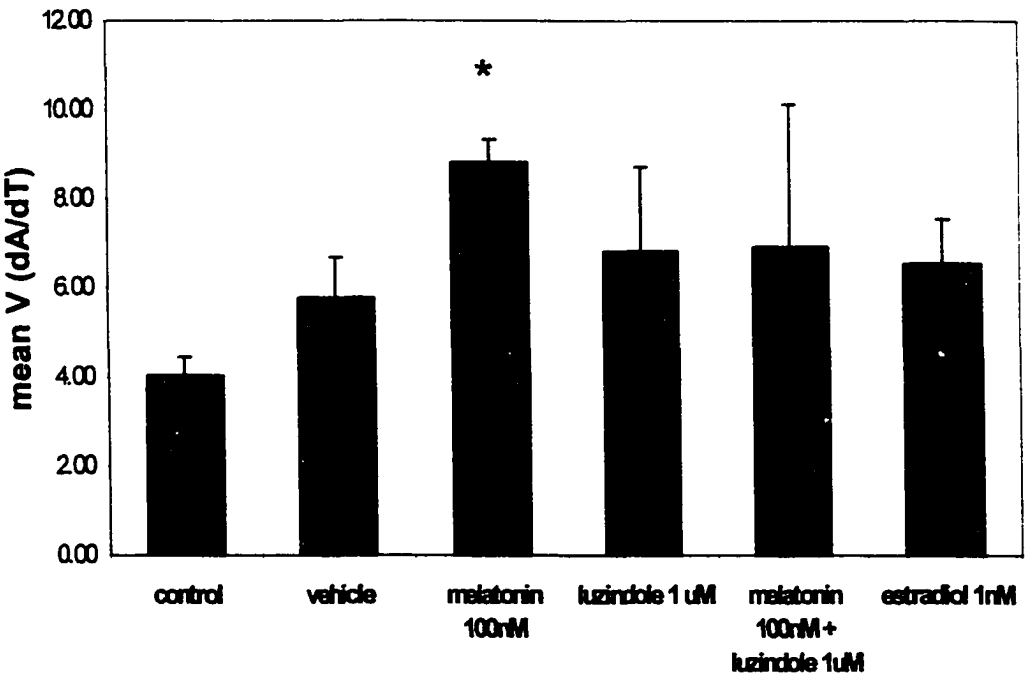

Figure 1. 18. Cytochrome C oxidase activity by microtiter plate method (colorimetric measurement of oxidized DAB) in MCF-7 cells 18 hours after treatment with vehicle, melatonin, luzindole, or 17β-estradiol.

The enzyme reaction rate (mean V/minute) was standardized to cell number. Only 100 nM melatonin was significantly different from control (*P<0.01 by one way ANOVA with Fishers comparison of means test). The addition of 1 uM luzindole to the 100 nM melatonin treatment group returned cytochrome C oxidase activity to control values.

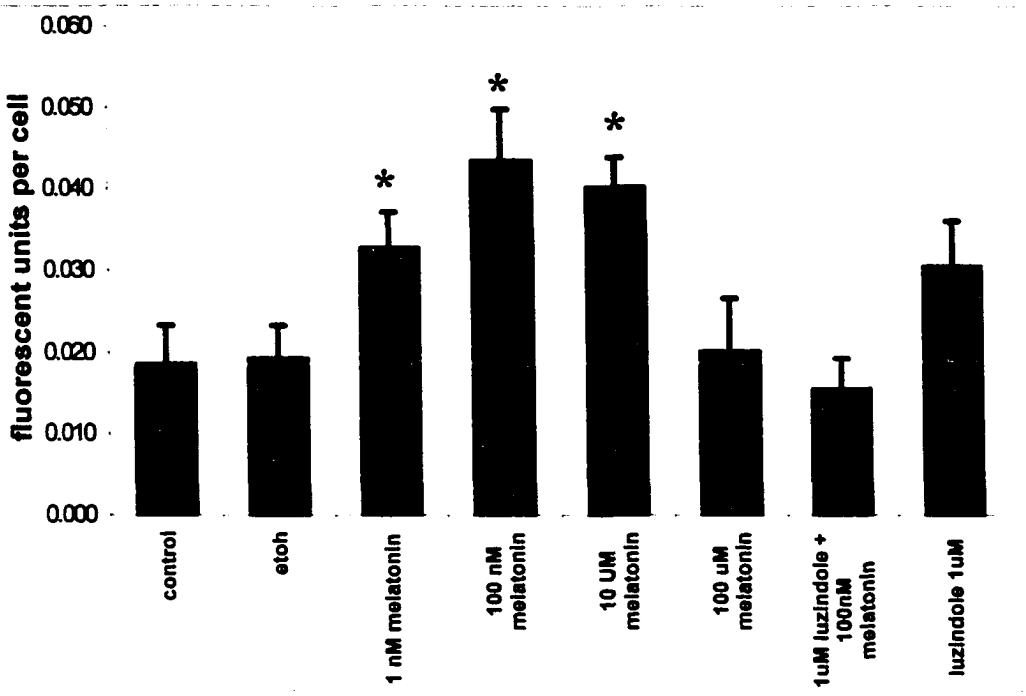

Figure 1. 19. Cytochrome C oxidase activity in MCF-7 cells (reduction of AlamarBlue) at 18 hours after treatment.

Data is reported as fluorescent units of AlamarBlue dye reduction during a four-hour incubation period per million cells. Melatonin treatments of 1 nM, 100 nM, and 10 uM were significantly higher than controls by one way ANOVA and Dunnett's comparison of means to control test. The addition of 1 uM luzindole to the 100 nM melatonin returned the activity of the enzyme to control values.

To rule out the possibility that the observed changes in enzyme activity were the result of direct chemical antioxidant activity, a cell free system containing medium, melatonin, and AlamarBlue dye was incubated and analyzed for fluorescent changes indicative of dye reduction. Melatonin dose response data of concentrations from 10 pM to 10 uM (figure 1.20) demonstrated the absence of dye reduction in the cell free system. This confirmed the melatonin effect as a modulation of cell metabolism and not a direct chemical artifact.

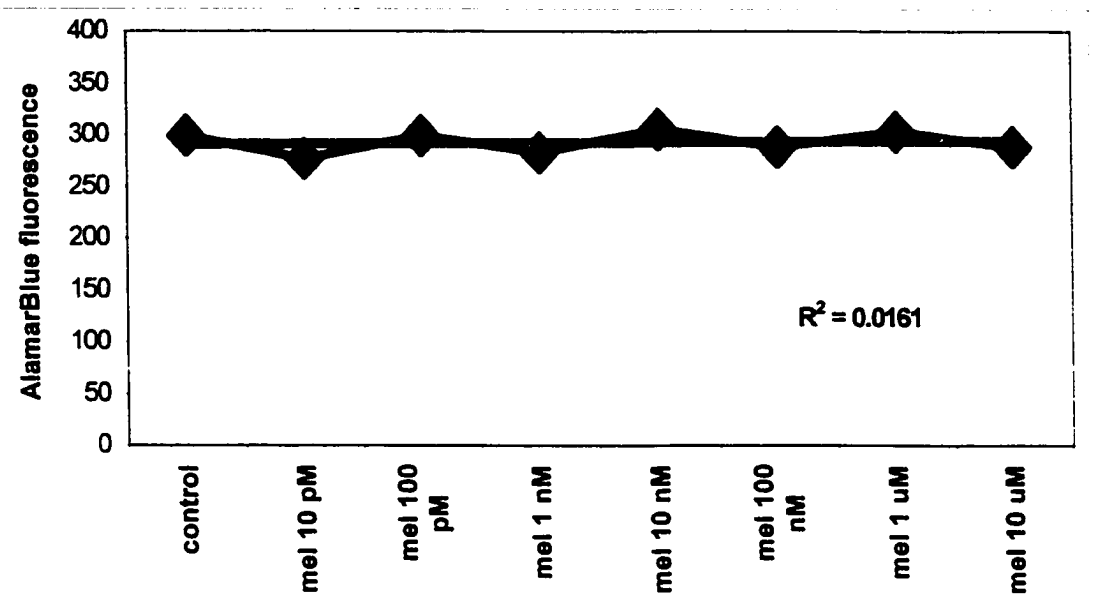

Figure 1. 20. Dose response analysis of melatonin with AlamarBlue dye in cell free culture medium.

To determine if AlamarBlue dye reduction was occurring by direct chemical action of melatonin, medium containing eight concentrations of melatonin was incubated with AlamarBlue dye according to the protocol described in materials and methods for MCF-7 analysis. Regression analysis shows no evidence of direct dye reduction by melatonin ($R^2 = 0.01$).

Mitochondrial bioergetic effects of melatonin on isolated rat liver mitochondria.

Further studies of melatonin induced bioenergetic effects determined whether melatonin would increase the enzymatic activity of isolated rat liver mitochondrial particles. To test this hypothesis, electron transport chain complex I (NADH dehydrogenase) and complex II (succinate dehydrogenase) activity in submitochondrial particles treated 20 minutes with either melatonin or vehicle were analyzed as described in materials and methods. The resulting data from these experiments was transformed to double reciprocal plots and analyzed by slope comparison within the context of linear regression. There was no significant increase in enzyme activity over controls in either

enzyme complex, although the expected Michaelis-Menton saturation kinetic curves were obtained (figures 1.21 and 1.22). This again suggested that the observed effect on oxygen consumption was not the result of a direct melatonin effect on isolated electron transport enzymes, but instead was related to the intact electron transport chain in the estrogen deprived MCF-7 cells.

Melatonin effects on ATP production.

The increase in oxygen consumption and electron transport activity implied that melatonin was either increasing overall cell respiration or was uncoupling oxidative phosphorylation in breast tumor MCF-7 cells. To test the hypothesis that melatonin treatment disassociated electron transport from ATP synthesis, cellular ATP levels were measured by luciferin-luciferase chemiluminescence. As shown in Figure 1.23, the 100 nM melatonin treatment resulted in a significant decrease of MCF-7 cell ATP levels. Thus, melatonin appears to act as an uncoupler of oxidative phosphorylation, and may exert its cytolethality in breast tumor cells via this cellular pathway.

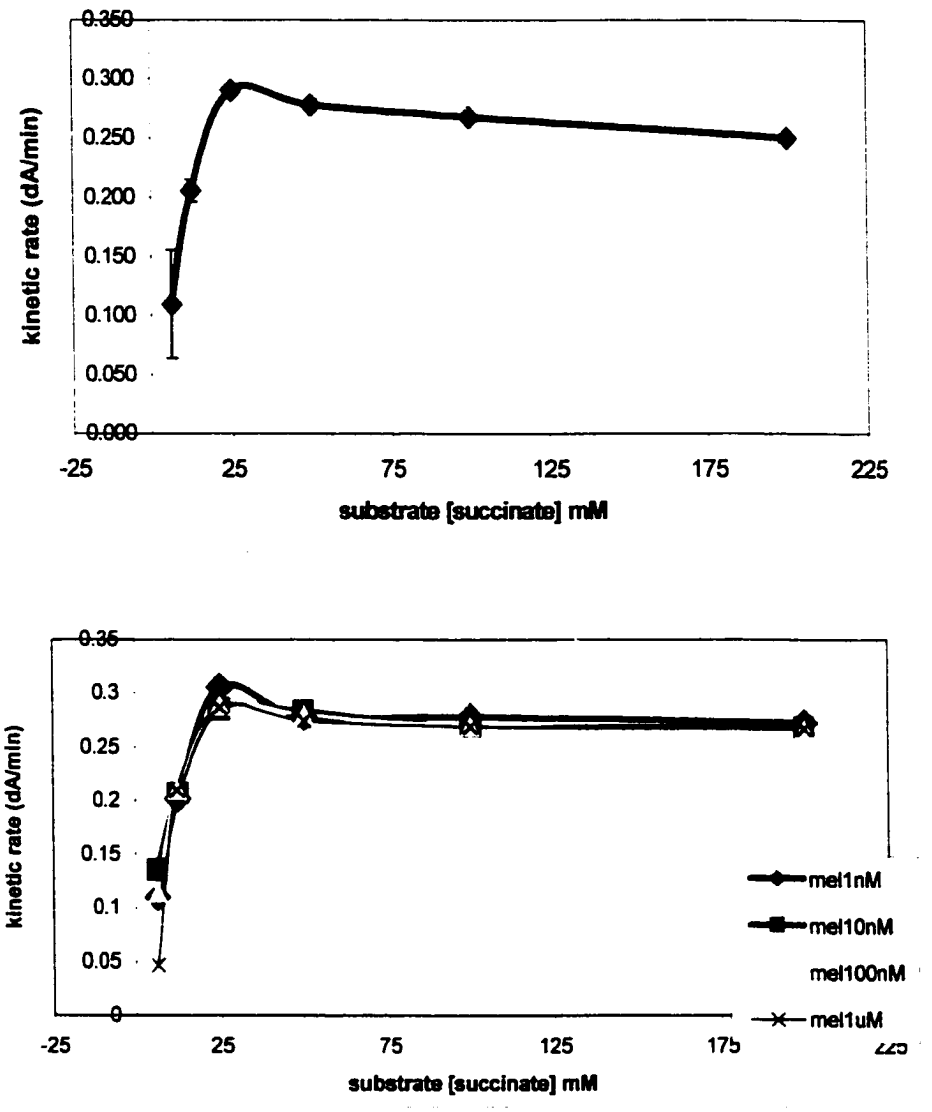

Figure 1. 21. Kinetic rates of mitochondrial electron transport chain complex II determined in isolated rat sub-mitochondrial particles following a thirty minute treatment with melatonin or vehicle.

The upper plot is of control data with succinate as the substrate but without melatonin treatment. Standard error bars represent three replicate experiments. The lower plot is a dose response of four concentrations of melatonin as shown. The saturation kinetic curves superimposed on the control values demonstrated no effect of melatonin treatment.

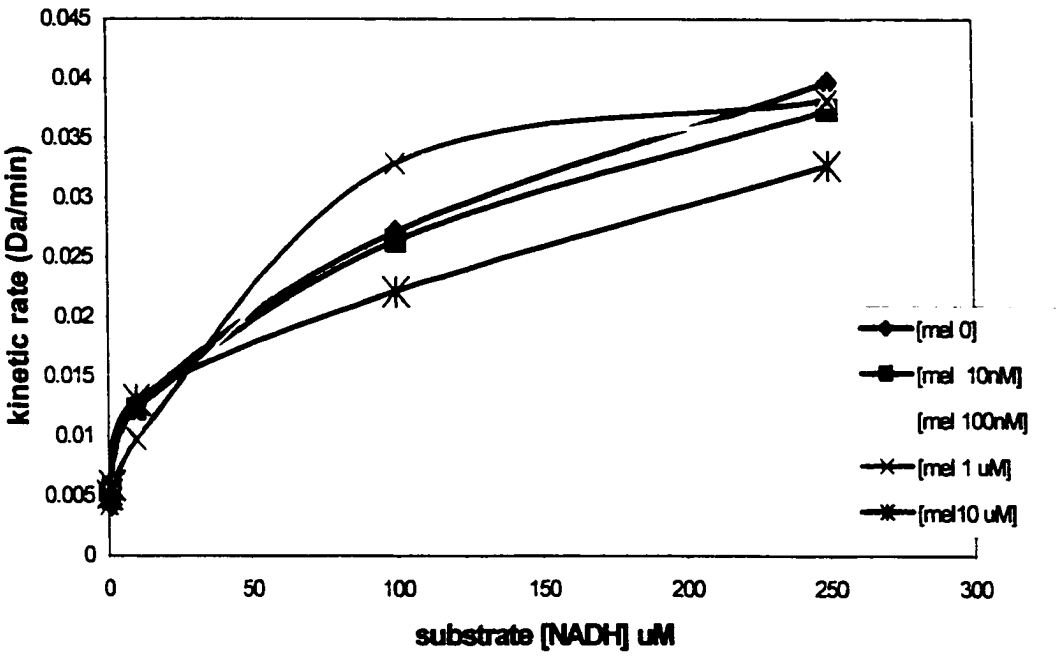

Figure 1. 22. Kinetic rates of mitochondrial electron transport chain complex I

Rates were determined in isolated rat sub-mitochondrial particles following a thirty minute treatment with melatonin or vehicle. There was no significant difference of any melatonin concentrations from control as determined by slope analysis of double reciprocal plots.

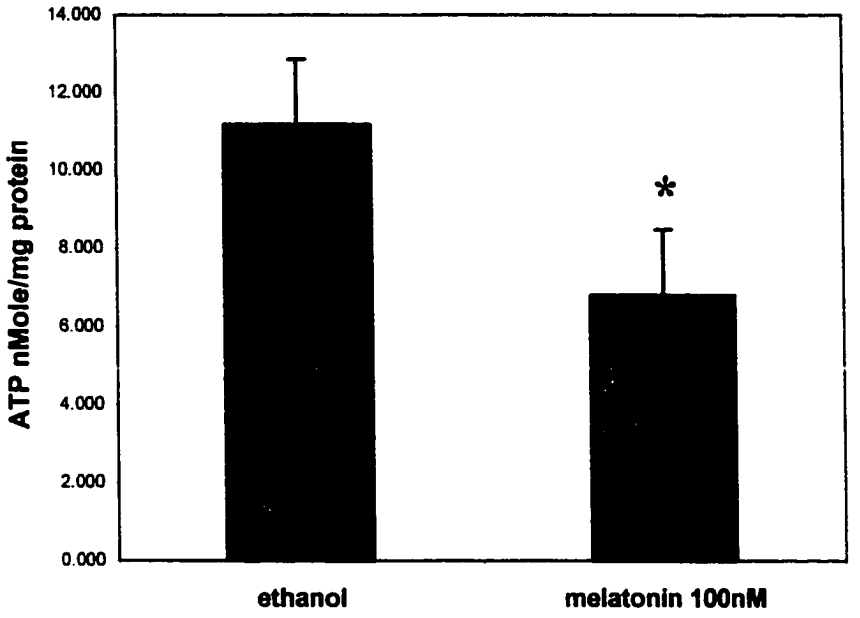

Figure 1. 23. ATP concentration in MCF-7 cells 21 hours after treatment with 100nM melatonin or vehicle (0.00005% ethanol).

ATP was measured by luciferin-luciferase chemiluminescent assay. Crude data (relative light units) were converted to nMole of ATP from a standard curve and reported as nMole of ATP per mg protein. Melatonin treated cells had significantly lower total ATP than vehicle controls ($p<0.05$ by Student's T test)

Correlation of cell number and cytochrome C oxidase activity dose response curves.

The temporal relation of cell death and mitochondrial bioenergetic perturbation was highly suggestive of a causal association. To further examine this association, the hypothesis was posed that disassociation of electron transport from ATP synthesis was intimately linked if not causally related to MCF-7 cell toxicity. It was further postulated that melatonin dose response curves of the two endpoints would be highly correlated if cell death was caused by bioenergetic perturbation. Data from experiments to test this prediction are presented in figures 1.24 and 1.25. Cells were grown in triplicate in 48 well microtiter plates and treated as described in previous experiments. Analysis was done for two endpoints; first, AlamarBlue dye reduction was used as a measure of

mitochondrial respiration following treatment with four concentrations of melatonin. The second endpoint, viable cell number, was measured concurrently by Trypan Blue dye exclusion assay. Figure 1.24 describes a linear regression analysis of cell number and dye fluorescence per cell. The coefficient of determination for the regression is -0.76 with a normal distribution of data, thus indicating that 76% of the cell number change is predictable by mitochondrial activity. Figure 1.25 shows regression analysis of triplicate means for cell number and fluorescence per cell vs. melatonin concentration. The polynomial regression curve fits of mean data (R^2 of 0.93 and 0.96) follow the "U" shaped dose response described by others [16;18] and demonstrate an inverse relationship between cell number and mitochondrial respiration.

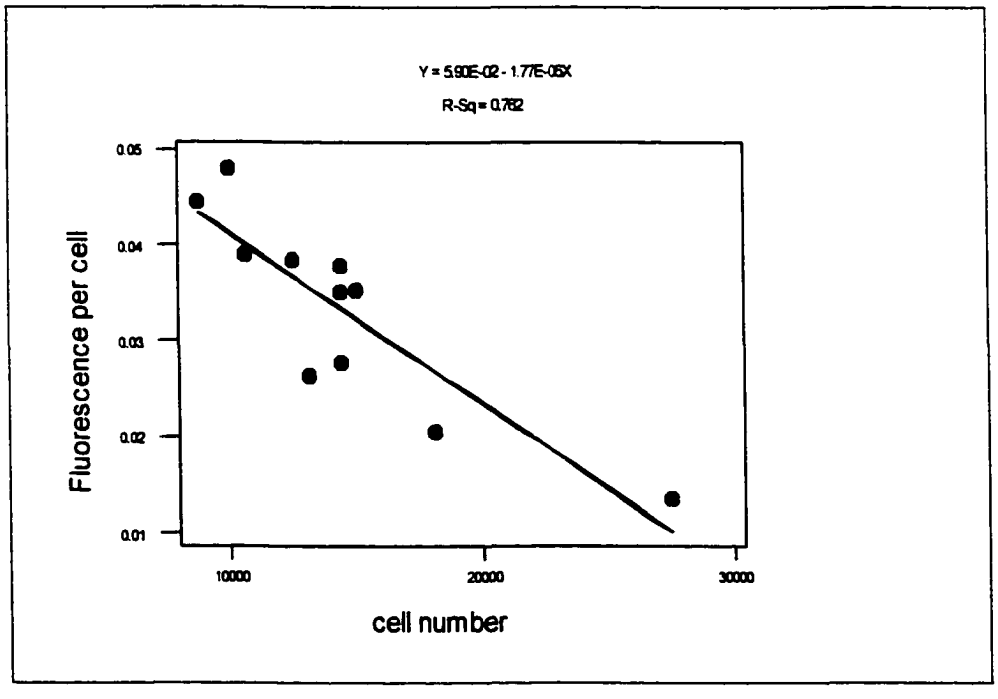

Figure 1. 24 Regression of cell number and AlamarBlue fluorescence.

MCF-7 cells 18 hours after melatonin treatment (doses of 1 nM to 100 uM). Linear regression plot of Alamar Blue fluorescence per cell (cytochrome C oxidase activity) vs. cell number demonstrated a relationship of cytotoxicity (cell number) to activity of Cox at the four dose groups shown in figure 1.25. Triplicate treatments were present at each dose level. (Analysis by Minitab software. $R^2 = -0.76$ with significance of the regression $p<0.01$ and normality of the distribution determined by Anderson -Darling test $p>0.1$)

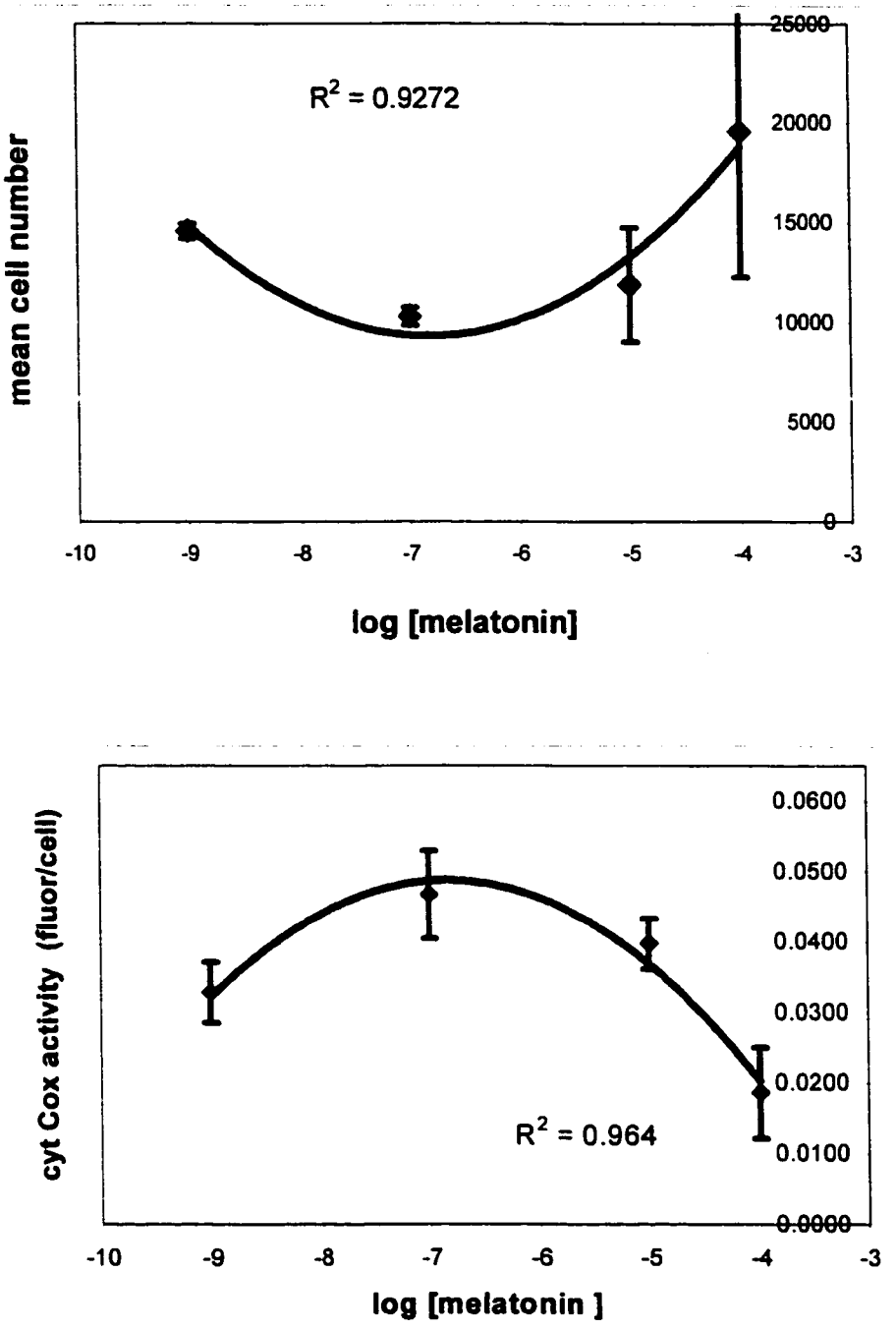

Figure 1. 25. Dose response data from MCF-7 cells 18 hours after treatment with melatonin.

The upper graph indicates cell number as a function of melatonin dose. The lower graph is a plot of cytochrome C oxidase activity (measured by AlamarBlue dye reduction) as a function of melatonin dose. Error bars represent one standard deviation of data points at each dose level. The curves were fitted by polynomial regression analysis of means for triplicate wells. R^2 was equal to 0.927 and 0.964 respectively.

DISCUSSION.

The cells targeted by melatonin in these studies were not rapidly dividing and were killed by physiologic levels of an endogenous hormone

Oncostatic agents can exert a number of cytotoxic effects on cancer cells, including inhibition of cell proliferation as well as acute cell death. Typical chemotherapeutic drugs target aspects of cell biology intrinsic to a more rapidly dividing cell population as their primary mechanism of differential cytotoxicity in tumor cells. Conversely, the acute cytotoxicity described in this series of experiments with MCF-7 human breast carcinoma cells involved cancer cells that were slowly growing and predominantly in G_1-G_0 phase of the cell cycle (figures 1.7 and 1.8). Furthermore, the cytotoxic agent, melatonin, was not a pharmaceutical agent but an endogenous hormone at physiologic concentrations of 10 pM to 100 nM [16;29;43;44].

Does in vitro data from cells grown in E- medium relate to in vivo physiology?

The physiologic doses of melatonin and estrogen used in these experiments are important considerations for *in vivo* implications of the studies. First, cytotoxic melatonin concentrations in the cell cultures were within a range that breast epithelium is naturally exposed (see Chapter 3 of this dissertation). Analysis of clinical gross fibrocystic breast disease patient aspirates demonstrated melatonin concentrations from 0 to 86 nM (table 3.1) compared to the present *in vitro* studies that were performed with concentrations of 0 to 100 nM melatonin.

Secondly, the final concentration of estradiol in the culture medium was estimated to be 0.114 pM from analysis of C-D extracted FBS. The significance of cell culture data from experiments with low estrogen concentration may be appreciated by considering the hormone levels during the menses phase of a normal menstrual cycle and the extremely

low levels found during and after menopause. Figure 1.1 is a graphic representation of the human menstrual cycle demonstrating plasma estradiol levels ranging through different phases of the cycle from low picomolar to 0.5 nanomolar concentration. Although, breast epithelial cell exposure to estrogen has not been measured *in situ*, clinical evidence suggests that it follows a cyclic pattern related to plasma levels. For instance, estrogen responsive proliferative changes (ductal cell mitosis) of breast development result with successive menstrual cycles but are inhibited by the anti-estrogen, tamoxifen [45]. Additionally, the swelling and pain associated with clinical conditions such as cyclic mastalgia are closely related to menstrual estrogen cycling [8;45]. Hence, it is apparent that *in situ* estrogen exposure of breast epithelial cells is either similar to plasma estrogen levels or at least fluctuates with a comparable pattern.

In addition to the monthly cycles of estrogen that breast epithelial cells are exposed, human melatonin levels follow a diurnal rhythm [8;45]. It is therefore probable that breast cells are exposed to low estrogen levels concurrent with melatonin peaks every 24 hours for approximately one week per month during the premenopausal years and more frequently during and after menopause.

Cell death was obvious in the proliferation and tritiated thymidine studies...

Acute toxicity of MCF-7 cells *in vitro* was apparent in low estrogen culture conditions combined with 16 -20 hour melatonin treatments. Figure 1.4 depicts a dose responsive decline in cell number to less than 40% of controls following melatonin treatment. This decrease in cell number was necessarily due to either lethal cytotoxicity or to decreased proliferation compared to control cultures. Since no change was observed in DNA synthesis, defined by tritiated thymidine uptake (figure 1.6), and cell cycle

parameters by flow cytometry (figure 1.7) were unchanged, the loss of cells was postulated to be the result of cell death.

Comet assays did not indicate evidence of apoptosis...

The type of cell death was suspected to be an acute necrotic process rather than apoptosis. Compared to the rapid swelling and dissolution of the cytoplasmic membrane in necrotic cell death, programmed cell death is an orderly and sequential destruction of the cell with cascading events resulting in enzymatic cleavage of proteins and DNA [46]. A hallmark of apoptotic cell death is the inter-nucleosomal fragmenting of DNA with characteristic 180-200 base-pair fragments of DNA [46]. Such cleavage patterns produce small segments of DNA that move rapidly through the agarose gel of the Comet assay and result in an elongated area (comet) when stained and imaged. Figures 1.9 and 1.10 describe the results of Comet assays performed on the MCF-7 cells after an 18 hour melatonin treatment. The tail moment (measure of DNA movement and staining intensity) was minimally different between treated and control cells as would be expected in absence of apoptotic fragmentation. On the other hand, the statistical mode of the DNA content parameter was nearly twice as high in the controls as the melatonin treated cells; a difference not evident on flow cytometry (figure 1.7).

There are two possible explanations for the lack of agreement between the two data sets. First, the Comet assay was calculated from 300 - 400 events per sample, while the flow cytometer measured 30,000 events. The potential for error is considerably higher with smaller sample sizes, however, the magnitude of difference in the Comet data (two-fold) was quite large. A second possibility to explain the lower mode of DNA content is that cells with degenerating plasma membranes but without apoptotic DNA

fragmentation would likely be destroyed by vortexing and alcohol fixation for flow cytometry analysis. In contrast, cell nuclei with large base pair fragmenting fixed in gel for the Comet analysis would be expected to stain and appear on the imaging system as cells with lower DNA content. Thus, the findings of both sets of experiments were compatible and indicated a process of necrotic cell death.

Dual staining with ethidium bromide and acridine orange did not show evidence of apoptosis...

Further examination of dual stained cell cultures by fluorescent microscopy was undertaken to visualize cells undergoing programmed cell death. The cytoplasmic membrane of viable cells is impermeable to ethidium bromide (EB) stain while acridine orange (AO) enters by active transport and stains the DNA. AO staining of early apoptotic stages allows visualization of apoptotic bodies as bright yellow-green areas compared to the uniform green staining of intact DNA. Cells with non-viable membranes allow entry of EB and stain bright orange in excitation wavelengths of 500 to 600 nm.

MCF-7 cells treated 16 hours with melatonin did not show visual evidence of apoptosis but did show a subjective increase in the number of EB stained dead cells and an overall more intensly yellow fluorescence of the DNA (figure 1.11). These subjective observations suggested that melatonin cytotoxicity was present, although large numbers of non-viable cells did not remain in the monolayer. This finding agreed with histology and electron microscopy data (figures 1.13 and 1.14) that suggested that both rapid degeneration (cell debris) and autophagocytosis of the dead cell bodies were present.

Flow cytometry didn't show apoptotic changes...

Further evidence for a pathway other than apoptosis was provided by the lack of sub G_1 or sub G_2 peaks on flow cytometric analysis. Apoptotic populations of cells typically

demonstrate decreased brightness (lower channel) of DNA staining thought to be the result of early DNA fragmentation [47]. The lessened intensity of nuclear stain shifts the peak (G_1 or G_2) to the left, appearing as a sub G_1 or sub G_2 area. This classical change was not apparent in the MCF-7 cells (figure 1.7); however, an undefined sub G_1 irregularity was present in the melatonin treated group but only in smaller sized cells (figure 1.8D). The smaller sized cells (figure 1.8A) were more numerous in the control than treatment groups but were substantially less prevalent in all cells by 18 hours. This apparent size change suggested cytotoxicity from melatonin and/or metamorphosis from metabolically inactive G_0 cells to active G_1 cells growth stimulated by the fresh medium. It is unlikely that the small cells represented a sub-population of the MCF-7 line as suggested by their slightly but consistently lower DNA content compared to the larger cells. (i.e. The modes of smaller populations were at channels 64 and 67 for treatment and control, while the larger cells were at 70 and 71 respectively.) If this were the case, a sub-population would be equally represented at 9 hours and 18 hours in control cells even if not in treated ones. A more probable explanation is that the small cells represented inactive G_1-G_0 cells appearing to have lower DNA content due to lesser staining of tightly packed heterochromatin. Hence, MCF-7 cell cycle characterization indicated that the cells were highly synchronized in G_1-G_0 (figure 1.7), and suggested that cytotoxicity was concurrent with increased metabolic demand on small (inactive G_0) cells moving to a larger size (active G_1).

Evidence of cytotoxic morphologic changes was visible on light and electron micrographs.

Acute cytotoxicity in the form of necrotic cell death was confirmed by light and electron microscopy. Figure 1.13 displays one of many pale staining "ghost" like bodies

in the melatonin treated cells. In addition to these obviously degenerating cell bodies, a number of inclusion bodies were present within the cytoplasm of otherwise normal cells. A 15,000 x transmission electron micrograph (figure 1.14) of the inclusion body in figure 1.13, identified it as a phagocytized cell in advanced stages of degeneration. The results of these experiments, therefore, demonstrated that melatonin treatment of the MCF-7 carcinoma cells resulted in acute necrotic cell death accompanied by autophagocytosis.

A further finding of the electron microscopy experiment was morphologic alterations of mitochondrial ultrastructure in the melatonin treated cells. Figure 1.15 shows an MCF-7 cell 18 hours after melatonin treatment displaying effects ranging from near normal organelles to swollen cristae, degenerate cristae, and dissolution of outer mitochondrial membrane. Similar ultrastructural changes were previously described in melatonin treated MCF-7 cells grown in medium that was not C-D extracted of estrogen and furthermore, were associated with changes suggestive of cellular differentiation as well as cell death [16]. Thus, negative effects of melatonin on mitochondria appear to be associated with morphologic changes in malignant phenotype and to MCF-7 cell death.

Cellular bioenergetic respiration has been established as a point of differential growth control between normal and tumor cells...

Over the last three decades, it has become increasingly clear that cancer is a disease programmed by genetic errors, although the controlling mechanisms that select for survival of the genetic errors are not clearly defined. Surprisingly, tumor cell bioenergetic pathways were suggested nearly three-quarters of a century ago to be differentially selective in tumor progression [48]. Biochemical studies by Warburg et al. [48] demonstrated that cancer cells, in general, display an increased utilization of glycolytic metabolism as a source of ATP. Such means of anaerobic energy production

is an obvious survival advantage for rapid, unregulated growth spatially removed from the vascular system's immunologic and physiologic control. An additional growth advantage comes from a cytoplasmic redox status that is highly reduced from the increased NADH levels of glycolytic glucose utilization [49].

The mitochondrion appears to be an important point of neoplastic growth control...

Although anaerobic metabolism is well established as a primary means of tumor cell energy production, recent evidence strongly implicates the mitochondrion as an important regulatory control point [17;26;50-52]. First, apoptotic triggers such as cytochrome C release and Bcl-2/Bax ratios indicate a mitochondrial role in programmed cell death [53]. Additional evidence of mitochondrial involvement in tumor growth was demonstrated in MCF-7 cells depleted of mitochondria by repeated ethidium bromide passage [17]. The cells displayed a more differentiated phenotype defined both by morphology and by loss of anchorage independent growth, but replacement of mitochondria returned the cells to their original malignant phenotype. The phenotypic changes, therefore, appeared to be the result of bioenergetic disruption rather than direct effects of EB, and suggested the mitochondrion as a necessary part of MCF-7 cancer cell growth [17]. Finally, cancer cells typically have fewer mitochondria, but their individual electron transport activity (e.g. membrane potential) is higher than that of non-transformed cells and may be integral to their malignant phenotype [54-58]. Thus, the dogma that cancer growth is independent of aerobic metabolism is being replaced with an understanding that tumor cells dependent on anaerobic respiration remain reliant on mitochondrial ATP for normal function and maintenance of malignant characteristics.

Anaerobic tumor metabolism utilizes mitochondrially produced ATP to "prime" glycolysis...

The dependence of tumor cell phenotype on aerobic respiration, even though the bulk of ATP production comes from glycolysis, emphasizes an intriguing relationship of the two pathways. For example, increased activity and transcription of hexokinase II (HKII) is a common phenotype in a wide variety of tumor cell types [59-65][review[66]], and suggests a common mechanism for the entry of glucose into the glycolytic pathway. In addition to increased transcription and enzyme activity, the HKII binding affinity of glucose was increased as much as 100-fold in a hepatoma cell model compared to normal liver [59]. These factors, in combination with evidence of a reduced feedback inhibition to glucose-6-phosphate [59], indicate that abnormal response of HKII is common if not a prerequisite for successful tumor growth.

Mitochondrial involvement in tumor glycolysis is also suggested by the findings suggesting that 70% of HKII be bound to mitochondrial porins while normal cell mitochondria have virtually none bound [67]. Furthermore, there is a considerable amount of data to define HKII porin binding as a regulatory mechanism of anabolic metabolism (for example, insulin) [51]. This mechanism, known as the insulin acceptor theory [68], defines insulin mediated HKII binding to mitochondrial porin as a mechanism providing the enzyme ready access to mitochondrial ATP, and additionally, a more efficient means of glucose phosphorylation for glycolysis.

In spite of the obvious tumor survival advantages, anaerobic metabolism would be inefficient if phosphorylation of glucose depended on low cytosolic concentrations of ATP and random diffusion for enzyme binding and phosphorylation. On the other hand, the utilization of aerobically produced ATP to prime the glycolytic cascade by a

strategically located HKII with high glucose binding affinity allows virtually uncontrolled production of glucose-6-phosphate [51]. Thus, a common pathway of cancer cell selective advantage appears to copy a mechanism similar to insulin-dependent anabolic metabolism and likewise, requires mitochondrial contributions to glycolytic energy production.

Increased oxygen consumption was present in melatonin treated cells suggesting increased respiration or uncoupling of oxidative phosphorylation...

Perturbations of aerobic respiration were temporally associated with the death of melatonin exposed MCF-7 cells in C-D extracted medium. Figure 1.16 demonstrates a dose responsive increase of oxygen consumption in treated vs. control cells, with both the 100 nM melatonin dose and the 1nM estradiol significantly higher ($p<0.05$) than vehicle control when standardized to cell number. Interestingly, the magnitude of oxygen consumption rate increase in estrogen treated cells was similar to that of DNA synthesis seen in figure 1.6, however, the melatonin treatment resulted in no change in tritiated thymidine uptake. Hence, a valid argument can be made that estrogen, but not melatonin stimulated increased oxidative phosphorylation to provide ATP for DNA synthesis and cell cycle advancement.

Uncoupling of oxidative phosphorylation (ox-phos) must have been present...

Evidence of increased basal respiratory rate in the melatonin treated cells was further indicated by experiments measuring activity of electron transport chain complexes. Significantly greater activity of succinate dehydrogenase in MCF-7 cells following melatonin treatment was evident in the MTT assays described in figure 1.17. Further melatonin studies described a significantly elevated Cox activity over controls (figure 1.18) by a microtiter plate assay that measured the ability of complex IV to accept

electrons from cytochrome C. In addition to the microtiter plate assay data for Cox, figure 1.19 demonstrates data from the AlamarBlue dye assay, which also measured activity of complex IV. If the oxygen consumption and mitochondrial complex activity were resulting from increased metabolic activity of the cell, increased DNA synthesis would have been expected as was seen with tritiated thymidine uptake following estrogen treatment (figure 1.6). Together, the combined mitochondrial respiration data and tritiated thymidine data strongly suggested that uncoupling of oxidative phosphorylation was present.

Confirmation of mitochondrial ox-phos uncoupling was evident from the data presented in figure 1.23. In this experiment, cytoplasmic ATP concentration determined by chemiluminescent luciferin-luciferase analysis was significantly reduced to 61% of controls following melatonin treatment ($p<0.05$). Thus, the combination of increased electron transport and a 39% decrease of ATP production further implicated the effect of melatonin as one uncoupling oxidative phosphorylation.

Uncoupling of oxidative phosphorylation produces toxicity through at least three separate mechanisms. The first result of toxicity is a decrease in the chemiosmotic electrical gradient ($\Delta\psi$) that drives not only ATP production, but also the import/export mechanisms of the mitochondria. Disruption of $\Delta\psi$ inhibits the ability of the mitochondrion to exchange ADP/ATP, shuttle structural and apoproteins, amino acids, and to regulate osmolarity [49]. Mitochondrial swelling and disruption of cristae ultrastructure would be the expected morphologic result from this target of toxicity [1]. The second mechanism is the disposition of energy that otherwise would have been utilized by proton pumping. Uncoupled electrons release energy as heat (e.g. brown fat

metabolism) or as reactive oxygen species (ROS) such as superoxide anion radical [1]. Cellular toxicity resulting from damage at this target would affect membrane components of organelles and the cell membrane [1]. Finally, phosphorylation of glucose would be a sensitive target in cells utilizing mitochondrial respiration to provide ATP to porin associated hexokinase II as described above. Such a target would be quickly lethal to energy dependent vital functions such as ion transport, DNA synthesis, and fibrilar infrastructure of the cell.

The melatonin effects on respiration and cell death were receptor mediated...

Melatonin effects on cell biology are mediated at least in part through G-protein coupled surface receptors with both high (mel-1) and low (mel-2) affinity binding [19;20]. The melatonin receptor antagonist, luzindole, (2-benzyl-N-acetyltryptamine) competitively inhibits melatonin binding with greatest affinity to mel-1 (e.g. rabbit retina K_d = 20 nM) [19;69].

The addition of luzindole to the 100 nM melatonin treatment returned cell number to control values (figure 1.4). Similar to luzindole's effect on cell number, antagonism of melatonin surface receptor inhibited the mitochondrial respiratory rate increase (oxygen consumption in figure 1.16, succinate dehydrogenase in figure 1.17, cytochrome C oxidase in figure 1.18, and AlamarBlue in figure 1.19). Although the possibility remained that melatonin's effect was due to direct anti-oxidant activity, it seemed unlikely from the data. First, the melatonin responses in all cases were eliminated by luzindole (figures 1.4, 1.16, 1.17, 1.18, and 1.19). Secondly, the melatonin respiratory effect was not present in isolated mitochondrial particles (figures 1.21 and 1.22), and finally, it was not present in cell free medium containing AlamarBlue (figure 1.20).

Thus, the combined data from experiments with the melatonin competitive antagonist, luzindole, indicated that a receptor-mediated pathway was responsible for the cytotoxic effects described in this report.

The melatonin effect on cytochrome C oxidase was present within 30 minutes...

Cytochrome C oxidase activity was increased as early as 30 minutes following melatonin treatment (figure 1.26). Rapid up-regulation of estrogen early responsive genes (e.g. c-*myc* and c-*fos*) has been previously described following melatonin treatment of MCF-7 cells [11]. Although inhibition of these metabolism-stimulating genes could modulate mitochondrial respiratory rate, the uncoupling of electron transport from ATP synthesis shown in figures 1.16, 1.17, 1.18, 1.19, and 1.23 would not be an expected result. It was therefore likely that melatonin either uncoupled ox-phos via an early transcribed gene unrelated to estrogen, or directly affected the electron transport chain.

Interestingly, others have suggested that melatonin was associated with increased levels of the mitochondrial uncoupling protein, thermogenin (review [15]). A melatonin induced un-coupling protein with effects similar to thermogenin would be postulated to be inhibited by the receptor antagonist, luzindole, and return electron transport activity to the level of controls as shown in figures 1.17, 1.18, 1.19. If this hypothesis were true, an early gene that modulates bioenergetic activity in the mitochondria would be transcribed at the same time as c-*myc* and c-*fos*.

A second mechanism through which melatonin could disrupt electron transport is the direct shuttling of electrons bypassing the proton pumping subunit of cytochrome C oxidase. Papas et al. proposed that the normal mitochondrion allowed "slips" of electrons through cytochrome C oxidase to alleviate an electron back-pressure in states

when cellular respiration outpaced ATP production [70]. This metabolic state would be expected in MCF-7 cells following the induction of c-*myc* by melatonin in low estrogen medium. The mechanistic model that Papas proposed involved electron movement directly to the CuB moiety of complex IV bypassing the proton pumping of sub-unit II. If melatonin localized in the lipid of the mitochondrial inner membrane were able to accept and release an electron down an energetically favorable pathway within cytochrome C oxidase, it could function to augment the electron "slips" proposed by Papas. Its inhibition by luzindole could be explained if the "slips" produced by melatonin were only present when respiratory enzymes such as those upregulated by a receptor mediate c-*myc* pathway were increased by melatonin treatment.

Since MCF-7 cell death and bioenergetic disruption was not present when luzindole was included in the treatment, it must be concluded that a receptor-mediated pathway was involved in the cytotoxicity observed. However, the second postulate above suggests that effects on the cancer cells could result from a combination of direct and receptor mediated functions of the hormone. Thus, while MCF-7 cancer cells were killed by melatonin in association with bioenergetic disruption of electron transport, further research is necessary to fully define the molecular targets and pathways.

Cells grown in estrogen containing FBS or co-exposed to estrogen were rescued from melatonin cytotoxicity...

Others have shown that a major mechanism of melatonin oncostatic effects on MCF-7 cells is mediated through the estrogen response pathway through as yet undefined mechanisms [review [4-6]]. Transcriptional down-regulation of the estrogen receptor is a likely candidate for one mechanism with effects evident within 12 hours [71]. The significance of estrogen receptor down-regulation, however, is questionable in the

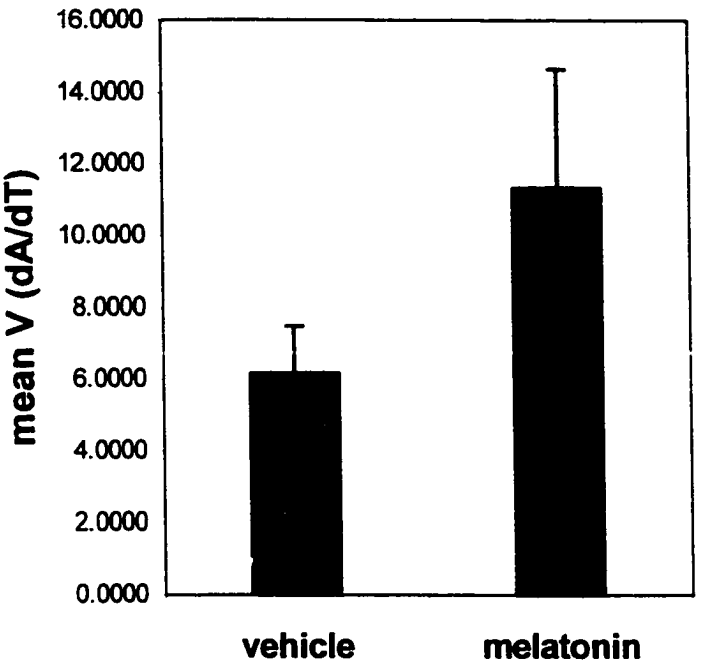

Figure 1. 26 Cytochrome C oxidase activity by microtiter plate method

Colorimetric measurement of oxidized DAB in MCF-7 cells incubated for 30 minutes after treatment with vehicle (0.00005%) or 100 nM melatonin was used to determine the rate of cytochrome C oxidase activity. The enzymatic rate of DAB oxidation (Mean V/minute) was standardized to cell number. Melatonin (100 nM) was different from control with P=0.067 by Student's two tailed T test and p=0.03 by one tailed Student's T test.

current studies since the medium was depleted of nearly all estrogen. Moreover, melatonin proliferation studies using estrogen-containing medium showed little effect of melatonin on growth rate until 4 to 7 days of culture, and suggested late as well as early effects of the hormone [16;71]. Thus, the early MCF-7 cell cytotoxicity from melatonin suggested that interaction with an estrogen pathway may be involved but without the direct influence of estrogen. For example, cell death was eliminated by FBS complete culture medium (figure 1.5) or by the addition of 1 nM estrogen to the C-D extracted medium (electron microscopy data not shown). It was therefore probable that estrogen

modulated the expression of factors that rescued MCF-7 cells from melatonin induced death.

Two interactions of melatonin and an estrogen pathway...

Two interactions of melatonin and an estrogen pathway were likely in the MCF-7 carcinoma cells. First, melatonin up-regulation of estrogen early response oncogenes (c-*myc*, c-*fos*, and *tnf*-α) [11] has been previously shown to induce tumor cell glycolytic enzymes and cell division kinases [72]. The increased glycolitic metabolism and cell cycle advancement would be expected to increase utilization of ATP as well as increase mitochondrial respiration. Uncoupling of oxidative phosphorylation however, would prevent adequate synthesis of ATP and result in cell death.

On the other hand, estrogen rescue from cytotoxicity could result from induction of cytochrome C oxidase proteins. Previous studies describe the regulation of mitochondrial protein transcription by steroid hormone trans-activation [73-75]. Specifically, one direct estrogen effect is the transactivation of mitochondrially encoded cytochrome C oxidase (Cox), subunit proteins which are involved in proton pumping through complex IV [49;76]. For example, Cox subunit II protein was increased as much as 16 fold in pituitary GH_4C_1 cells by the presence of 1 nM estradiol [76]. Thus, dramatic variations in Cox subunit II protein would not be a surprising finding associated with estrogen cyclic variations during the menstrual cycle as well as during menopausal fluctuation and decline of ovarian estrogen. Since cytochrome C oxidase is the final member of the electron transport chain [77], and a key regulatory point [49;77;78], up or down regulation of subunit genes would quickly regulate the flow of electrons through the chain.

Furthermore, cytochrome C oxidase activity is increased by ADP and results in increased $\Delta\Psi$ to drive synthesis of ATP [60]. The practicality of dual regulation by estrogen and ATP is two-fold. First, elevated protein levels of Cox during estrogen induced growth would accommodate energy demand by proliferating or secreting breast tissue. Secondly, a more sensitive means of regulation would be possible during dynamic fluctuations of metabolism associated with lowered ATP levels. Hence, transcription of Cox proteins suggests a regulatory point responsive to estrogen controlled growth genes in the aerobic pathway of ATP production, and may be a critical point for melatonin modulation in estrogen deprived MCF-7 cells.

If estrogen early response growth genes were turned on without estrogen induced Cox transcription, would production of ATP be out of balance with ATP consumption?

The mitochondrial bioenergetic disruption and the accompanying cell death described in this report would be a probable outcome of three concurrent cellular events. First, breast tumor cells with decreased Cox levels in the absence of estrogen would have limited electron transport activity to synthesize ATP. Secondly, uncoupling of oxidative phosphorylation would increase the activity of electron transport without increasing ATP synthesis. Finally, increased glycolytic activity would provide higher levels of reduced NADH substrate for electron transport as well as demand increased amounts of ATP for the phosphorylation of glucose-6-phosphate.

There is evidence that this type of estrogen/melatonin gene regulation controls mitochondrial and glycolytic bioenergetic pathways...

Bioenergetic disturbance in the absence of estrogen with uncoupling of oxidative phosphorylation has been demonstrated in the present data. Additionally, stimulation of glycolysis by melatonin is highly suggested by the work of others. Yokayama et al.

reported and validated an analytic method for quantification of melatonin by its dose responsive effect on intra-cellular pH (a surrogate measure of lactic acid production) [79]. A second suggestion of increased glycolysis by melatonin is the regulatory control of glycolysis by estrogen response genes. Molis et al. reported the up-regulation of c-*myc*, *tnf*-α, and c-*fos* following exposure of MCF-7 cells to melatonin [14]. These genes are known as "early response" growth stimulating genes and are commonly associated with estrogen mediated growth [80]. Estrogenic cell proliferation, however, is only seen with prolonged exposure to estrogen (>16 hours) suggesting that cell growth and division is further mediated by a secondary wave of nuclear transcription factors [80].

Although pathways of the putative second wave of transcription factors have not been elucidated, many of these may be key regulatory enzymes of glycolysis. For instance, recent studies have shown that the commonly amplified oncogene, c-*myc*, up-regulates the transcription of LDH-A isozyme [72;81]. The growth advantage for the cancer cell is two-fold. First, re-oxidation of NADH to NAD+ decreases NADH inhibition of the glycolytic pathway, and allows continued anaerobic energy production [review [49]]. Secondly, it has been suggested that c-Myc/Max may play a regulatory role in the transcription of a number of glycolytic enzymes (GPI, G3PDH, enolase, pyruvate kinase as well as HK and GK) [72]. Some, if not all of these enzymes act to control cell cycle advancement as well as regulate energy metabolism. For example, pyruvate kinase has been identified as a cell division control kinase (cdk19) as well as being a key regulatory protein of glycolysis[72]. Interestingly, the c-Myc/Max consensus binding sequence (CACGTG - E box) is identical to the carbohydrate response element in

the promoter region of glycolytic regulatory enzymes [72], and again suggests an intimate role of c-*myc* in bioenergetic control through glycolysis regulation.

Finally, an increase in MCF-7 cell glycolytic activity would elevate cytoplasmic NADH concentration and predict elevated spectrophotometric absorption at 340 nm. Such an increase was suggested in figure 1.27 with a 127% increase in the 340 nm O.D. of melatonin treated cytoplasmic extract compared to untreated vehicle controls ($p<0.1$). At the same time, ATP concentration was only 61% of the control value. Thus, it was likely that melatonin treatment of MCF-7 cells in estrogen deplete medium stimulated an increase in glycolytic activity in conjunction with oxidative phosporylation uncoupling that would agree with the data presented herein.

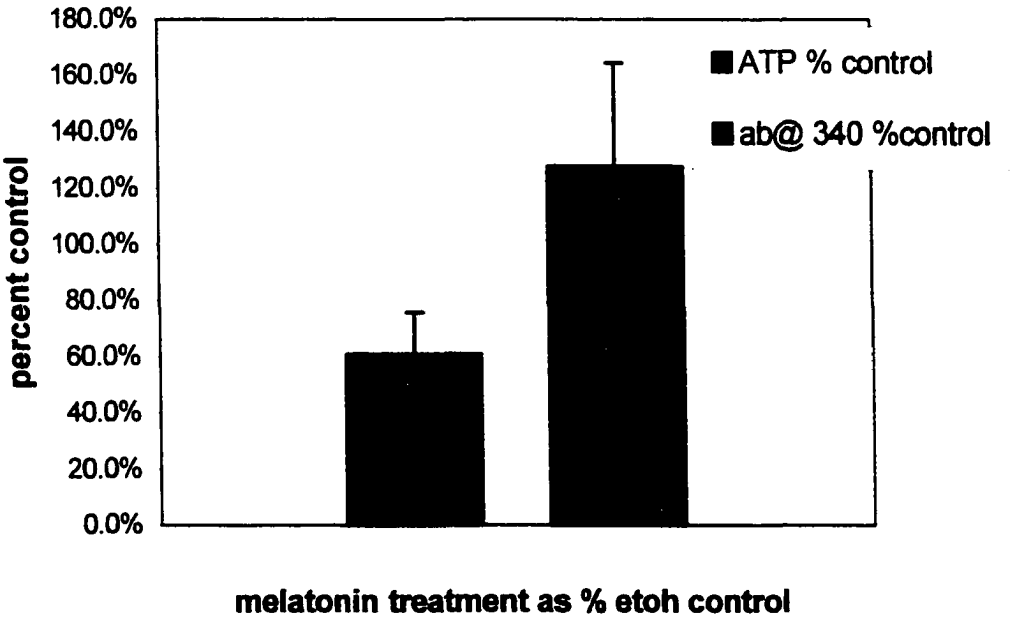

Figure 1. 27. Cytoplasmic extracts of MCF-7 cells treated with 100 nM melatonin for 20 hours.

ATP concentration analyzed by luciferin-luciferase assay was 61% of vehicle control cells ($p < 0.05$). 340 nm spectrophotometric O.D. of sample aliquots was 127% of controls but was not significantly different at the 95% level of confidence ($p<0.1$). Measurements were standardized to protein with the BCA protein analysis kit and represent triplicate samples.

CONCLUSION.

The data presented in Chapter 1 of this dissertation demonstrated the following:

1) The hormone melatonin in physiologic concentrations exerted a cytotoxic effect on cultured MCF-7 human breast carcinoma cells.
2) Moreover, the experimental results defined and described bioenergetic dysregulation of cells following melatonin treatment as an increase of electron transport chain oxidative activity and a concurrent decrease in cellular ATP levels.
3) Further studies demonstrated that these effects were abolished by the melatonin G-protein coupled receptor antagonist, luzindole.
4) Finally, the temporal and dose responsive relationship of cell death and mitochondrial dysfunction strongly suggested that a novel oncostatic mechanism targeting mitochondrial respiration was responsible for the cytolethality shown in this breast cancer cell model.

Thus, given these intriguing findings, I postulate (see Figure 1.28) that melatonin stimulated early up-regulation of glycolytic regulatory proteins and Cdc kinases through the induction of c-*myc* (as shown by others) and possibly other early transcribed genes [72]. I further hypothesize that growth in charcoal dextran extracted medium resulted in low levels of estrogen-dependent subunit proteins (as reported in other estrogen responsive cell types [76]) and a resulting limitation of electron passage through Cox. Uncoupling of oxidative phosphorylation by melatonin then bypassed the Cox blockade and increased the movement of electrons through the complex while inhibiting the

amount of ATP available to the cell (as suggested by the present data). Concurrently, growth genes (such as c-*myc*, c-*fos*, c-*jun*) induced by melatonin [11] drove the cell energy demand via unregulated glycolytic pathways [82], thus depleting an already compromised mitochondrial source of ATP. Finally, ATP requirements were not met, and the lack of energy triggered acute cell death (as demonstrated by the present data).

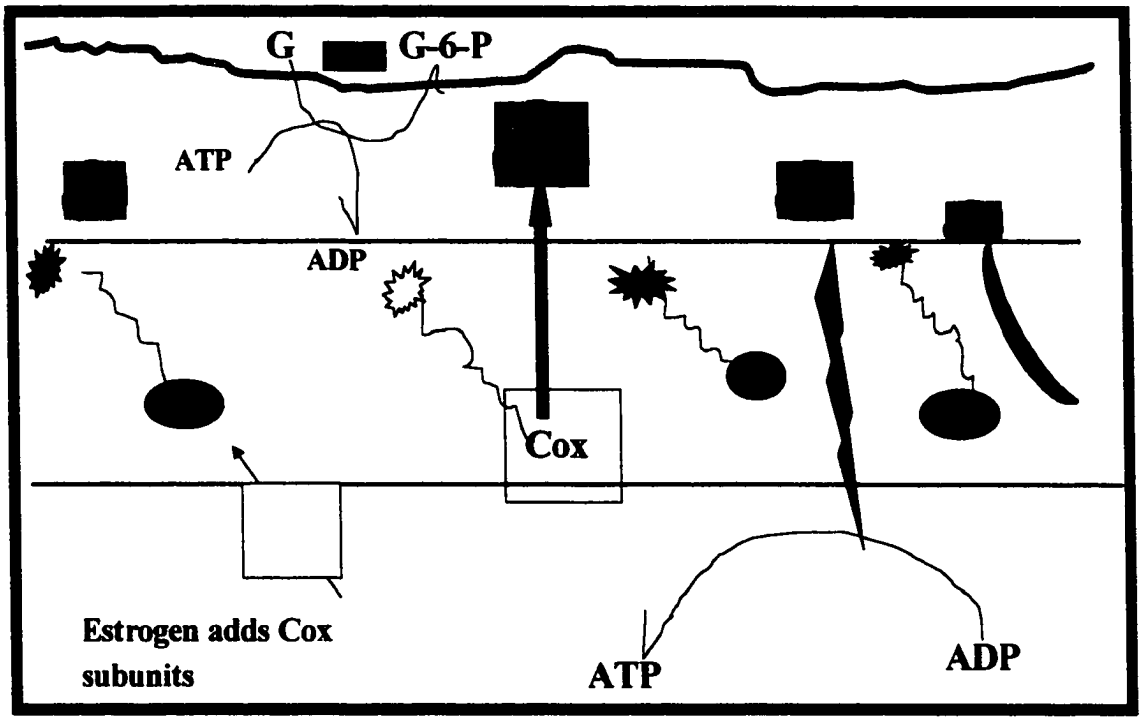

Figure 1.28 Diagram of postulated melatonin effect on estrogen deprived MCF-7 cells.

In the absence of estrogen, Cox subunits (yellow squares) are limited in the mitochondrial inner membrane (parallel lines) and thus restrict the number of functional electron transport complexes (green). ATP is depleted by overactive HKII phosporylation of glucose (G) in the tumor phenotype. Melatonin mediates the uncoupling of oxidative phosphorylation (directly or indirectly through an uncoupling protein – red half moon shape), and decreases the proton motive force available for ATP synthesis. The hormone further activates glycolytic enzymes, and causes increased activity of the restricted electron transport chain. Estrogen rescue induces increased Cox subunit protein, and thereby augments the limited electron transport chain function to overcome the melatonin effects.

Taken together, these data suggested a mechanism whereby peak levels of melatonin at periods of low estrogen exposure exerted selective toxicity on energy dysregulated cells. It is tempting to speculate that pulses of melatonin in periods of low estrogen (menstrual cycling and menopause) may serve to inhibit pre-neoplastic growth through metabolic toxicity to cells with poorly regulated energy production. Thus, although MCF-7 carcinoma cell death mediated by melatonin is novel oncostatic mechanism, it more importantly suggests a potential therapeutic target unique to cells with bioenergetic and growth dysregulation exemplified by the MCF-7 human breast carcinoma cell line.

SECTION I CHAPTER 2

DIFFERENTIATION IN MCF-7 CELLS TREATED WITH MELATONIN

INTRODUCTION.

The experiments in Chapter 1 describe a cytotoxic mechanism through which melatonin treatment of cultured MCF-7 cells resulted in acute death associated with mitochondrial bioenergetic disruption. Interestingly, data from other recent studies [17;52] suggest that mitochondrial function is necessary to maintain the neoplastic phenotype of MCF-7 cells. The authors reported that depletion of mitochondria with ethidium bromide produced a line of MCF-7 cells (rho$^-$) that lost anchorage independent growth and were more sensitive to cytotoxic drugs. Furthermore, the phenotypic changes were reversed with the transfer of normal mitochondria back to the rho$^-$ MCF-7 cells. These provacative findings suggest the possibility that melatonin may exert anti-neoplastic effects on MCF-7 cells by causing cell differentiation.

Definition and description of cell differentiation

Terminal differentiation is a process of cell maturation that leads to a final functional state with an inability to divide and reproduce [25]. It is a biological antithesis of cancer because the cells develop a highly specialized function, cannot perform in any other capacity, and ultimately die when there is no longer need of their specialized activity [83]. Epithelial germinal cells differentiate into glandular secretory cells or to squamous protective coverings and are guided by the growth factors and hormonal stimuli of their micro-environment [30;84]. In breast tissue, the squamous pathway is a common non-cancerous form of pathology in response to abnormal growth conditions and is frequently found in association with pre-cancerous lesions [1;30]. Thus, insight into the mechanisms triggering breast cancer squamous cell differentiation as opposed to pre-

neoplastic development may offer a biologic alternative that would eliminate cancer cell immortality and convert the malignant phenotype to a non-tumorigenic cell.

General morphology of breast cells and characteristics of the MCF-7 cell line:

Breast epithelium is composed primarily of simple cuboidal ductal cells with glandular secretory functions that vary under hormonal control [30]. As components of milk are formed due to influence of progesterone and prolactin, cytoplasmic granules form and fuse with the plasma membrane and are released [84]. Non-glandular epithelium in other organs (e.g. skin) functions for mechanical protection of the underlying tissues and terminally differentiates into a flattened squamous epithelium [84]. With changing growth conditions, the MCF-7 breast carcinoma cell line undergoes phenotypic variability and, specifically, may demonstrate morphologic changes reminiscent of the squamous epithelium (figure 2.1). On the other hand, under normal culture conditions, the MCF-7 cells display typical neoplastic morphology with obvious pseudopodia, multiple nucleoli, and anisokaryosis (figure 2.1).

Morphology of MCF-7 cells and changes following melatonin exposure:

Hill et al. described changes in MCF-7 cell morphology suggestive of a more differentiated phenotype after four days of melatonin treatment [16]. In a similar study, Crespo et al., confirmed Hill's findings in addition to demonstrating that the effects were reversible by estrogen [85]. Both authors observed a decrease in surface microvilli and described prominent nucleoli, which were frequently single and centrally located.

Figure 2. 1 MCF-7 cell culture phase contrast micrograph.

After five days in C-D extracted phenol red free medium containing 1 nM melatonin, two MCF-7 cells (above) demonstrated squamous epithelial morphology in monolayer culture. Other cells (arrowheads) demonstrated typical MCF-7 morphology with multiple nucleoli and active mobility from pseudopodia. The cell cluster to the right had multiple cells with anisokaryosis, multiple nucleoli, large nuclear to cytoplasmic ratio, and irregular cytoplasmic volume characteristic of epithelial cancer cells.

Neoplastic cells frequently demonstrate large and often multiple nucleoli. Although sometimes found in benign tissues, the presence, number, and size of nucleoli are roughly correlated with degree of malignancy [1]. This intra-nuclear structure is a production and modification center for ribosomal RNA transcripts where rRNA's are synthesized and associated with ribosomal proteins and the non-nucleolar 5S rRNA. Its light microscopic appearance and staining is apparent because of the concentration of both RNA and protein surrounded by DNA. The nature of neoplastic growth requires large amounts of protein synthesis and correspondingly large numbers of ribosomes [86]. Thus, the

transition from multiple nucleoli to one suggests a more organized transcription process and possibly a less active cell.

Another structural feature of some neoplastic cells is the development of motility through the formation of pseudopodia. These membrane extensions allow amoeboid movement of cells through the mechanism of polymerization and de-polymerization of actin filaments [86]. This ability aides in the escape of cancer cells from a growth limited micro-environment and provides a clonal evolutionary advantage enabling metastasis to more desirable nutrient conditions [46]. Interestingly, the Hill and Crespo studies report decreased size and presence of pseudopodia following melatonin treatment in addition to a cytoplasm smaller (i.e. less active) than typical untreated control cells.

Furthermore, prominent bundles of filaments were identified by both investigators [16;85] following exposure of the MCF-7 cells to melatonin. Intermediate filaments (IFs) are the "cables" that cross the cytoplasm and provide structure to the cell [86]. Keratin filaments, a type of IF categorized by its keratin subunit protein, compose one major group found in tissues of epithelial origin and become most prominent in the terminal differentiation of skin [46]. Different cytokeratins arise in different types of epithelium, but serve a similar function of mechanical protection and have been used as a cytological marker of differentiation [87]. Crespo [85] visually identified the IF bundles in melatonin treated MCF-7 cells as cytokeratin and presented a conclusion that the filaments were further morphologic evidence of cell differentiation.

METHODS AND MATERIALS.

Materials, Cell model, and culture conditions.

MCF-7 human breast adenocarcinoma cells were obtained from American Type Culture Collection (ATCC, Rockville MD) at passage 154. Cell cultures were maintained in a humidified incubator at 5% CO_2 and 37^0C. All reagents and supplies were purchased from Sigma, St. Louis, MO unless otherwise specified. Cells were maintained in Dulbecco's Modified Eagle's Medium (DMEM) supplemented with fetal bovine serum (FBS 10% v/v), MEM non-essential amino acids (1% v/v), penicillin-streptomycin (1% v/v), hydrocortisone (200nM), sodium pyruvate (1 mM), and insulin (0.003 unit/ml). For experiments, cells were grown in phenol red free medium supplemented with C-D extracted FBS for electron microscopy experiments or 5% FBS for cornified envelope and flow cytometry.

Electron microscopic morphology studies.

MCF-7 cultures were grown for 18 hours in the presence of 1 nM or 100 nM melatonin, 0.00005% ethanol, or 1 nM estradiol. The flasks were harvested by trypsin digest, rinsed once in PBS, and immediately fixed in glutaraldehyde. Slides were prepared by osmium tetraoxide post-fixation, sequential dehydration, infiltration, and plastic imbedding prior to staining and examination.

Cornified envelopes.

Cornified envelopes were prepared and identified with little modification of the method of Sun et al. [88]. Briefly, MCF-7 cells were seeded at a density of 10^6 cell per T75 flask with 5% FBS-phenol red free DMEM and culture conditions as described previously. Twenty-four hours after passage, ten flasks were treated with either 1 nM melatonin or 0.00005% ethanol. Medium was replaced every three days and the cells

trypsin harvested on the eighth day. Cornified envelopes were counted in 900 ul of cell suspension by phase contrast microscopy following a 5-10 minute treatment with 100 ul of 2% SDS 1%β–mercaptoethanol solution. An aliquot from each flask was counted by hemocytometer and Trypan Blue exclusion to standardized envelopes to cell numbers.

Flow cytometry.

MCF-7 cells were seeded at a density of 1.25 x 10^6 cells per T75 flasks with culture conditions as described for cornified envelope experiments. Twenty-four hours after passage the cells were treated with 0.00005% ethanol, 1 nM melatonin, all trans retinoic acid (1 pM, 100 pM, or 10 nM), or 1 nM melatonin plus retinoic acid. Following six days of treatment, the flasks were trypsin harvested and prepared for dual-parameter flow cytometry analysis. First, they were rinsed with cold PBS to remove residual medium, re-suspended in 2 ml PBS, and finally ethanol fixed by adding 5 ml of absolute alcohol dropwise while vortexing. After removing the ethanol supernatant, the cells were stained with propidium iodide (10ug/ml with 40Ku RNAase), FITC labeled anti-keratin (K4, K5, K6, K8, K10, K13) primary antibody (Sigma catalog #F3418, 1:100 dilution), for staining controls, or a combination of the two for samples. The prepared cells were then analyzed on an EPICS IV fluorescence activated cell counter with 488 nm laser excitation wavelength. Filters used included a 515 nm longpass blocking filter, a 560 nm dichroic, and a 630 long pass and 530 short pass filter respectively for the red PI and green FITC wavelengths. Propidium iodide (DNA) was read on an integral scale of 256 channels and the FITC (keratin) read on a log integral scale with 30,000 events gated on forward angle light scatter.

RESULTS.

Morphologic changes- Small cells with single nucleoli...

Following 18 hour treatment with melatonin, many MCF-7 cells were obvious with small cytoplasm and large single nucleoli similar to those described by Crespo et al. [85]. Figure 2.2 is an electron micrograph depicting one such cell. A smooth cytoplasmic border with minimal microvilli and no pseudopodia were also evident, and suggested a metabolically quiescent cell. The cells in figure 2.2 also demonstrated well-defined tight junctions to a neighboring cell indicating an attempt to maintain some of the original epithelial function.

Figure 2. 2 A single MCF-7 cell after 18 hours treatment with 1 nM melatonin.

This melatonin treated cell displayed a more differentiated phenotype than the typical MCF-7 cell. Of note are the single large nucleolus (arrow), the smooth cytoplasmic border without pseudopodia, and the relatively scant quiescent cytoplasm. The tight junction with an adjoining cell was typical of normal breast ductal epithelium.

Morphologic changes--degenerate mitochondria.

Melatonin treated MCF-7 cells with single nuclei, and small cytoplasm frequently demonstrated degenerate mitochondria in cultures grown 18 hours in C-D extracted FBS

containing DMEM. Apparent swelling and loss of structural definition of the cristae were present, and in some cases, loss of the mitochondrial membrane was evident.

Figure 2. 3 An MCF-7 cell treated for 18 hours with 100 nM melatonin. Note the degenerate mitochondria.

This cell was one of many melatonin treated MCF-7 cells demonstrating morphologic variations suggestive of differentiation. Findings in these cells were single nucleoli, decreased pseudopodia, and mitochondrial alterations. Several mitochondria had ultra-structural changes such as degenerate and distorted cristae (arrows) with others minimally affected (arrowhead).

Morphologic changes–intermediate filament bundles.

Pronounced filament bundles were obvious in many MCF-7 cells as early as 18 hours after treatment with melatonin (figure 2.4). These bundles were of size consistent with intermediate filaments such as cytokeratins. This observation is in agreement with the findings of Crespo et al. [85] although cytochemical confirmation of the filament identity was not done in either study. Subjective evaluation of electron microscopy grids suggested the greater prevalence of the filament bundles in cells with the single nucleoli

and abnormal mitochondrial morphology described in previous paragraphs. This further suggested that they were related to cellular differentiation.

Figure 2. 4 Electron micrograph of MCF-7 cell showing prominent intermediate filament bundles.

After 18 hours treatment with 100 nM melatonin, the cell at the left demonstrated prominent intermediate filament bundles with the morphologic appearance of cytokeratin.

Cornified envelopes.

To further explore the hypothesis that melatonin induces terminal differentiation in MCF-7 cells, cornified envelopes were enumerated as described in materials and methods. There was a significant increase ($p = 0.02$) in number following 1 nM melatonin treatment, although the total number of envelopes was low in both groups (less than 1% of all cells). Figure 2.5 compares the melatonin treated cells to vehicle control. Each bar represents five replicate flasks and the data was repeated in two separate

experiments. As expected, there was no difference in phase contrast morphologic appearance of the cornified envelopes between treatment and control groups.

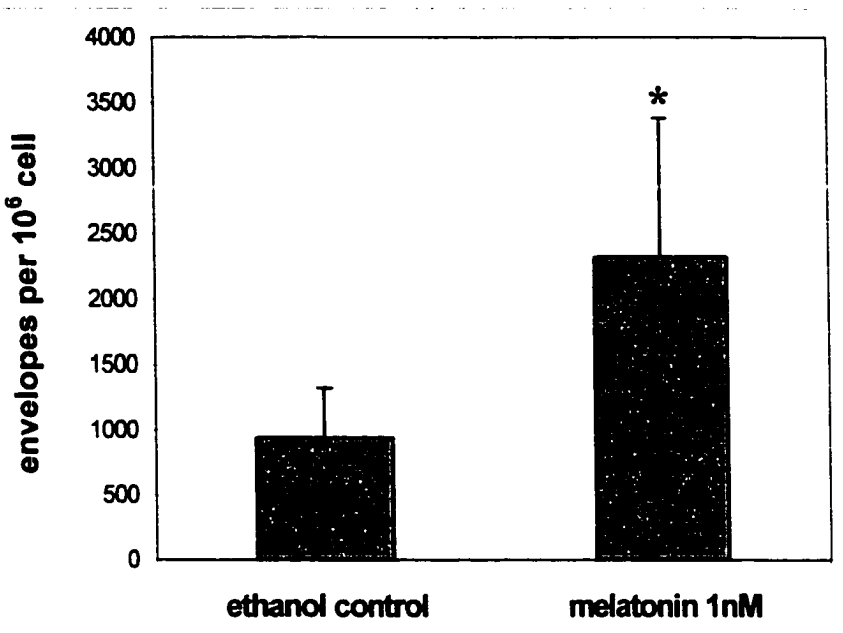

Figure 2. 5 Cornified envelopes in melatonin and vehicle control treated MCF-7 cells.

Cornified envelopes were significantly more numerous in 1 nM melatonin treated MCF-7 cells than vehicle control (0.00005% ethanol) (*p=0.02 by two tailed Student's T test).

Flow cytometry.

The morphologic changes and findings of increased cornified envelope number in melatonin treated cells led to further exploration of keratin changes in the MCF-7 cells. The postulate that melatonin would induce a quantitative cytokeratin increase was investigated with the use of an EPICs model fluorescence activated cell sorter and dual fluorescent staining. If keratinization was increased in the G_1-G_0 population of cells, keratin immunostaining (FITC on the Y-axis of the histograms in figure 2.6) would be predominant in the dimmer regions (propidium iodide on the X-axis) of DNA staining. A

gating region was placed around this area and compared between control, 1nM melatonin, all-trans-retinoic acid (atRA at 1pM, 100pM, and 10 nM), and a combination of atRA (100 pM) plus melatonin (1 nM). As shown in figure 2.6, there was no difference in any treatment groups from control either visually in the histograms or by analysis of data mean or mode. The keratin antibodies were monoclonally specific against several cytokeratins (K4, K5, K6, K8, K10, K13, and K18) and would not identify changes if increases in one were counter-balanced by decreases in another.

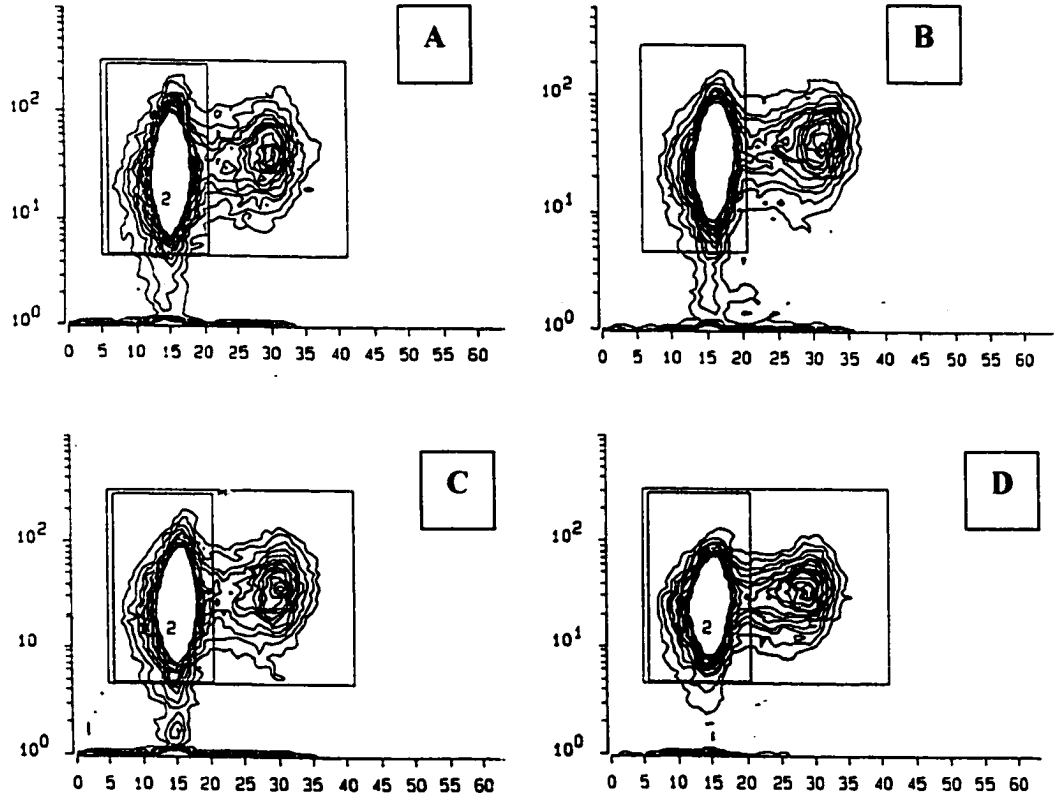

Figure 2. 6 Flow cytometry dual parameter histograms.

The above histograms are from MCF-7 cells treated as follows: A) Ethanol control 0.00005% B) Melatonin 1 nM for three days C) All trans retinoic acid 100 pM for three days D) Pretreated 24 hours with 1 nM melatonin then retinoic acid 100 pM plus 1nM melatonin for three days. DNA staining (propidium iodide) is shown on the X-axis and keratin immunostaining on the Y-axis. There was no visual difference between histograms and no significant differences between modal analysis of treatment groups.

DISCUSSION.

Data presented in Chapter 1 strongly suggested alterations of aerobic metabolism in melatonin treated MCF-7 cells, which resulted in acute cell death. Following melatonin treatment, obvious morphologic changes were present in MCF-7 cells grown for 18 hours in charcoal dextran extracted FBS medium. These changes included a tendency for cells to have single nuclei, smaller cytoplasmic volume, altered mitochondrial ultra-structure, and increased presence of intermediate filament bundles (figures 2.2, 2.3, and 2.4). The current set of experiments (Chapter 2) were performed to further examine the possibility that melatonin affected MCF-7 cell metabolism by inducing MCF-7 cells to undergo terminal differentiation. The experiments were conducted to examine keratin formation in the cells following melatonin treatment in medium containing reduced concentration of steroid hormones (i.e. 5% FBS).

Enumeration of cornified envelopes has been described as a measure of differentiation in the epithelium of both skin and respiratory tract [88;89]. Similarly, morphologic changes following melatonin treatment of MCF-7 cells suggested that a similar process occurred in the breast epithelial carcinoma cells. Additionally, given that MCF-7 cells have the ability to differentiate in culture, [17] and furthermore, to undergo squamous transformation [30], it was postulated that melatonin would increase cornified envelope number in cultured MCF-7 cells.

Data in figure 2.5 demonstrated a significant increase in the number of cornified envelopes following melatonin treatment (data was the result of $n = 5$ and was repeated in two separate experiments). Although the increase was significant ($p = 0.02$), it was present in less than 1% of all cells and suggested two conclusions. First, melatonin did

indeed increase the formation of cornified envelopes but secondly, the number of cornified cells was a small percentage of the total population.

This finding in itself is of minimal significance to the clinical treatment of transformed cells (i.e. cancer), however, more importance may reside in questions regarding non-transformed cells. For example, 1) Does melatonin prevent transformation of breast cells following periods of rapid estrogenic growth by causing terminal differentiation? 2) Is the melatonin effect on breast cells synergistic with hormones known to regulate growth and differentiation (e.g. retinoic acid and estrogen)?

The flow cytometry experiments described in figure 2.6 were designed to address combined retinoic acid and melatonin effects on MCF-7 cell differentiation. Two assumptions were made in the design of these experiments. First, the assumption that cytokeratins would increase in more differentiated cells was necessary to allow measurement of cytokeratin fluorescence as a quantitative endpoint. The second assumption was that the total amount of cytokeratin would increase without qualitative change in type of cytokeratin (an assumption that did not prove true).

Experimental results did not show the expected differences between melatonin or retinoic acid treatments and control cells. There was an increase between the melatonin/retinoic acid combination treatment and controls, although the magnitude of the difference was small. There are two possible reasons for failure of the flow cytometry experiments to agree with findings of increased cornified envelopes and morphologic presence of intermediate filament bundles. First, pancytokeratin immunostaining would not differentiate between different cytokeratins if increases of one type were balanced by decreases of another [89;90]. It also would not identify types of

intermediate filaments other than the specific keratins targeted by the monoclonal antibodies of the stain [90]. Secondly, the number of cornified envelopes was small (less than 1% of all cells) and thus, the increase in keratinization may not have been detectable by the flow cytometer.

CONCLUSION.

The contribution of melatonin to cellular differentiation of MCF-7 breast cancer cells appeared to be small, however, it was clearly present. Morphologic simplification of nuclear and cytoplasmic architecture and the formation of intermediate filaments defined a change of cells to a more quiescent phenotype. Furthermore, increased numbers of cornified envelopes indicated a modulation of cell physiology toward terminal squamous differentiation. Although, the findings of these experiments were not conclusive, the studies demonstrated that the hormone caused at least some MCF-7 cells to have a phenotype suggestive of terminal differentiation. Finally, the mechanisms responsible for changes in cell morphology and cornified envelope number as seen in these experiments presented interesting possibilities for future studies of cancer prevention.

SECTION I CHAPTER 3

PRELIMINARY BIOASSAY STUDIES OF MELATONIN, 17β-ESTRADIOL, TGFβ, AND ELECTROLYTE CONTENT IN HUMAN GROSS FIBROCYSTIC BREAST DISEASE FLUID SAMPLES

INTRODUCTION

Breast epithelial cell secretion may represent autocrine/paracrine homeostatic control mechanisms against the numerous growth-promoting peptides and steroids necessary to maintain a gland whose function is to rapidly proliferate at the time of pregnancy and lactation. Previous studies suggest that MCF-7 human breast carcinoma cell growth is inhibited by exposure to breast cyst aspirate fluid [91;92], in spite of its content of mitogenic peptides and hormones [93-96]. Furthermore, several components of cyst aspirate fluid have been identified as biomarkers of breast cancer risk [97-101]. Thus, an understanding of cyst fluid bioactivity and elucidation of its growth-inhibiting mechanisms may be invaluable in the prevention and treatment of breast cancer.

Breast cysts: definition and incidence.

The term "gross fibrocystic breast disease" (GFBD) has been used as a clinical description of any non-cancerous breast change associated with fluid filled cystic structures [30]. GFBD is the result of secretory dilation of normal breast ductal architecture, which may be associated with normal aging [30]. Although clinically palpable cysts affect about 7% of women, histologic tissue examination from post-mortem studies indicates that dilatory pathology is present in approximately 70% of all middle and older aged women [102]. Thus, it is reasonable to assume that the pathological changes involved in breast cyst formation may represent a widespread aging development of the general cancer aged population [102].

Anatomy of the breast in relation to cysts and cancer

Both breast adenocarcinoma and GFBD arise from the epithelial cells of the terminal lobular unit in the breast ductal system [103]. Anatomically, the ductal cells are

separated from blood vessels by a basement membrane, connective tissue, fat, and finally, the endothelium of adjacent capillaries. They are exposed to their own luminal secretions that are biochemically unique and different from blood and extracellular fluid [104]. Although ductal cells secrete relatively large quantities of milk during lactation, only a small fluid accumulation is present during non-lactating periods [review [105]]. This fluid provides a medium that appears to be a secretory product of the ductal cells [92;105;106] and bears considerable similarity to GFBD fluid [107]. Thus, two conclusions may be made. First, the breast ductal cells have greater exposure to the micro-environment of their paracrine and autocrine secretions than they do from the blood and extra-cellular fluid compartments. Secondly, GFBD fluids represent the breast cell micro-environment for 7% of the population and may provide insight and understanding for a much larger proportion of all women.

Risk of cancer in GFBD patients and relation to general population

GFBD cysts are considered to have a low or zero risk of breast cancer development when no other pathology is present [30;102]. Patients with concurrent hyperplasia (20% of cases) however, demonstrate relative risk factors of 2 to 4 and those with nuclear atypia (10-12% of cases) have RR as high as 5 [102]. A 10-fold risk may be present if there is a family history of breast cancer [102]. Interestingly, Wrensch et al. [108] reported almost identical relative risks in a large cohort study with 30,000 person years follow-up using nipple aspirate fluid cytology as a predictor of risk. The authors found the relative risks of 1.8, 2.5, and 4.9 for patients with normal cytology, hyperplasia, and atypical hyperplasia respectively compared to non-secreting controls. It therefore appears that GFBD patients and nipple fluid secretors have common risks of pre-

neoplastic pathology with cancer risk predicted similarly by nipple aspirate and cystic fluid. If so, GFBD fluid would be representative of the ductal fluid from fluid secretors in nipple aspirate studies and would represent 72% of all women in the 30 to 50 year age group. This again suggests that the information achieved from studies of GFBD fluid may have far wider implications than the 7% of women with GFBD.

Characterization and biochemistry of cysts

Needle aspirates of cysts have been categorized as type I and type II according to the ratio of sodium and potassium content in the fluid. Type I cysts are defined as having high potassium and low sodium (ratio >1:3), and are associated with increased cancer risk patients (RR= 4.62) [100]. Histological examination of tissue from the higher risk cysts shows an apocrine epithelial morphology [109] although the significance of the risk relationship to electrolyte content in these cysts is an observational association with undefined underlying mechanism of action. The risk relationship appears valid, however, since cyst type is also associated with risk biomarkers such as the growth factors (EGF, bFGF, and TGFβ) [94;98;101;110], and hormones such as estriol, estrone, dehydroisoandrosterone [96], and estradiol [94]. Additionally, a number of peptides such as gastrin releasing peptide (GRP) [111], gross cystic disease fluid protein (GCDFP-15) [95], interleukins 6 and 8 [112], and angiotensin converting enzyme (ACE) [113] have been significantly related to cyst type and indicate the diverse nature of the fluid. Unfortunately, in spite of these significant associations with risk biomarker hormones, growth factors, and breast cancer [100], cyst fluid electrolyte content appears not to be a consistently reliable biomarker in all studies [114].

Breast cyst aspirate fluid is rich in mitogenic hormones:

Cyst fluid is rich in mitogenic hormones and peptide growth factors. Biochemical analysis identifies high estrogen (estradiol, estrone, and estriol) concentrations with estriol levels greater than 1000 times that found in serum, and androgens (e.g. dehydroepiandrosterone) in quantity up to 500 ug/ml [93;96;104]. Petrakis et al. found levels of estrogen (estradiol and estrone) in ductal fluid samples up to 45 times the serum level with large variation between patients [104]. Rose et al. [115] identified elevated levels of estrogen as well as prolactin in GFBD fluid and found prolactin in some cases at levels previously reported to stimulate growth arrested (G_0) breast carcinoma cells [107]. In a later study, significant prolactin and growth hormone activity was identified in a cyst fluid bioassay that was not detected by parallel immune assay [115]. Thus, cyst fluid would be expected to have a highly mitogenic effect *in vitro* and especially so for estrogen responsive cells.

Cyst fluid also contains the mitogen, EGF...

The concentration of epidermal growth factor (EGF) in GFCD fluid is positively correlated with breast cancer risk in numerous studies and is proposed as a biomarker for breast cancer [93;94;98;99]. In addition, EGF is elevated in cystic fluid with a significant difference between cysts having apocrine metaplasia (high risk-low Na/K ratios) and those having flattened epithelium (low risk-high Na/K ratios) [94;116]. Finally, the finding of significantly higher EGF concentration in cystic fluid of cancer and atypia patients compared to those with non-proliferative lesions further supports an association of EGF and cancer risk [98].

In addition to clinical and epidemiological studies, *in vitro* laboratory data with breast cancer cells demonstrate the mitogenic effects of EGF [117]. Proliferation of

MCF-7 cells in culture was stimulated even in the absence of estrogen if EGF or factors from estrogen conditioned medium were present [117]. Interestingly, the mitogenic effect of EGF was abolished by the addition of melatonin. It appears therefore, that homeostatic mechanisms that control proliferation of breast cells *in vivo* must modulate EGF as well as estrogen and prolactin.

Mito-inhibitory agents associated with ductal cell growth

Needle aspirates from GFBD patient as well as nipple aspirates from healthy volunteers contain a multitude of mitogenic agents including growth factors and estrogens, often in high concentrations relative to blood levels [93;95]. In spite of growth-promoting agents in cyst fluids, the relative risk of breast cancer is less than 2.0 in both GFBD patients and nipple fluid secretors when no other pathology is present [102;108]. Given these findings, the presence of strong mito-inhibitory factors is highly probable, although few studies have addressed the anti-cancer relevance of such postulated endogenous growth-blocking agents. Thus, it is a logical assumption that growth promoting and growth inhibiting factors are delicately balanced and that alteration of the normal balance may be a strong indicator of cancer risk.

Many factors that inhibit breast cell proliferation *in vitro* are present in cystic fluids. For example, interleukins 6 and 8, oncostatin M, basic fibroblast growth factor (bFGF), and transforming growth factor beta (TGFβ) are present in cyst fluid with higher concentration in cysts of Na/K ratio greater than 3. These growth factors have all been categorized as endogenous agents that inhibit the growth of transformed cell lines *in vitro* although direct mechanisms of action have not been defined [101;105]. Other agents with obscure relation to breast growth such as angiotensin converting enzyme (ACE) and

enkephalinase have also been identified in cyst fluid samples, with the higher concentrations of ACE significantly associated with type II cysts. The authors postulated that these proteins served a proteolytic function to degrade peptide mitogens but the regulatory control pathways were not discussed [113]. Undoubtedly, many other growth inhibitors are also present that respond to the diverse number of growth promoters.

TGFβ, a potent mito-inhibitory factor in epithelial cells...

TGFβ is a potent mito-inhibitory agent in epithelial cells [25] and may be a significant antagonist of uncontrolled growth in breast epithelium. Lack of responsiveness to TGFβ was a grave prognostic marker in human colorectal tumors [118] and was associated with increased invasiveness in human breast cancer [119]. Furthermore, TGFβ is a component of GFBD fluid with a significantly ($p<0.001$) higher concentration in type II (lower risk) cysts. It was also identified in ten of ten benign breast fibroadenomas but in none of 36 invasive adenocarcinomas by immuno-histochemistry [120]. These reports taken together would suggest that TGFβ activity in the breast epithelium is a significant contributor to physiologic defenses against cancer.

Mito-activators and mito-inhibitors may oppose each other, but bioassay analysis could evaluate both together

The cell growth effects of GFBD fluid result from hormone-growth factor combinations with the overall effect due to a variety of different agents [93-96;98;99;101;107]. Because the combined effects of mitogens and growth inhibitors complicate the interpretation of analytic findings from cyst fluid, accurate prediction of cancer risk is difficult. A solution to this problem is the development of bioassay procedures that define the desired endpoint, cancer cell growth, and allow *in vitro* analysis of all cyst fluid constituents simultaneously. There are three specific advantages

to this approach. First, an *in vitro* model of cancer cell growth is rapid and inexpensive but quantifies the effects of growth responsive agents and their interactions together. Secondly, the bioassay is useable in combination with analytic techniques for fluid analysis and with epidemiological tools for patient data analysis. Thirdly, cell biology mechanistic information may be ascertained from the study data and could be used in future treatment and prevention studies.

GFBD fluid treatment of cells in vitro

GFBD cystic fluid was found to significantly inhibit the growth of cultured MCF-7 carcinoma cells [91] and significantly stimulate 17-oxidoreductase activity in the reductive direction (estrone to estradiol). This suggests that mechanisms antagonistic to estrodiol-mediated proliferation must have been induced. In a second study, using ER positive MCF-7 and ER negative MDA-MB231 breast cancer cells, 7 of 21 and 17 of 20 samples, respectively, demonstrated significant decreases in growth rate [92]. The authors postulated that the growth rate changes were due to modulation of estrone sulfatase, which catalyzes the conversion of sulfated estrone to the biologically active free estrone and finally to the more potent estradiol. Estrone sulfatase activity was inhibited in 19 of 21 MCF-7 treatments but stimulation of estrone sulfatase activity was found in 11 of 20 of the MDA sample treatments. The argument therefore, was that the inhibition of estrone sulfatase activity in ER positive MCF-7 cells decreased their proliferation by reducing the amount of available estradiol. This hypothesis, however, does not answer the question of why a larger percentage of cysts inhibited growth in the ER- cell line that should be non-responsive to estradiol. A plausible answer would be

that mito-inhibitory substances were present in the fluid and played a more important role than the effects on estrone sulfatase.

Melatonin may be involved in the prevention cancer cell growth

Melatonin, best known as a pineal gland neurohormone, has intriguing potential as a breast cancer preventative agent. Melatonin concentration in breast tissue has been demonstrated to be three orders of magnitude greater than serum levels and has been inversely correlated with severity of histologic nuclear grade in breast adenocarcinoma ($p<0.006$) [82]. *In vitro* carcinoma cell studies have shown melatonin to down-regulate estrogen receptor [14], inhibit estrogen induced growth [12;121], induce sublethal morphologic changes [16], alter cell cycle dynamics and DNA synthesis [122;123], and augment the anti-proliferative action of tamoxifen by a factor of 100 [124]. Other melatonin oncostatic effects, either alone or in combination with chemotherapeutic drugs, include anti-proliferative, immunostimulatory, and anti-oxidant effects [6]. Data from Cos et al. [117] strongly indicates that physiologic concentrations (1nM) of melatonin modulate the growth stimulatory effects of EGF in MCF-7 breast carcinoma cells. Additionally, a recent study by Molis et al. showed melatonin to significantly stimulate the production of TGFβ [11].

In addition, melatonin antagonized the mitogenic effects of prolactin in MCF-7 and ZR75-1 breast carcinoma cells [18]. Conditioned medium from MCF-7 cells treated with melatonin also inhibited growth of MCF-7 cells, thus indicating that melatonin may act through induction of autocrine factors [117]. These studies in combination suggest that melatonin may indeed have a major regulatory role in the growth of breast ductal cells and in the modulation of breast cancer development.

In summary, cystic fluid contains many agents that can affect cancer cell growth and metabolism. Agents in cyst fluid such as estrogen undoubtedly exert a positive influence on cancer growth [30], while the presence of agents that inhibit cancer cell growth are reported in laboratory *in vitro* studies [91;92]. This balance between disease promotion and protection (homeostasis) is not a new theme in biological systems of disease [1]. Thus, it is a reasonable hypothesis that breast cells recognize abnormal biologic activity and secrete autocrine/paracrine agents that create a protective micro-environment. Moreover, the finding that breast cell proliferation was decreased after cystic fluid treatment [91] suggests an anti-cancer role for the cyst secretions. Finally, the identification of growth inhibitory factors such as TGF β [92], lend further credence to a hypothesis that cystic fluid at least in part protects against breast neoplasia.

Significance of bioassay for cyst fluid analysis

Breast cancer biomarkers found in GFBD fluid such as epidermal growth factor (EGF), gross cystic disease fluid protein (GCDFP-15), and electrolyte ratios have been previously reported [94;98-100]. Additionally, a number of biochemical characteristics such as hormone and growth factor concentrations have been strongly associated with higher risk cyst types [93;94;96;99;101]. Unfortunately, the significance of single biomarkers and biochemical correlations are easily lost in the complexity of agents found within breast cysts. The advantage of bioassay analysis, therefore, is to measure a single response (e.g. cancer cell growth rate) to a complex exposure of agents in the fluids. Conversely, the disadvantage is that specific biomarker identification is still limited to the correlation study of single agents. None the less, bioassay data adds a layer of depth to the understanding of breast cell responses to agents of their micro-environment.

Exposure of breast epithelial cell lines to human breast cystic fluid provides a model system to study the breast epithelial cell behavior in a simulated micro-environment. The value of this sort of bioassay is three-fold. First, biochemical analysis can be done directly on the fluid samples. Secondly, *in vitro* endpoints such as cancer cell growth are easily related to the biochemical findings. Finally, the most important aspect of the bioassay study of breast cysts is that the laboratory analytic and *in vitro* data can be related to the human populations at risk with the tools of epidemiology.

Specific aims of the experiments...

The first specific aim of these experiments was to analyze and demonstrate the existence of melatonin in human breast cyst fluid specimens. After demonstrating this novel finding, determination of the variation in concentration was necessary to support a hypothesis of melatonin mediated growth modulation of breast ductal cells. A second aim was to establish protocols and procedures for preparation, storage, and administration of breast cyst fluids to an *in vitro* bioassay model. The third aim was to establish laboratory methods to use an MCF-7 breast cell model for proliferation assays with cyst fluid exposure. The final aim was to develop preliminary data for biochemical analysis of TGFβ, 17β-estradiol, melatonin, sodium, and potassium as well as data from the MCF-7 proliferation assays. And finally, the goal of these specific aims was to explore the feasibility for use of the MCF-7 bioassay model in future population studies.

METHODS AND PROCEDURES:

Choice of cell model

The MCF-7 human breast carcinoma cell line was isolated from a pleural metastasis and has been widely used as an estrogen receptor positive breast cancer cell model [125].

Although it originated from a malignant tumor, the MCF-7 cell line has been reported to retain estrogen [71;125], progesterone [125], prolactin [18], and retinoid [126], responsiveness in addition to the wild type p53 genotype [125]. As with any cancer cell line however, the risk of genotypic drift is present. To minimize this possibility, the following studies were completed with MCF-7 cells limited to passage number 157 through 172. Additionally, care was taken to ensure that the cells retained responsiveness to estrogen induced proliferation and to avoid phenotypic drift of morphology by visual examination under phase contrast microscopy.

Cyst fluid sample acquisition and preparation...

Aseptic needle aspirates of cysts containing 0.5 ml or more of fluid were taken from GFBD patients seen at the University of Colorado Health Sciences Center University Hospital. The samples were coded for laboratory use with no personal identification and patient permission granted as required by the (University of Colorado) University Hospital human subjects review board. After collection by the attending physician, the samples were stored at -80^{0}C. The frozen samples were shipped to Colorado State University on dry ice and immediately returned to -80^{0}C storage upon arrival. Samples were handled with appropriate OSHA-approved precautions for blood-born pathogens.

Samples were received in two groups with potential variability inherent in their resulting data. The first samples (number 1, 2, and 3) were collected in the late fall and winter of 1997-98 and remained in storage for over 12 months before use in the bioassay. These samples, additionally, were thawed and refrozen twice during that time for preliminary analysis of melatonin in the spring of 1998. The remaining samples were collected in late spring of 1998 and analyzed in the fall. Inherent differences in the time

of collection, freeze-thaw handling, and length of time between melatonin analysis and bioassay make the data from these samples questionable. For these reasons, the proliferation data from samples 1, 2, and 3 was not included in cell proliferation studies.

Endogenous synthesis of melatonin from serotonin...

MCF-7 cells were seeded in T-75 flasks at a density of 5 x 10^6 cells per flask and maintained in phenol red medium with 10% FBS as described previously (Chapter 1). After 24 hours, triplicate groups were treated with 10 ml of either control medium, or medium containing 100 nM, 10 uM, or 1 mM concentrations of 5-hydroxytryptamine (serotonin). After an additional 24 hours of incubation, the cultures were examined under phase contrast microscopy for evident cytotoxic morphologic changes or decreases in cell number. After qualitative (morphology) and quantitative (cell counts) evaluation for cytotoxicity, the 1 mM serotonin treated triplicate samples and the control medium were submitted for melatonin analysis by radioimmunoassay. The R.I.A. was performed by the method of Rollag and Nisewinder [31] by personnel of the Animal Reproduction and Biotechnology Laboratory (ARBL) at Colorado State University, Ft. Collins CO.

Effects of filtration and storage on melatonin content...

To determine the effects of filtration on cyst fluid melatonin levels, three samples were prepared with and without passage through a 0.2 um filter (Gelman Sciences, Ann Arbor MI). The cyst fluid was vortexed for 30 seconds after thawing at room temperature. Duplicate samples of 100 ul were prepared, diluted with PBS to one ml volume, and kept on ice until analysis. After passing one set of samples through a 0.2 um filter, the samples were submitted for R.I.A. melatonin analysis to the ARBL laboratory.

Fluid characterization: electrolytes by atomic absorption spectroscopy...

Samples were analyzed for sodium and potassium content by flame ionization atomic absorption spectroscopy. Commercial sodium standard solutions (Fisher, Houston TX) were diluted with 1% nitric acid in double de-ionized water to concentrations of 0.125, 0.250, 0.500, 1.0, and 2.0 ug/ml. A standard curve was prepared as shown in figure 3.10 with Na concentration on the X-axis and absorbance at 589 nm (sodium lamp) on the Y-axis. Data was integrated and recorded with Varian Spectra 300/400 software. Potassium standards were prepared in similar fashion from commercial stock standard solution (Fisher, Houston TX) and diluted with 1% nitric acid in double de-ionized water to concentrations of 0.3125, 0.625, 1.25, 2.5, and 5.0 ug/ml. A standard curve is shown in figure 3.10 with concentration of K on the X-axis and absorbance at 766.5 nm (potassium lamp) on the Y-axis. Data was again collected using the Varian Spectra system. The cyst fluid samples were diluted in 1% nitric acid-double de-ionized water with final dilution factors of 1000X for potassium and 1,000X or 2000X for sodium. Analytic blanks were prepared form 1% nitric acid in double de-ionized water.

Fluid characterization: analysis of melatonin...

Cyst fluids were thawed and submitted to the ARBL laboratory. The analysis was performed by the I^{125} competitive radioimmunoassay method as described by Rollag and Niswender [31]. The samples were kept on ice and delivered either undiluted or diluted with PBS gel as recommended by the laboratory. Results were reported as pg/ml with detection limit of the method at 0.45 pg/ml (1.9 picomol / liter).

Fluid characterization: analysis of estradiol...

Samples of the bioassay treatment medium containing cyst fluids were submitted to the Cornell University diagnostic laboratory, Ithaca NY for radioimmunoassay analysis

of 17β-estradiol. The samples were packed on ice and sent by overnight Federal Express delivery. The results were reported as pg/ml.

Proliferation bioassay...

Proliferation assays were conducted in 48 well microtiter plates seeded at 50,000 cells per well in DMEM supplemented with 10% C-D extracted FBS and insulin, sodium pyruvate, non-essential amino acids, hydrocortisone, and penicillin-streptomycin as described in Chapter 1. Quadruplicate wells were seeded for each fluid sample and six wells seeded for the untreated control. The cells were allowed 24 to 48 hours for adherence to the wells before treatments were begun. Maintenance of stock and treatment cultures was conducted at 37^0C, 5% CO_2, and in a humidified atmosphere as previously described (Chapter 1).

Cyst fluids were added to culture medium in 16.7% v/v concentration for bioassay treatments. The samples were removed from -80^0C storage, thawed at room temperature, vortexed for 30 seconds, and added to 10% C-D extracted FBS medium. Cyst volumes ranged from less than one ml to over 10 ml and in some cases were not adequate for treatment of the full set of culture plates. In the case of inadequate sample volume, cyst dilution was completed in medium and concentrations of melatonin and estradiol adjusted accordingly. Control wells were treated with medium that was diluted with Hank's Balance Salt Solution (16.7% v/v).

Cells harvested by trypsin digest at 16, 40, 90, and 160 hours were counted with an electronic particle counter (Elzone 180 Particle Data inc.). Briefly, medium was removed and wells rinsed once with 1X trypsin EDTA (Sigma). Trypsin was then added and incubated for 5 minutes at 37^0C. The cells were loosened from wells and the clumps

disengaged by gentle flushing through a pipette tip, then added to 500 ul of cold medium. Each well was rinsed once with 500 ul of cold PBS and checked microscopically to ensure complete removal of cells. The cell pellet was separated from trypsin containing supernatant by low speed centrifugation, re-suspended in 1 ml of cold PBS, and added to 9 ml of counting buffer. Triplicate counts were averaged for each sample.

Elisa assay for TGFβ...

TGFβ1 analysis was performed with an enzyme immunoassay (TGF-β1 EASIA, Biosource Europe, Belgium). The principle of the method involves the competitive binding of sample TGFβ and horseradish peroxidase (HRP) labeled TGFβ to bound antibody in a microtiter plate. After rinsing and adding the HRP substrate-chromogen, TMB, the O.D. at 450 nm is inversely proportional to TGFβ concentration. The cell culture medium collected from 160 hours of culture was stored for 10 days at -20^{0}C and thawed immediately prior to TGFβ analysis. The procedure used in the current experiments generally followed the manufacturer's protocol. Briefly, the provided calibration standard (2 ng/ml) was serially diluted in 5-fold increments to produce standards of 400, 80, 16, and 3.2 pg/ml. The wash solution was prepared by diluting 1 ml to 199 ml of double de-ionized (DDI) water (200X). The positive control was reconstituted with 0.5 ml DDI water, extracted with 2.5 M acetic acid (100ul/100ul), vortexed, and incubated at room temperature for 15 minutes. It was then diluted 20 ul to 500 ul of dilution buffer for a final dilution of 1:52. Cell culture medium was extracted with the provided acid containing extraction solution (500ul/50ul), vortexed, and incubated at room temperature for 10 minutes with continuous shaking. It was then diluted with 0.5 ml dilution buffer to a final dilution factor of 1:2.1. Coated assay wells

were secured to the provided frame with positions noted and labeled for standards, samples, and controls. Sample, standard, or control (200 ul) was pipetted into the appropriate well followed by 50 ul of TGFβ (horse radish peroxidase) HRP conjugate. The plate was then incubated for two hours at room temperature on a horizontal shaker at approximately 700 RPM. The liquid was aspirated from each well followed by three rinses with wash solution. Within 15 minutes after the final wash. 100 ul of chromogen was added and the plate incubated 60 minutes in the dark on a horizontal shaker. Stop solution (100 ul) was added and the absorbance at 450 nm read on a Bio-tek Elx 800 microtiter plate reader. A standard curve was prepared as shown in figure 2.4 and concentrations calculated from the linear regression curve equation.

Statistical analysis...

Regression analyses and correlations were calculated with Minitab or Microsoft Excel software. Minitab software residual analysis was used to evaluate the normality of regression distributions and non-parametric (Spearman's rho) correlations used when applicable. Coefficient of determination (R^2) was used as a measure of association for regressions and "p" values were calculated as a measure of significance for each R^2. Data was considered statistically significant when "p" was less than 0.05. Anderson-Darling tests of normality were considered significantly normal when $p>0.1$.

RESULTS.

General characteristics: analysis of cyst fluid

Characterization of GFBD cyst fluid involved analysis for melatonin, 17β-estradiol, sodium, potassium, and Na/K ratio. Values from cyst biochemical analysis are listed in table 3.1 and include mean, median, and mean excluding samples 1, 2, and 3. The most

remarkable observation of this data was the almost 100-fold difference between mean concentration of melatonin in cysts collected in the winter months (#1, #2, and #3) and those collected in the spring months. This difference was not statistically different ($p>0.05$) due to the small number of samples and large standard error of the respective means, but the magnitude of difference strongly suggests that a larger sample size will prove significant seasonal variation.

On the other hand, 17β-estradiol concentration in the cysts did not appear to vary with time of year. All of the ten samples contained measurable estradiol with ranges from 180.2 to 1685.0 picomoles per liter. Interestingly, all but one of the samples were within a relatively narrow range of 180 to 800 pM with the outlier having a concentration of 1685 pM estradiol. Unfortunately, patient personal data such as age and menstrual status were unavailable for the specimens thus introducing a possible source of confounding for estrogen studies and leaving open the possibility of the outlier resulting from ovulatory menstrual estrogen levels.

Sodium potassium ratios were readily divided into those greater and less than Na/K=3.0. However, further analysis showed no correlation between the grouping and other endpoints.

MCF-7 cells are able to synthesize melatonin from serotonin...

Data shown in Table 3.2 shows the concentrations of melatonin present in medium conditioned by MCF-7 cells grown 24 hours in 1 mM serotonin. The treated cells had a significantly higher concentration of melatonin ($p<0.001$ by Student's T test) indicating the ability to synthesize melatonin. There was no evidence of cytotoxicity from the

serotonin treatment indicated either by phase contrast morphologic evaluation or by cell number ($p<0.5$ by Student's T test).

Samples used for bioassay experiments...

Cell proliferation studies were done without including the cysts collected in the winter of 1998 to avoid four possible sources of error. First, samples 1, 2, and 3 were collected and stored for over twelve months prior to cell culture treatment producing a possibility of differential degradation of peptide factors versus the more stable lipid soluble hormones. Secondly, the first group of samples was thawed and refrozen twice prior to use in proliferation experiments further increasing the potential for degradation. Thirdly, this sample set may have contained seasonally related hormones unaccounted for by melatonin and estrogen analysis, but was too small to statistically adjust for these potential confounders. Finally, the laboratory reported difficulty in performing the assay with a resultant detection limit of ten to one hundred-fold higher than subsequent sets of samples. Because these sources of bioassay error would not likely affect the analytic characteristics of the fluids, the concentrations for estrogen, melatonin, and electrolytes were included in non-bioassay analysis.

Table 3. 1 Sodium, potassium, melatonin, and estradiol in cyst fluids

Cyst ID	Cyst fluid sodium mg/ml	Cyst fluid potassium mg/ml	Na / K ratio in cyst fluid	Melatonin in cyst fluid picomol/liter	17b-estradiol in cyst fluid picomol/liter
1	3.09	0.34	9.1	1293.1	472.6
2	1.00	4.65	0.3	N.D.	549.7
3	2.44	2.14	1.1	84051.7	859.4
7	0.76	5.22	0.2	53.4	397.0
8	0.42	0.09	4.7	127.2	1685.0
9	2.95	2.29	1.3	N.D.	307.7
11	2.76	0.40	6.9	33.2	558.1
12	3.65	0.32	11.4	235	230.0
13	0.16	2.91	0.1	24	440.7
14	0.90	5.06	0.2	141.6	180.2
Mean	1.81	2.34	3.53	8595.9	568.0
Median	1.72	2.45	1.2	90.3	456.7
Mean without #1, #2, #3	1.66	2.33	3.54	87.8	542.7

Results of sodium, potassium, melatonin, and estradiol analysis of breast cyst fluids. Samples for electrolyte determination were diluted either one thousand-fold or two thousand-fold with 1 % nitric acid in double deionized water prior to flame AA analysis. Original concentrations in units of mg/ml of cyst fluid are shown above. Concentrations of melatonin and estradiol are presented in units of picomoles / liter of cyst fluid. The cysts obtained in late fall and winter (#1, #2, and #3) appeared to have a higher melatonin concentration than the remainder collected in the spring months, suggesting a seasonal variation. The melatonin detection limit for sample #1, #2, and #3 was 30 pg/ml while the detection limit for remaining samples was 5.6 pg/ul.

Table 3. 2 Melatonin synthesis from serotonin substrate

	Concentration of melatonin in medium picomole/liter	Cell number (millions)
Serotonin 1	64.3	18.98×10^6
Serotonin 2	70.7	17.02×10^6
Serotonin 3	51.5	21.62×10^6
Control 1	N.D.	21.6×10^6
Control 2	N.D.	19.44×10^6
Control 3	N.D.	11.5×10^6

N.D. = below detection limit of 5.6pg/ml

Proliferation time course of cyst fluid treated MCF-7 cells...

Given that breast cells can synthesize melatonin and that it was present in a wide range of concentrations in patient cyst aspirates, the data in figure 3.1 was compiled to define a proliferation time course for cyst fluid exposed cells. There were two important observations from this data set. First, discernable differences in cell growth were not evident until 90-hours of growth. This was in agreement with the work of others using MCF-7 cells cultured *in vitro* with estrogen containing medium [16;71] and was coincident with near confluent growth of the culture. The second observation was that all of the cyst samples had a higher growth rate than the control set; a finding contradictory to that published by others [91;92]. An explanation of this anomaly probably resides in that the authors used filter sterilized cyst fluid and may have inadvertently removed many lipid soluble bioactive compounds that would have been present in the unfiltered samples used in the present experiments.

Effect of filtration on cyst fluid melatonin concentration

Filtration of GFBD fluids through 0.2 um mesh removes any material of larger size, including bacteria and cellular debris. Since ductal cell secretions are typically apocrine secretory products containing large concentrations of lipid and cellular debris [84], it is likely that the filtration process removed many of the lipid soluble hormones. Table 3.3 lists the results of paired samples analyzed for melatonin concentration with and without filtration. It is apparent from this data that melatonin was substantially removed from the filtered samples. Furthermore, if the loss of melatonin was due to removal of lipid containing apocrine material by the filter, it is highly probable that other lipophilic compounds such as estrogen were also removed. Thus, proliferation data published with filtered cyst fluid does not likely represent the effects of hormones such as melatonin and estrogen, and may not be a true representation of the overall bioactivity of the cyst fluids.

Table 3. 3 Loss of melatonin from cyst fluid after filtration.

	Melatonin concentration unfiltered sample	**Melatonin concentration Filtered through 0.2 um**
Sample 1	1293 pM	N.D.
Sample 2	N. D.	N.D.
Sample 3	84,052 pM	N.D.

N.D. < 30 pg/ml

Cell proliferation and dose response to melatonin

Proliferation data for 16, 40, 90, and 160 hours of growth are shown in figures 3.2 and 3.3. Polynomial regression analysis was used to fit an inverted "U" shaped curve to each sample. The coefficient of determination was greatest for the 160-hour plate with

R^2=0.85 and a significance of p=0.03. Residual analysis identified the regression as a normal distribution with an Anderson-Darling coefficient of p>0.84. The quadratic regression plotted in figure 3.3 implied that melatonin was permissive of MCF-7 cell growth in concentrations less than approximately 1 picomole per liter. At higher concentration (>10 pM), melatonin was associated with dose responsive decreases in cell numbers. This apparent relationship of melatonin to MCF-7 cell growth poses the intriguing possibility of a biologic "switch" with melatonin/mitogen interaction producing cell growth at low melatonin concentration and inhibition at higher concentrations.

TGFβ related to cell number.

TGFβ in the culture medium was postulated to inhibit MCF-7 cell proliferation in the cyst fluid bioassay. Results in figure 3.4 show a significant linear dose-response of cyst TGFβ concentration in medium versus 160-hour cell number. The coefficient of determination (R^2=0.56) was statistically significant with p=0.05 and the regression data was normally distributed with an Anderson-Darling coefficient of p=0.83.

Melatonin versus TGFβ concentrations in culture medium

It was further postulated that culture medium melatonin concentration would correlate to TGFβ levels in support of a causal relationship. Although cyst fluid TGFβ concentration was not necessarily related to that found in culture medium, it was postulated that the two were highly correlated, and more so if melatonin were inducing TGFβ synthesis. Regression analysis of melatonin versus TGFβ in the 160-hour culture medium, however, did not support this hypothesis (figure 3.5). Since other factors could influence culture medium TGFβ concentrations, (e.g. degradation with time, dilution by

TGFβ in FBS, or volume dilution), future studies should evaluate the relationship of melatonin to TGFβ in the cyst fluid.

Table 3. 4 Concentration of melatonin, estradiol, and TGFβ in culture medium and 160 hour cell number.

Cyst ID	Cyst Melatonin in culture medium pMolar	Cyst 17b-estradiol in culture medium pMolar	TGFb pg/ul medium per million cells at 160 hours	Cell count at 160 hours**
Control	0.08		7.61	131,616
7	6.22	23.2	20.55	202,223
11	5.53	62.0	42.23	198,767
9	*0.24	51.3	126.54	147,908
14	23.6	30.0	16.07	188,867
12	27.4	26.8	37.06	158,132
13	2	36.7	7.77	207,233
8	2.65	35.1	8.75	190,530
1	215.5	78.8		178,672
2	*0.24	64.2		272,142
3	14008.6	50.1		198,655

Summary of the data for melatonin, estradiol, and TGFβ concentration in the culture medium, as well as cell number at 160 hours. Cysts #13 was diluted 2X, # 7 and #12 diluted 1.4X and # 8 diluted 8X before preparation of culture medium due to small volumes. The concentrations in table 3.4 reflect actual concentrations in culture medium after dilution. (* indicates samples below detection limit and are reported as ½ detection limit) (**Cells were initially plated at $5*10^4$ per well)

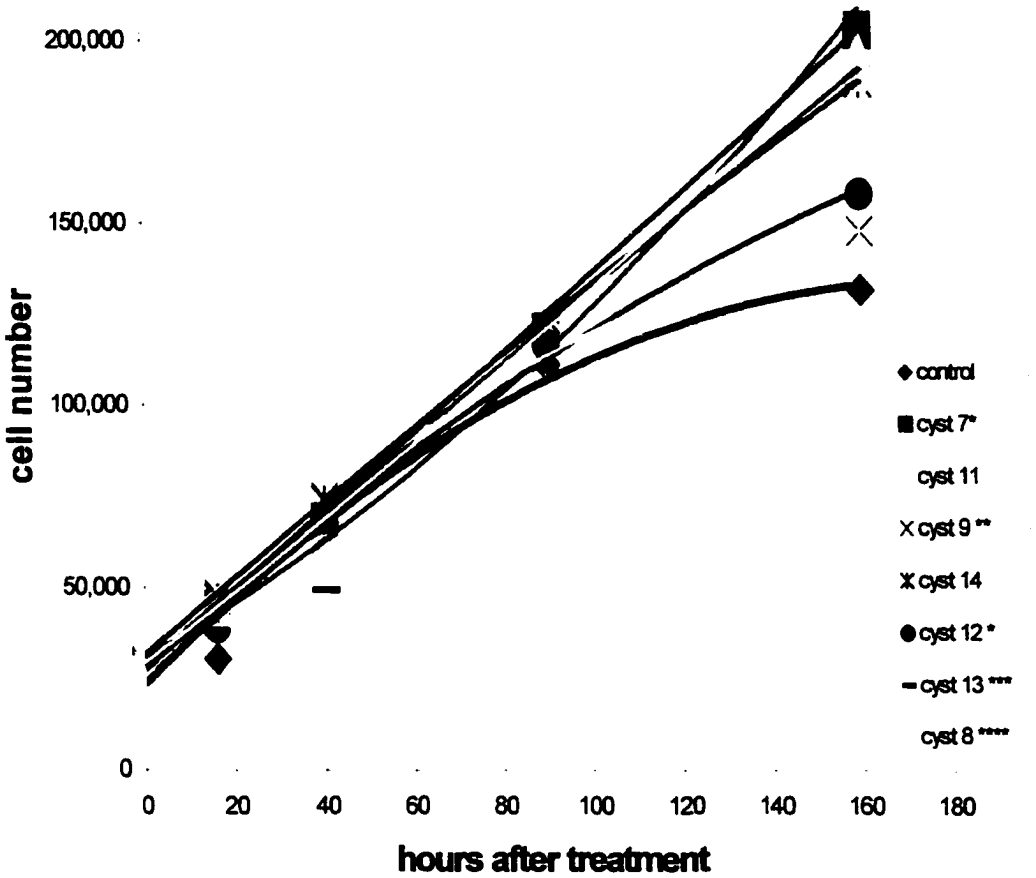

Figure 3. 1 Proliferation time course.

Growth curves for GFBD fluid treated MCF-7 cells. Cells were plated in quadruplicate wells and counted electronically at 0, 16, 40, 90, and 160 hours of growth. The 160-hour plate was re-fed with fresh medium-cyst fluids on the fourth day. Discernible differences in cell number were not present until about 90 hours of growth.

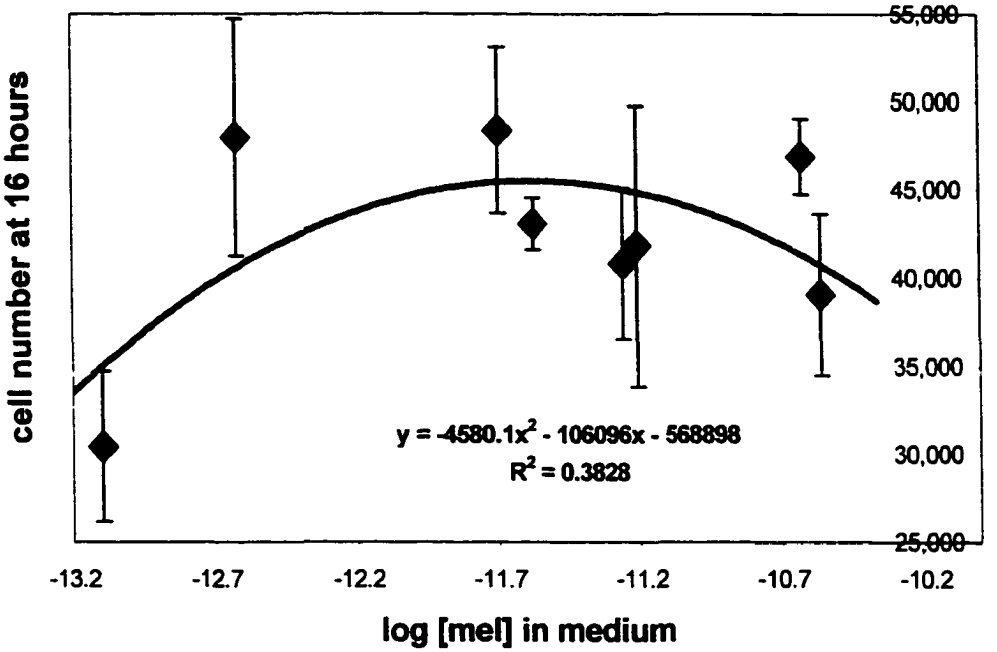

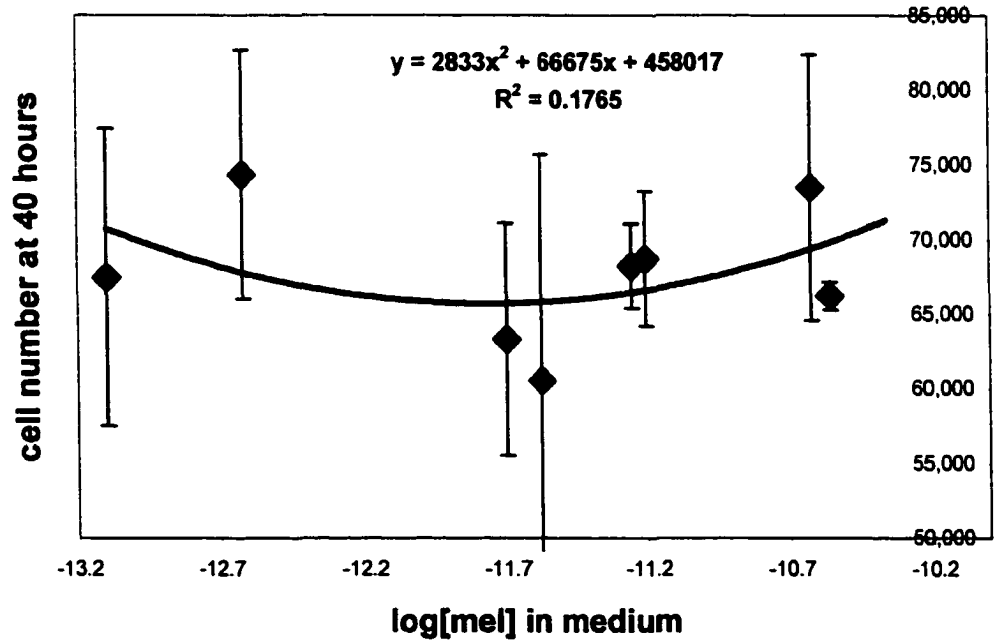

Figure 3. 2 Melatonin versus cell number at 16 and 40 hours.

Polynomial regression plots of logged melatonin concentration in the medium versus cell number at 16 and 40 hours of growth. Significant associations were not present at these time points, although the regression fit at 16 hours was suggestive of the 90 and 160-hour curves (figure 3.3).

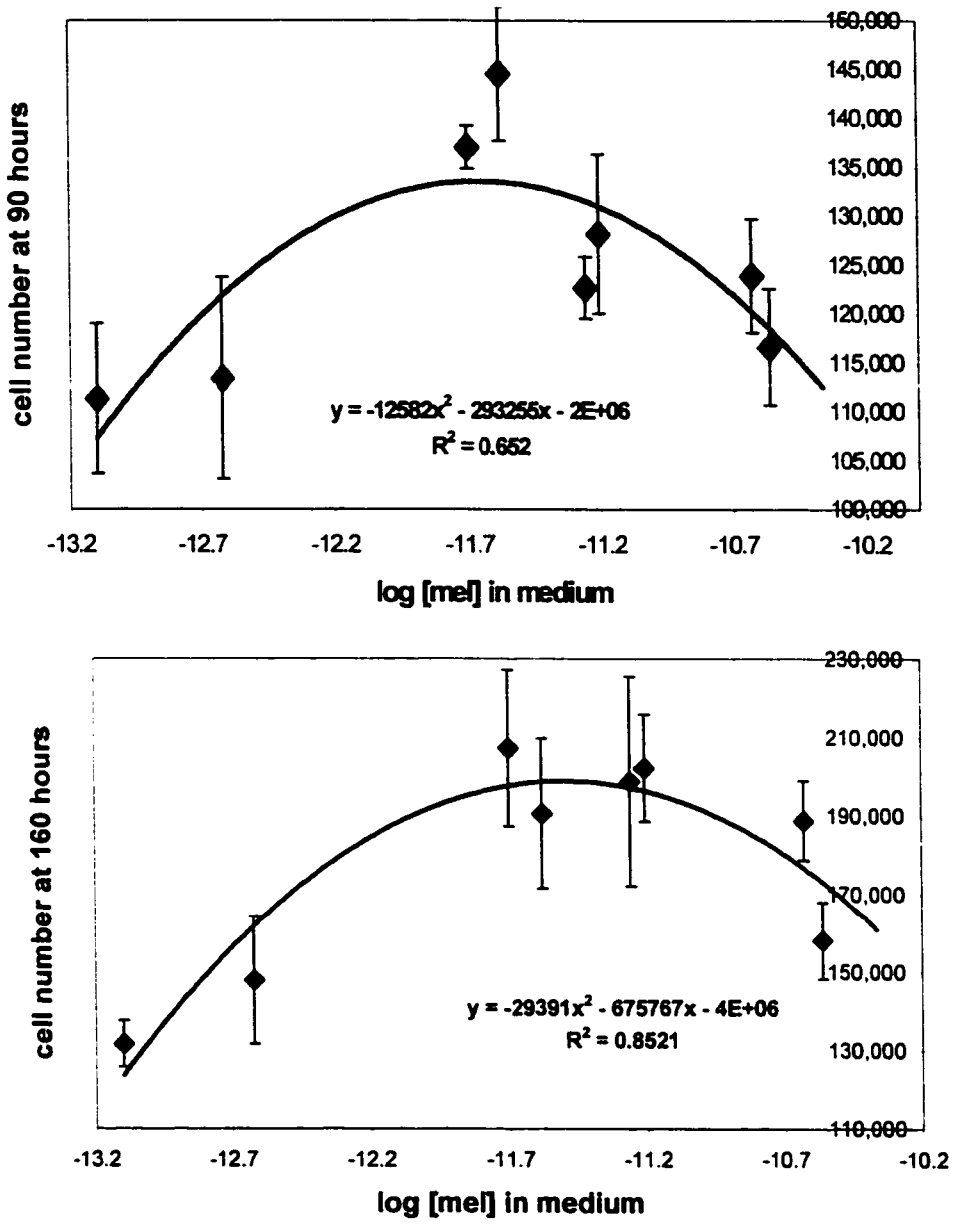

Figure 3. 3 Cell number vs. melatonin at 90 and 160 hours.

Polynomial regression plots of logged concentration of culture medium melatonin and cell number at 90 (upper) and 160 (lower) hours of growth. The coefficient of determination at 160 hours was R^2=0.852 with the significance of the regression p=0.03. Residual analysis demonstrated normal distribution of the regression data (Anderson Darling p=0.84). The growth inhibition suggested a critical regulatory point of mitogen mediated MCF-7 cell growth between 1 and 10 pM melatonin concentration.

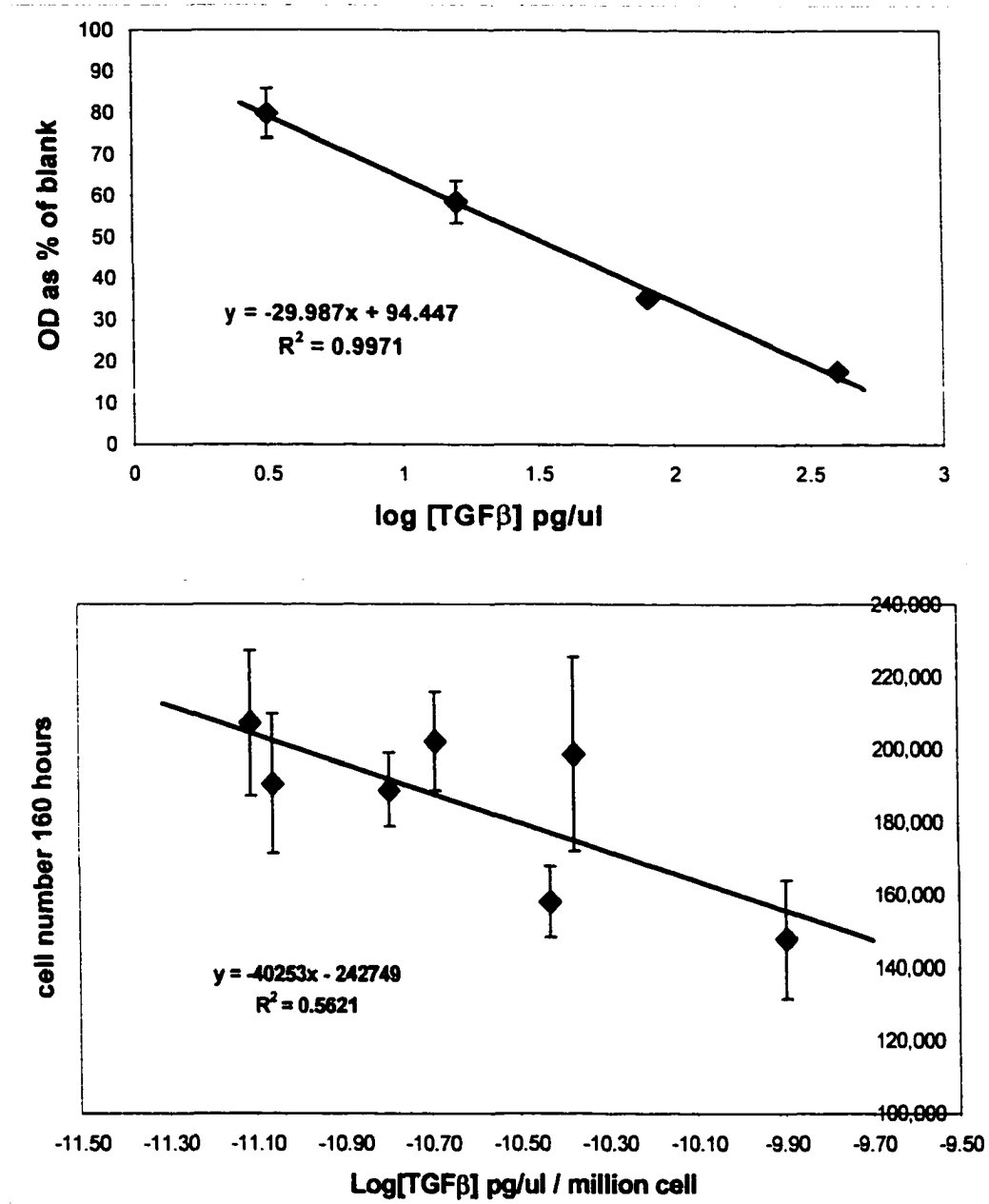

Figure 3. 4 TGFβ standard curve and TGFβ vs. cell number.

Standard curve for TGFβ analysis (upper). Error bars represent duplicate standards and are not visible under the lower two data points. The regression was linear with $R^2 > 0.99$. The lower chart is a linear regression of logged TGFβ concentration from culture medium collected over 160 hours versus cell number. The coefficient of determination (R^2=0.56) was a significant association with p=0.05 and the regression normally distributed (Anderson-Darling p=0.83).

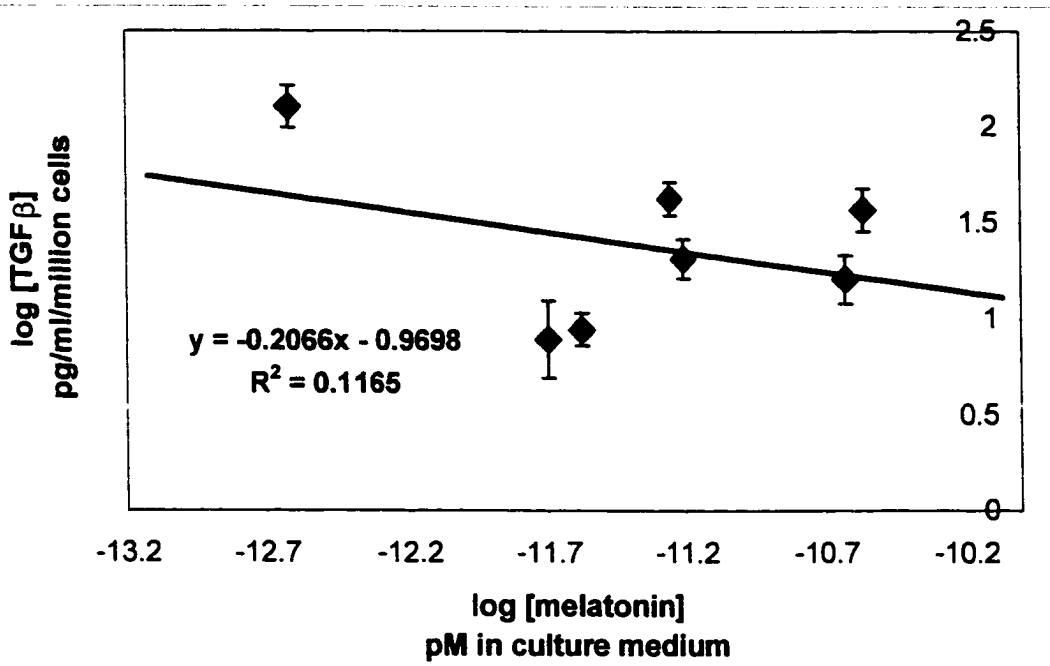

Figure 3. 5 TGFβ vs. melatonin.

Linear regression plot of logged TGFβ concentration collected from culture medium over 160 hours and logged initial concentration of melatonin. Error bars represent one standard deviation of quadruplicate samples. The regression association was not significant ($p>0.05$) and $R^2=0.12$.

Cyst concentration of melatonin versus 17β-estradiol.

The relationship of cyst melatonin and 17β-estradiol was not significant (figure 3.6; $R^2=0.0096$) although all cyst samples contained substantial amounts of estradiol (see table 3.1). Several factors could confound this lack of association. For example, estrogen is likely to vary within the cysts over the course of menstruation (see discussion in Chapter 1), while cyst fluid melatonin concentration would be less apt to change during a 12-hour diurnal rhythm. Exploration of this confounder would only be possible if patient data were available identifying the day of menstrual cycle that the sample was

collected. Since this information was not available in these preliminary studies, associations with menstrual cycles were not done.

Estradiol in culture medium association with TGFβ, Na/K ratio, or to cell number at 160 hours.

Analysis of estrogen concentration in the breast cyst fluid did not show significant linear correlation to TGFβ levels, Na/K ratio, or to cell number. Figure 3.7 indicates the result of regression analysis of 17β-estradiol to the growth inhibitory factor, TGFβ, in culture medium. The association was not significant with R^2=0.25 and $p>0.05$. Likewise, the association of estradiol and Na/K ratio was not significant in figure 3.8. Cell numbers, however, in cultures treated with cyst fluids (containing estrogen) were significantly higher (mean of cyst treatments vs. mean of control $p<0.05$). This did not appear to be a linear relationship with a regression coefficient R^2= 0.01 (figure 3.9).

These findings suggested that mitogens such as estrogen in the cyst fluids do indeed increase MCF-7 cell growth but not necessarily in a dose responsive manner. Furthermore, the data did not indicate any relation of estrogen to the mito-inhibitory agent TGFβ, nor to the putative cancer risk factor, Na/K ratio.

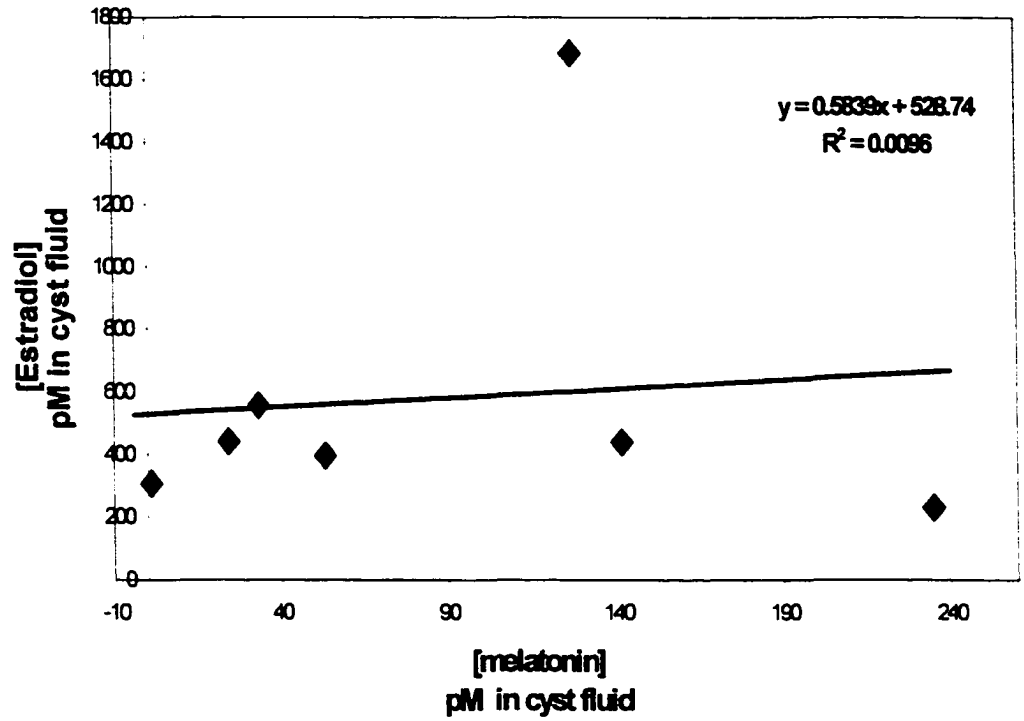

Figure 3. 6 Melatonin vs. 17β-estradiol in cyst fluid samples.

Concentrations of melatonin and estradiol from GFBD cyst fluids compared by linear regression analysis. The coefficient of determination R^2= 0.00096 was not significant with p=0.51. Residual analysis demonstrated that the regression was not normally distributed (Anderson-Darling p = 0.001). Re-analysis by non-parametric rank correlation (Spearman's rho) ρ=0.1 again showed no significant relation between estradiol and melatonin concentrations.

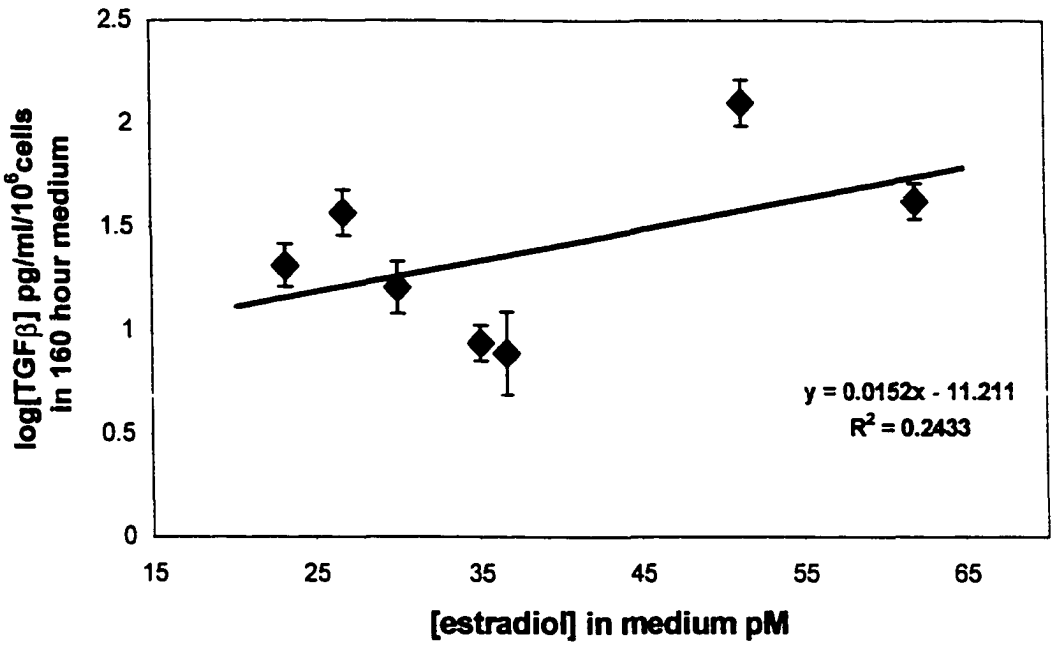

Figure 3. 7 Association of 17β-estradiol vs. TGFβ in culture medium.

Regression analysis of culture medium 17β-estradiol concentration versus logged concentration of medium TGFβ collected over 160 hours of cell growth. Error bars represent one standard deviation of TGFβ concentration for quadruplicate samples. The regression association was not normally distributed. Non-parametric analysis (Spearman's rho) failed to show significant correlation with p=0.18.

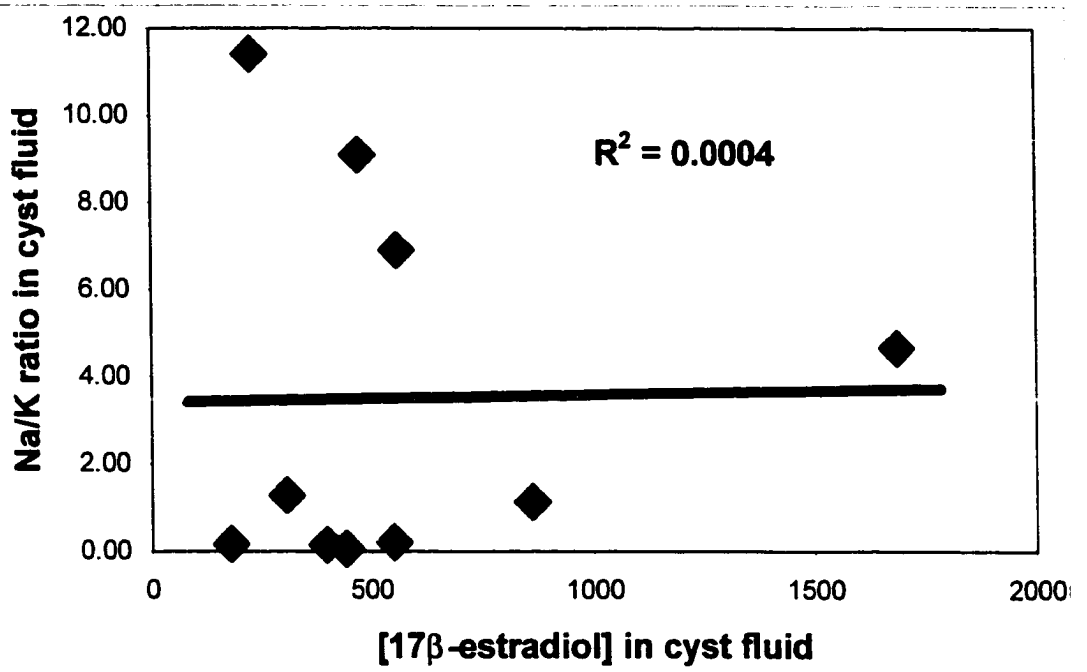

Figure 3. 8 17β-estradiol vs. Na/K ration in cyst fluids.

Association of estradiol concentration and Na/K ratio was not significant by regression analysis (R^2=0.0004). Cyst fluid sodium-potassium ratios did cluster in high electrolyte (Na/K>3.0) and low electrolyte (Na/K<3.0) groups, but there was no relation of mean estradiol by Student's T test.

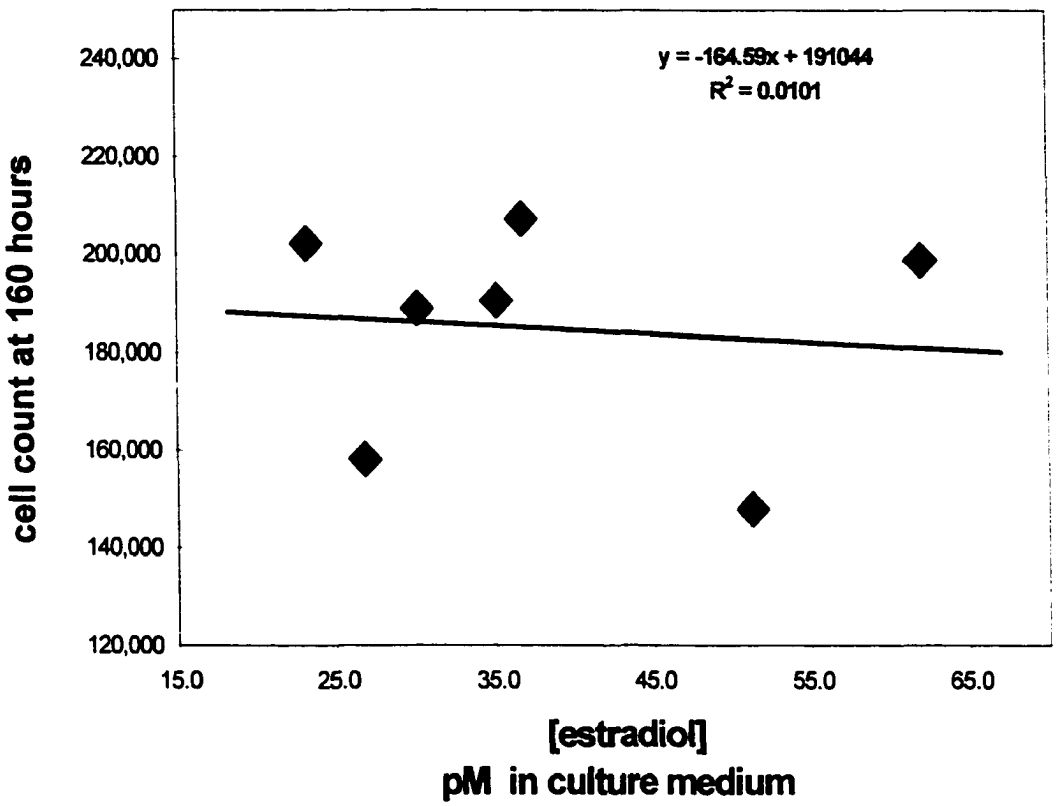

Figure 3. 9 Estradiol vs. cell count at 160 hours.

Regression analysis of estradiol concentration in the culture medium and cell number at 160 hours of growth. Coefficient of determination was $R^2 = 0.01$ and was not significant with $p = 0.83$. Residual analysis indicated a normally distributed regression data set (Anderson-Darling $p = 0.123$).

Ratio of sodium and potassium to cancer cell growth.

To determine the effects of Na/K ratio on the MCF-7 cell bioassay, cyst fluids were diluted with double deionized (DDI) water and analyzed by flame ionization atomic absorption spectroscopy. Standards were prepared from commercially available solutions (Fisher, Houston TX) and diluted to prepare standard curves (figure 3.10). All ten cyst samples were used in the analysis due to the unlikely probability of changes in electrolyte content due to storage artifact. Na/K ratio was compared to 160-hour cell numbers by

regression analysis with no significant association (figure 3.11). To further ensure that artifact was not responsible for changes in electrolyte content of samples 1, 2, and 3, the regression was repeated excluding these three with no change in results (data not shown). Additionally, although it was possible to divide the cysts into ratios greater and less than 3.0 as described by others [97], there was no association of mean cell number between high and low electrolyte ratios by Student's T test. Thus, the current data with limited sample size shows no association of MCF-7 cell growth to NA/K ratio.

Could Na concentration have altered cell growth by changing the culture medium osmolarity?

GFBD fluids may contain substantial quantities of sodium and potassium as was found in table 3.1 data. To assure that changes in MCF-7 cell growth were not from alterations of culture medium osmolarity, the analyses in figure 3.12 were performed. Sodium concentration was not related to cell number at either 16 or 160 hours (R^2=0.18, p=0.19 and R^2=0.23, p=0.16 respectively). The calculated changes in culture medium sodium concentration due to the most and least concentrated cysts were 23 meq/l and 7meq/liter (normal concentration = 135-145 meq/l). Similar analysis of potassium concentration showed no significant association to cell growth.

Melatonin association with Na/k ratio.

Regression analysis of melatonin concentration and Na/K ratio in figure 3.13 identified no apparent linear association. It is notable that the cyst fluids readily divided into low and high (Na/K > 3.0) groups, however, analysis of mean melatonin was not significantly different between groups by Student's T test.

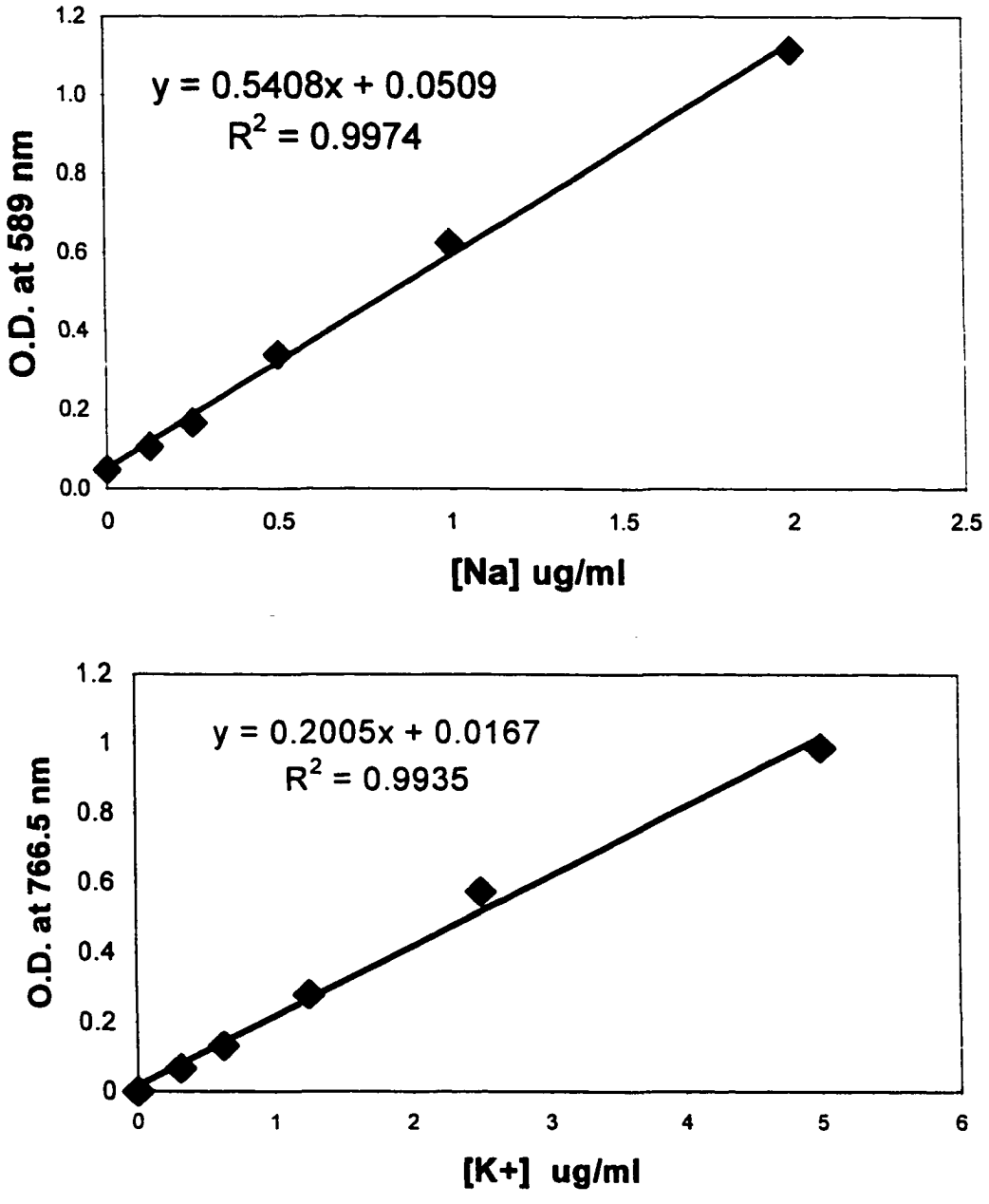

Figure 3. 10 Standard curves for atomic absorption analysis of sodium and potassium.

Standard curve for atomic absorption analysis of sodium (upper) and potassium (lower) were linear with R^2>0.99. Commercial standards were diluted in 1% nitric acid and double de-ionized water. Samples were diluted 1000-2000x in the same matrix and concentrations calculated from the regression analysis formulas as follows:

[K] ug/ml = (OD - 0.0167)/0.2005
[Na] ug/ml = (OD -0.0509)/0.5408

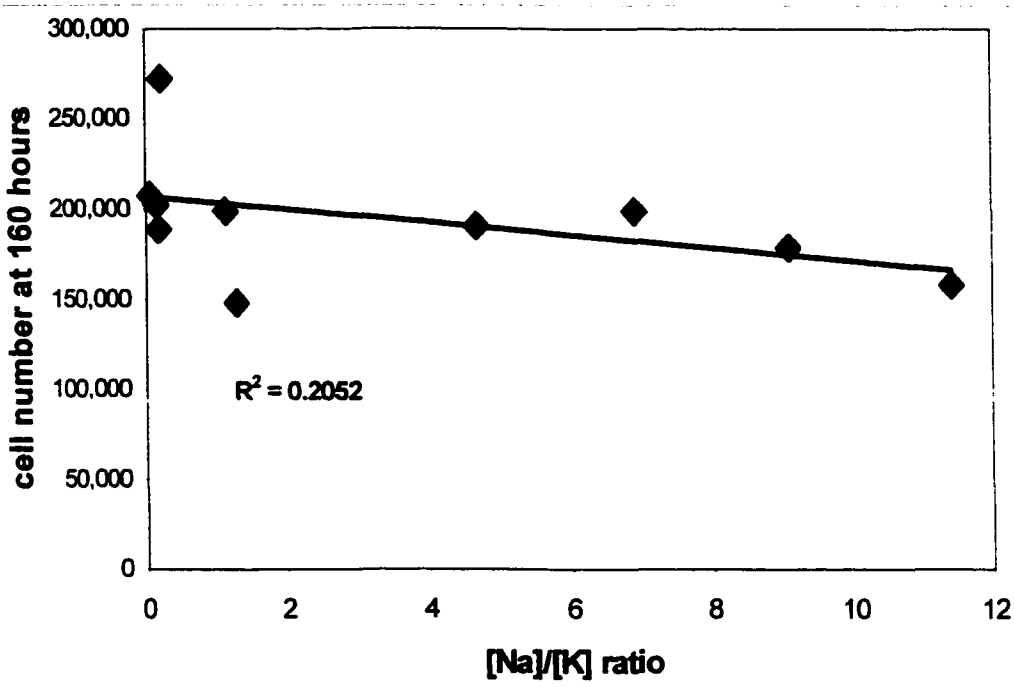

Figure 3. 11 Na/K ratio vs. cell number at 160 hours.

Linear regression plot of sodium-potassium ratio versus cell number. The coefficient of determination was R^2=0.20 and the association was not significant with p=0.19. The cysts can be divided into groups with Na/K ratios of greater and less than 3.0, but no relationship was found to MCF-7 cell proliferation by either Student's T test of [Na/[K] means (not shown) or by regression analysis.

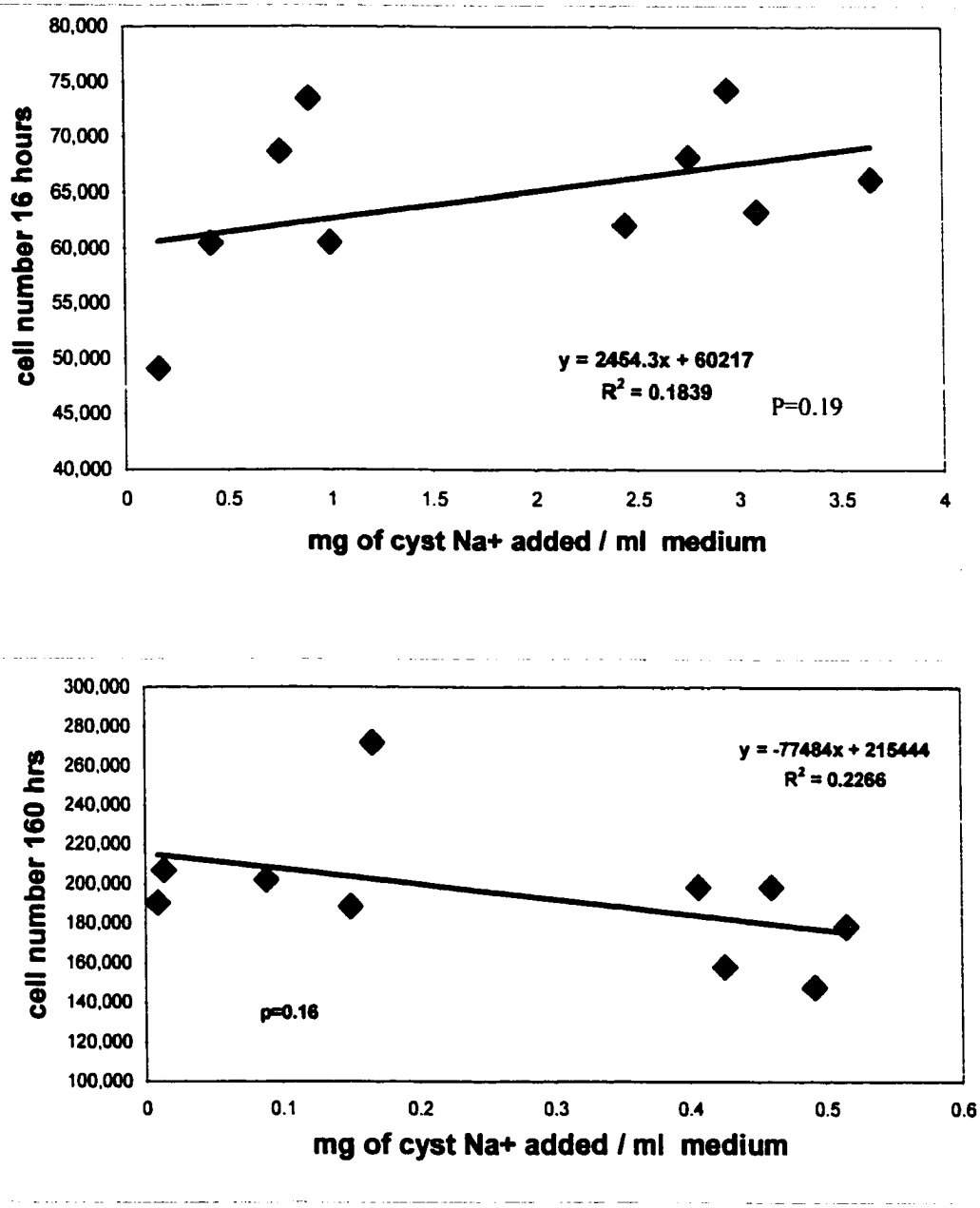

Figure 3. 12 Growth effects of Na concentration of added cyst fluid.

Regression plots are shown of mg sodium added per ml medium versus cell number at 16 hours (upper) and 160 hours (lower). The slopes of these curves were not significant at either time point (p=0.19 and p=0.16) confirming the assumption that sodium concentration would not affect growth due to osmolar changes. The highest cyst sodium concentration was 3.65 mg/liter = 91 meq/liter and lowest was 0.16 mg/ml=4 meq/liter. Culture medium dilution with the cyst fluid resulted in a calculated sodium change of approximately 7 meq/liter and 23 meq/liter. (normal levels = 135-145 meq/l)

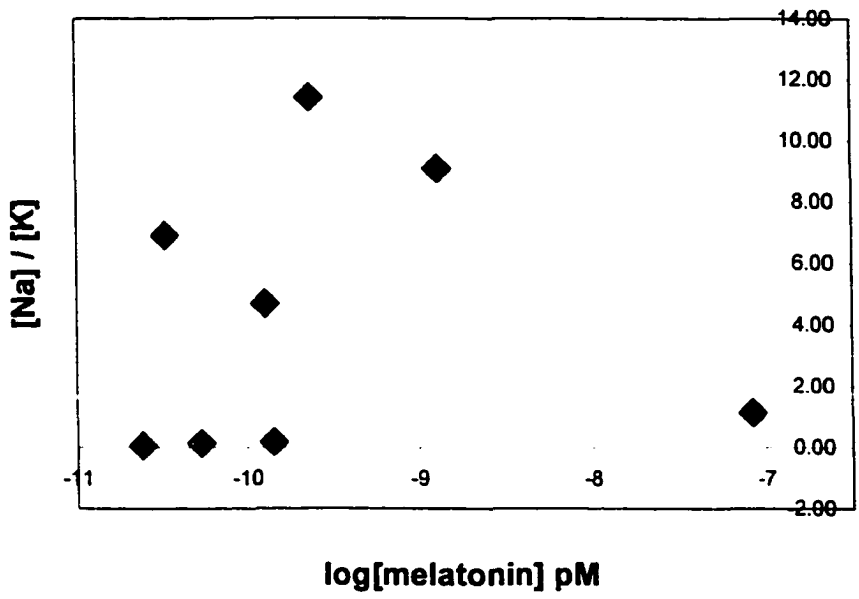

Figure 3. 13 Melatonin versus Na/ K ratio.

Scatter plot of cyst fluid log melatonin concentration and sodium-potassium ratio. There was no significant relation by either regression analysis or non-parametric rank correlation (Spearman's rho). Cyst fluid Na/K ratios were readily divided into two groups with ratios above and below 3.0 but no relationship was found with melatonin concentration by Student's T test analysis of group means.

DISCUSSION.

Previous studies (see Chapter 1) implied a possible role for melatonin in cancer cell growth regulation at an early time point in estrogen-free culture medium. Chapter 2 suggested an effect by melatonin in inducing differentiation in a small percentage of cultured MCF-7 cells. Other researchers have reported effects by melatonin in inhibition of MCF-7 cell proliferation in estrogen containing medium [10;18;42;83], down regulation of estrogen receptor [14;71], and up regulation of TGFβ [11]. In combination, these findings suggest that melatonin may serve a cancer inhibitory function in the breast. The current experiments, therefore, were conducted to establish bioassay methodology to

study melatonin effects of breast ductal fluids on the proliferation of MCF-7 breast carcinoma cells.

This set of experiments provided preliminary information for development of a GFBD fluid bioassay...

The set of ten samples in this study were used to establish laboratory methodology, collect preliminary data, and examine the feasibility of conducting a larger population based bioassay-biomarker study. Several intriguing and novel findings resulted from the data described herein, as well as the methodology required for performing the MCF-7 cell bioassay. First, procedural notes in the methods and material section outline techniques for preparation and handling of cyst fluids, conducting proliferation bioassay, and biochemical analysis of the samples. Secondly, suggestions of the data from this sample set pose important questions for future studies. For example, how does the seasonal variation of melatonin concentration relate to cancer cell growth? Is there a growth permissive-non-permissive "switch" concentration of melatonin in the cyst fluids between 1 and 10 pM concentration? Is TGFβ concentration in cyst fluid a biomarker of future cancer risk? Do seasonally high winter melatonin concentrations have a greater affect on cancer cell growth than the springtime samples used in these experiments?

Is melatonin present in GFBD cyst fluid?

The first assumption required for a bioassay was that the ductal cell fluid secretions were comparable to GFBD fluid and that melatonin was present in the fluid. Analysis of ten GFBD fluid samples obtained from the University of Colorado Health Sciences Center revealed that melatonin was indeed present in the fluids, and surprisingly, in concentrations as high as 86 nM (Table 3.1). Coupled with evidence suggesting the similarity of GFBD fluid to nipple aspirates (discussed in introduction), this defined a

role for GFBD fluid in bioassay-biomarker studies of cancer cell growth. Of further significance, GFBD fluid represents the breast micro-environment of 7% of the population and may represent ductal secretions for 70% of all women.

Can MCF-7 cells synthesize melatonin from serotonin?

A second assumption of melatonin's role as a cancer cell growth modifier was that ductal cells were able to actively concentrate and/or synthesize the hormone. If, for example, the presence of melatonin in cyst fluid was due to random accumulation, then its concentration could not be responsive to growth stimuli of the ductal micro-environment. Therefore, the hypothesis was posed that MCF-7 cells have the enzymes necessary for biosynthesis of melatonin from its precursor, serotonin. It was reasoned that a transformed cell, such as MCF-7, would not develop a functional mutation detrimental to its own growth. Hence, the ability of MCF-7 cells to synthesize melatonin strongly suggested that non-transformed ductal cells also have the same characteristic.

Hormone alterations from preparation of cyst fluid samples by filtration...

Growth effects of GFBD fluids on breast cells relate to a number of water soluble peptide growth factors and lipophilic hormones as discussed in the previous pages. An important consideration, therefore, was the preparation of the fluids to maintain their original content of growth regulating agents. Table 3.3 lists the analytic results of three cyst samples prepared either with or without sterile filtration. It was obvious from this data that filtration causes very substantial losses of melatonin. The most likely source of the lost lipophilic hormone was removal of cellular debris from the apocrine cystic secretions. It was further likely that other steroid hormones such as estrogen concentrated in lipid material would also be retained on the filter membrane and equally

lost from the specimens. Thus, filter sterilization of cyst fluids will undoubtedly result in erroneous interpretation of hormonal responses in cyst fluid bioassay of MCF-7 cell growth.

Two previous investigations of cyst fluid growth effects on MCF-7 cells [91;92] followed similar procedures to those described herein with the exception of filter sterilization. The authors demonstrated an inhibition of cell growth compared to HBSS treated control cultures in contrast to the significantly increased cell numbers that we observed in the current studies. This growth inhibition could have been due to endogenous peptide growth factors such as TGFβ, but probably does not reflect the true interactions of hormones such as melatonin and estradiol. Thus, conclusions about cancer cell growth in the presence of GFBD fluid should consider alterations of fluid hormone content due to filtration artifact.

Storage and handling of samples...

Stability of cyst fluid samples was not directly addressed in the present experiments but must be considered suspect in specimens stored for long time periods or those that are thawed and refrozen. First, the fluid contains a number of proteolytic enzymes [113], which would be likely to degrade peptide growth factors but not steroid or indole hormones. Additionally, compounds such as retinoids, indoles, and steroids may be more stable in storage, but could undergo photolytic degradation if exposed for long periods to laboratory lighting. Thus, samples with prolonged time before freezing, exposure to light, or those that are thawed and refrozen would likely have differential degradation of growth active agents.

Some suggestion of this effect was present in cell proliferation data from samples #1, #2, and #3 (table 3.4). It was obvious that sample #1 and #3 have melatonin concentrations at the very high levels previously associated with significant growth inhibition of MCF-7 cells [4;12;18]. Surprisingly, the 160-hour MCF-7 cell numbers were as high or higher than any other samples. It was of concern that these specimens were stored for over twelve months and were thawed twice before the bioassay cell proliferation studies. Therefore, until further controlled experiments are undertaken to define the stability of GFBD fluid samples, it should be assumed that these samples are labile.

Time course of cyst fluid treated MCF-7 cell growth...

Proliferation curves in figure 3.1 failed to show substantial growth association to melatonin concentration before the 90-hour time point but good separation of the 160-hour curves. This agreed with *in vitro* melatonin treated MCF-7 proliferation data showing melatonin growth inhibition on the fourth to sixth day of culture [16;125]. There were two points made by this observation. First, bioassay studies should be conducted through at least 7 days of culture to determine growth inhibitory effects of melatonin. Secondly, the biologic mechanism of growth inhibition at this time was not likely a direct effect of estrogen receptor down regulation since melatonin effects on ER appear as early as six hours [71]. The fourth to six day of culture coincides with monolayer confluence and may suggest interactions of melatonin and growth factor signal transduction pathways related to contact inhibition of the epithelial cell growth. Hence, bioassay data on growth factor and hormone interactions from cyst fluid treated MCF-7 cells may offer future biologic insight to the modulation of cancer cell growth.

Modulation of MCF-7 cell growth by GFBD cyst fluid melatonin...

The melatonin concentration dose response data in figure 3.3 depicts an inverted "U" shaped curve with peak values between 1 pM and 10 pM concentrations. Interestingly, others have shown similar growth inhibitory effects of melatonin in MCF-7 *in vitro* studies becoming obvious at 1 to 10 pM concentration in culture medium [16;18]. At melatonin concentrations less than 1 pM on the left side of the figure 3.3 curve, it appeared that growth was stimulated, but at the higher concentrations, growth was inhibited. This relationship posed an interesting hypothesis that melatonin may serve the function of a growth permitting "on/off" switch whereby low levels allow proliferation of breast cells and high levels inhibit growth. It is notable that melatonin receptors, have been described with high affinity (K_d approximately 300 pM) and low affinity (K_d approximately 6 nM) binding [19-21]. The 1-10 pM "on/off" switch-point suggested by the current cyst fluid data would be a likely concentration to see the beginning of downstream high affinity receptor effects. Likewise, the maximum *in vitro* growth inhibition of MCF-7 cells in Chapter 1, figure 1.1 was at 100 nM concentration and would correspond to near saturation of the low affinity receptor. Thus, further studies in cancer and non-transformed cells could provide valuable insight to the physiologic mechanisms of breast cell proliferation controlled by cyst fluid melatonin.

Melatonin as a biomarker of breast cancer risk in GFBD patients...

The value of melatonin as a biomarker is complicated by the apparent variability from seasonal concentration, which was of a magnitude large enough to overshadow any individual variations. Future study, however, may determine specific melatonin interactions with hormones (e.g. estrogens) or growth factors (e.g. EGF or TGFβ) that define its growth-controlling mechanisms, and thus, allow use of the interactions as

biomarkers. Furthermore, multivariate approaches to data analysis could be used to adjust for seasonal contributions to growth rate and contributing effects of other agents. In conclusion, melatonin does indeed appear to be directly associated with cancer cell proliferation *in vitro*. Future study is needed to define specific interactions with downstream targets, and to unravel the effects produced by multiple receptor binding and seasonal contributions to the growth inhibition.

TGFβ as a biomarker of MCF-7 cancer cell proliferation...

TGFβ is a member of a superfamily of growth-modulating factors with multiple isotypes (summarized in ref [25]) and at least three surface receptors [25]. Its signal transduction pathways are not completely understood, but appear, at least in part, to modulate epithelial cell growth by regulating c-*myc* transcription, Rb phosphorylation, and cyclin dependent kinase activity [25].

*TGF*β analyzed in the conditioned cell culture medium resulted from TGFβ produced by the MCF-7 cells, TGFβ from cyst fluid, and TGFβ from the FBS containing medium. However, there are three caveats to the assumption of TGFβ bioassay results accurately defining cancer risk. First, individual variations in the GFBD patient's ability to respond or to synthesize TGFβ would not be reflected in bioassay data. In this case, the cell model response would over or under-represent the contribution from the patient. Secondly, individual patients may produce high levels of TGFβ in response to under-expressed receptor, thus showing an exaggerated MCF-7 response. Indeed, failure of TGFβ receptor expression has been previously defined in the progression of breast and colon cancer [118;119]. Finally, individual patients may have normal TGFβ synthesis as well as response to receptor, but have altered TGFβ inducing factors such as melatonin.

The bioassay results of this scenario would show abnormally high TGFβ concentrations from the MCF-7 cells.

In spite of these potential sources of error, data from the current set of experiments did indeed demonstrate a significant dose responsive association of TGFβ and MCF-7 cancer cell growth. Figure 3.4 shows a linear inverse association of cell number and TGFβ in 160-hour cell culture medium. Future studies to examine this relationship will require comparison of cyst fluid TGFβ and cell culture medium content with particular scrutiny of outlying data points that could suggest TGFβ production and receptor abnormalities. In addition, experiments addressing the specific changes associated with melatonin seasonal concentration changes will be necessary to elucidate its full spectrum of activity. Caution, however, must be used with TGFβ bioassay data since some MCF-7 lines have been reported not to have TGFβ responsiveness [127].

Was melatonin concentration associated with TGFβ?

The postulated association of melatonin and TGFβ was not present in this set of experiments. Three possibilities could explain the lack of relationship. First, although melatonin induces TGFβ *in vitro* [11], other factors may overshadow the contribution of melatonin. A second potential error in TGFβ analysis of culture medium was the unknown stability of the growth factor at 37^0 culture conditions, thus limiting the measurable differences between samples. Finally, the relationship may not be robust enough to identify with only seven samples. Studies with larger sample size and analysis of cyst fluid TGFβ content will undoubtedly confirm or disprove this association.

Bioassay of MCF-7 growth association to 17β-estradiol...

Although dose responsive associations of estrogen and cell number were not found, it was apparent that the cyst fluid had a mitogenic effect on the MCF-7 cells (figure 3.9). Two hypotheses for future study arose from this observation. First, it is possible that some cysts could represent a higher cancer risk to patients because of exceptionally high estrogen. For example, cyst #8 had estradiol content of over 1.6 nM and was well beyond the range in the remaining samples. A second hypothesis would associate the higher risk patients with decreased mito-inhibitory agents. Thus, future studies must provide an understanding of the balance between mitogens (e.g. estrogen) and mito-inhibitors (e.g. melatonin or TGFβ).

Was there any relation of estradiol, Na/K ratio, or TGFβ?

There was no significant association of cyst fluid estradiol to either Na/K ratio or to TGFβ levels (figures 3.7 and 3.8). One explanation of the insignificant relationship was that culture medium estradiol levels were within a range of 23 to 78 pM (table 3.4) and may have not varied greatly enough to initiate biologic variability. Exploration of this hypothesis will be possible in studies with larger sample size that will undoubtedly provide a wide range of estrogen concentrations (cyst estrogen concentrations in table 3.1 ranged from 180 pM to 1.68 nM).

Was Na/K related to MCF-7 cell growth?

The previously postulated association of Na/K ratio and breast cancer [100] was not supported by the MCF-7 cancer cell proliferation data in these studies. Figure 3.11 demonstrates a 160 hour regression plot of Na/K ratio versus cell number with a slope significance of p=0.19. The curve hinted at a weak linear relationship that may prove

more robust with a larger number of samples, although the relationship may prove to be an association with osmolarity of the MCF-7 cell growth medium.

Was cell growth affected by electrolyte osmolarity due to Na concentration?

GFBD fluid samples contained 4 to 91 meq/liter of sodium (0.16 to 3.65 mg/ml shown in table 3.1) compared to an approximate culture medium concentration of 140 meq/l. In diluted medium, the sodium concentration would decrease by 5% to 16%. To address the question of sodium induced growth effects, regression analysis data showed no significant association between the mg sodium added to culture medium and cell number at 16 and 160 hours of growth (figure 3.12). Thus, it was highly unlikely that any changes in MCF-7 growth described in the present study are due to osmolar effects of sodium.

Was Na/K ratio related to melatonin concentration?

Because electrolyte ratios have been proposed as breast cancer risk factors by some investigators, Na/K ratios were included in the present study as a correlation endpoint for other agents potentially related to cancer risk. Figure 3.13 graphically presents the correlation data of cyst fluid melatonin versus sodium/potassium concentration. The association was not significant ($p>0.05$) and presented no suggestion that melatonin concentration was related to electrolyte concentration. It is however, worth noting that Na/K ratio in figure 3.11 was not significantly associated with MCF-7 cell growth. Thus, the lack of melatonin relationship to electrolyte ratio makes no implication about melatonin-cancer growth effects because, at least in this study, Na/K ratio is not associated with MCF-7 breast carcinoma cell growth

CONCLUSION.

In vitro bioassay of GFBD fluid provides a novel means to study cancer risk...

Bioassay of GFBD fluid with the MCF-7 breast carcinoma cell model provides a novel approach to the understanding of breast cancer risk in GFBD patients. First, fluid samples allow biochemical analysis of the ductal epithelium micro-environment. Secondly, patient data, when available, could define parameters for epidemiological data correlating to bioassay results. Thirdly, *in vitro* proliferation and cytokine production can be measured in response to a simulated micro-environment. Finally, bioassay procedures allow mechanistic insight to cancer cell biology responses to components of ductal cell secretions.

In summary, the significant findings of the present study...

There were a number of important points determined by this set of preliminary studies, including both method development and intriguing questions for future research. The following list summarizes the novel findings and considerations for continuing studies with GFBD fluid bioassay:

1. Care must be taken in cell proliferation experiments to avoid loss of lipid material in filtration, loss of active agents during storage, and to ensure appropriate time course evaluation of cancer cell growth.

2. A substantial amount of melatonin was present in GFBD fluid and appeared to have a distinct association with MCF-7 cell growth rate. However, the specific growth relationship may vary with concentration of melatonin, probably due to predominant effects of the high or low affinity receptor, nuclear receptor, or melatonin anti-oxidant activity.

3. TGFβ from cyst fluid treated medium had a significant negative association with cancer cell growth although its production may be due to factors other than melatonin.

4. Cyst fluid (containing estradiol) increased the growth rate of cells over non-cyst fluid treatments, but showed no dose responsive relation to melatonin, TGFβ, or electrolytes.

5. Electrolytes and electrolyte ratios were not related to MCF-7 cell growth, melatonin, estradiol, or TGFβ.

The experiments presented in Chapter 3 provided insight to the role of melatonin and TGFβ as modulators of cancer cell growth. Obviously, in spite of several statistically significant associations, the sample size was small. However, the findings were highly suggestive of growth regulation by these mito-inhibitors, and further defined laboratory methodology for a larger scale investigation of GFBD fluid effects in the MCF-7 cell bioassay.

SECTION II CHAPTER 4

ANALYSIS OF 8-OXOGUANINE ADDUCTS BY GAS CHROMATOGRAPHY MASS SPECTROMETRY

INTRODUCTION.

8-oxoguanine, a cancer biomarker.

DNA base hydroxylation has received recent attention for a putative role in carcinogenesis as well as a value in cancer biomarker studies [128-133]. Specifically, biologic significance has been postulated for base mispairing and mutagenic G to A transitions following oxidation of guanine bases to 8-oxoguanine (8-OHG) [25;130;134]. An alternative to mutation is cellular repair of the damaged DNA by base excision, nucleotide excision, or excision of multiple DNA bases [135] [134] [25]. After repair, the biological marker, 8-OHG, is excreted into the circulation and ultimately in urine [134;136]. Biomarker studies of blood and urinary 8-OHG excretion are therefore of potential value to identify cancer risk populations and to characterize occupational and environmental exposures to DNA damaging carcinogens.

Formation of 8-OHG is suggested to be a biomarker for oxidation of deoxyguanosine by the hydroxyl radical.

The hypothesized path of 8-OHG formation results from hydroxyl radical (OH*) attack on the N=C double bond at the guanine 7-8 position [137-139]. The source of OH* is probably from iron catalyzed intra-nuclear reduction of hydrogen peroxide (HOOH) [137;138;140;141], which is an oxidant by-product of mitochondrial metabolism as well as cytochrome P450 mediated oxidation [134;137;142]. Thus, 8-OHG from xenobiotic metabolism or enhanced aerobic respiration represents a biomarker of respiratory oxidative stress and P450-metabolized environmental chemical exposures in addition to being a marker of cancer risk.

Gas chromatography mass spectroscopy (GC-MS) analysis of 8-OHG.

Precise and accurate analytic procedures are needed to identify the minute quantities of 8-OHG bases in biological samples [143]. GC-MS analysis of 8-OHG is especially valuable because it provides positive identification of the target compound by mass ion spectra as well as retention time [142;144], and further provides excellent sensitivity (low femptomole) with minimal sample requirements (ug quantities) [142-144]. On the other hand, the weakness of GC analysis is the necessity to volatilize the analyte for introduction to the GC column. To provide adequate vaporization, 8-OHG is derivatized into a highly non-polar product with an inherent risk of unwanted chemical interactions during the reaction. In particular, oxidation of guanine may produce excessive quantities of 8-OHG artifact in the analysis [143;145].

The current studies were undertaken to establish QC/QA procedures of 8-OHG analysis.

Although 8-OHG analysis has been an integral part of biomarker population studies [131;132;135], its accurate, precise, and sensitive analysis has not been clearly validated for the analytic techniques used in the studies. Indeed, validation of 8-OHG analytic methodology could be considered a necessary prerequisite for reliable interpretation of population data.

Hydroxyl radical adducts (e.g. 8-OHG) have been identified by various techniques including high performance liquid chromatography, antibody linked assays, and GC-MS. Relative merits of the procedures are discussed elsewhere (review [143]), although well defined quality control data is scarce. With this in mind, the studies presented herein were conducted first to evaluate a commonly used GC-MS method utilizing isotopically labeled 8-OHG as an internal standard with careful attention to precision and accuracy of

the data. Secondly, the experiments were designed to develop and evaluate an isotopic dilution method with modifications and improvements over previously reported analytic techniques. Detailed quality control parameters are presented for both methods with identification and description of error sources.

Analysis of 8-OHG with an internal standard method.

GC-MS analysis of 8-OHG with quantification based on calculations from a pre-derivatized labeled internal standard has been previously reported [128;129;142;143;146]. Procedurally, the method utilizes a labeled derivatized 8-OHG to spike samples and standards, followed by calculations based on mass comparisons of target and qualifier ions (HP Chemstation software as described in methods). Although data from the method has been used in multiple studies [129-132], quality control parameters have not been published for the analytic procedure. Specifically, valid concerns for method repeatability stem from the unexplored stability of the derivatized compound, the unidentified amount of oxidation artifact, and unknown precision and accuracy both between and with-in assays [143;145].

Isotope dilution analysis.

Isotope dilution has been used for two decades to control analytic error in the GC-MS analysis of organic compounds [147]. The isotope dilution principle exploits the identical chemistry of an isotopically labeled surrogate added to the analyte matrix at the beginning of the analysis. Since the chemistry is the same, factors that change the quantity of target analyte, also affect the surrogate by exactly the same degree. When the sample is purified and separated on the GC column, the surrogate and target compound elute together and are introduced into a mass spectral detector. The MS then identifies

relative ratios of surrogate and analyte by the atomic mass difference of the labeled and unlabeled principal and qualifier ions. Thus, the proportion of surrogate recovered is identical to the percent target analyte recovery and results in a very accurate quantification of the compound (reviewed [147]).

Specific aims of the studies.

The primary goal of this study was to explore GC-MS procedures for 8-OHG analysis, and to establish a viable and practical method utilizing the sensitivity and definitive identification characteristics of the gas chromatograph interfaced to a mass spectral detector. Furthermore, the goal was to validate the precision, accuracy, and detection limit of the resulting method, as well as to establish parameters of any weaknesses of the analysis. Specific aims were as follows:

1) Critically evaluate an internal standard method of analysis for precision, accuracy, and stability of derivatized internal standard.
2) Develop methodology and techniques for an isotopic dilution method with modifications of previous reports including the application of a data analysis algorithm, use of dynamic instrument tuning, validation of labeled surrogate storage stability, and definition of daily calibration control standards.
3) Define criteria for 8-OHG analysis including inter-assay and intra-assay precision, accuracy, guanine oxidation artifact, evaluation of column degeneration, and instrument detection limit.
4) Evaluate room temperature derivatization or ethane thiol addition to aid in the control of oxidation artifact.
5) Establish quality control and quality assurance parameters for data analysis.

MATERIALS AND METHODS.

Generally used reagents and supplies were purchased from Sigma, (St. Louis, MO) unless otherwise stated. Gas chromatography supplies and glassware were purchased from Fisher, (Houston TX); VWR, (San Francisco CA); Hewlett Packard, (Wilmington DE); or Pierce, (Rockville MD). Specialty products and standards were purchased as indicated in text.

DNA extraction.

DNAzol extraction.

DNAzol is a complete and ready to use, DNA extraction reagent (Life Technologies, Rockville MD) for cells or tissue. The procedure is based on the use of a guanidine-detergent lysing solution, which permits selective precipitation of DNA from a cell lysate. The reagent protocol is rapid (10 to 30 minutes with recovery of 70 to 100%) and permits isolation of genomic DNA from a large number of samples in large or small volumes [148;149].

Briefly, the procedure for 10 to 30 million cultured cells is as follows. One ml of reagent is added to the cell suspension and pipetted gently to lyse the cells. The DNA is precipitated with 500 ul of absolute alcohol. After 1 to 3 minutes the DNA is visible and may be gently spooled on a pipette tip or adhered to the tube wall. It is then washed twice with 95% ethanol, air dried 5 to 15 minutes, and re-suspended in 8 mM NaOH. DNA concentration is measured spectrophotometrically with one O.D. unit at 260 nm equal to 50 ug/ml of DNA. Purity of the extract is considered good for an absorbance ratio of 260 nm/280 nm between 1.7 and 1.9 [150]. (NOTE: for the data presented herein, purity was considered acceptable with a ratio between 1.8 and 2.0 based on the

calibration of the Beckman Du 640B spectrophotometer in the molecular toxicology laboratory, Department of Environmental Health, Colorado State University).

DNA extraction by high salt method.

The DNA high salt extraction protocol generally follows the method of Miller et al. [151]. The principle involves detergent lysis of the cells, precipitation of cellular debris and proteins with saturated NaCl at 4^0C, and precipitation of DNA with ethanol. Further clean-up is achieved with proteinase K and RNAase digestions and ethanol washes. Briefly, the procedure was performed as follows. Lysis buffer was prepared to contain 10mM Tris HCl, 400 mM NaCl, and 2 mM EDTA at pH 8.0. Prior to use, 200 ug/ml of proteinase K and 0.5% SDS were added to the lysis buffer. For extraction of DNA from 5 to 15 million MCF-7 cells, two ml of lysis buffer was added to the trypsin harvested pellet and incubated for 10 minutes at 37^0C, then pipetted vigorously to homogenize the cell lysate. The proteinase digestion was continued overnight at 37^0C. Saturated NaCl (670 ul) was added to each tube, refrigerated for 15 minutes, then centrifuged at low speed (240 x g) for 20 minutes. The supernatant was transferred to a high-speed centrifuge tube, and 5 to 10 ml of absolute alcohol added. DNA was visible at this point. The tubes were centrifuged at 19,000 x g for 5 minutes, rinsed with 70% ethanol, and re-centrifuged at 19,000 x g. The supernatant was discarded with care to avoid losing the DNA pellet visible at the bottom of the tube. The pellet was air dried briefly and re-suspended in 150 ul TE buffer (10 mM tris-HCl, 1mM EDTA at pH 8.08). One ul each of RNAase A and RNAase T1 was added to each sample and incubated at 37^0C for 1 to 2 hours. (Note: a master 3:1 mix of RNAase A, 10 mg/ml and RNAase T1, 100,000 U/ml was prepared with addition of 2 ul). After incubation, 100 ul of 5M ammonium acetate was added and thoroughly mixed, followed by 500 ul of ethanol. At this point, the

samples were stored or centrifuged and re-suspended in water or TE buffer, and quantified spectrophotometrically by A260 nm absorption as previously described [150].

DNA extraction with chloroform and isoamyl alcohol.

The chloroform:isoamyl alcohol procedure generally followed the original method of Mumur [152] with unpublished modifications from the laboratory of Dr. Don Malins (Pacific Northwest Research Foundation) and Rusty Thomas (Colorado State University). Briefly, 4.5 ml of ice-cold PBS was added to 10 - 15 million cells, followed by 300 ul of RNAase A (1000 U/ml) and 2 ml of lysis buffer. The samples were incubated at 37^0C for one hour prior to the addition of 250 U proteinase K. They were then further incubated at 60^0C overnight. After cooling tubes to room temperature, 1.8 ml of 5M sodium perchlorate was added followed by 10.6 ml chloroform:isoamyl alcohol (24:1) and the tubes were mixed vigorously for one minute. After centrifugation at 1500 RPM for 10 minutes to separate layers, the aqueous layer was transferred to a new tube. The extraction was repeated three times with care to avoid contamination from the lower layer. Following the last extraction, an equal volume of chilled isopropyl alcohol was added and the tubes gently inverted until precipitated DNA was visible. Samples were frozen at -80^0C for 30 minutes then thawed 10 minutes at -20^0C before centrifugation (5000 RPM) in a refrigerated Sorvall high-speed centrifuge. Supernatant was discarded and the tubes dried 5 to 10 minutes. One ml chilled 70% ethanol was added to wash the DNA, followed by centrifugation at 1500 RPM for 10 minutes. The supernatant was again discarded. The pellet was dried 5 to 10 minutes and re-dissolved in either de-ionized water or TE buffer. Purity and quantification was performed as described above.

Analysis of 8-oxoguanine and 4,6-diamino-5-Formamidopyrimidine (Fapy-A) by GC-MS with labeled internal standard.

The internal standard method of analysis used in the present experiments generally follows the procedure described by Malins et al. [129]. The principle involves the separation of tetrakis-trimethylsilated forms of 8-oxoguanine (8-OHG) and Fapy-A by gas chromatography and identification by electron ionization mass spectroscopy with selected ion monitoring (reviewed [142]). Quantification of 8-OHG was calculated from a standard curve prepared with previously derivatized and stored ring-labeled standard, and routine computerized data analysis by Hewlett Packard Chem Station software (quantification menu).

Preparation of standards and calibration curve.

Briefly, standard curve preparation was done as follows. Unlabeled 8-OHG and Fapy-A (Sigma) and N^{15}-C^{13} ring labeled standards (Cambridge Isotope Laboratories inc., Andover MA) were weighed and added to Reacti-vials (Pierce, Rockford IL). A derivatizing solution of BSTFA (N,O-bis[trimethylsilyl]trifluoroacetamide + 1% trimethylchlorosilane) and acetonitrile (3:2) was added to each standard giving final concentrations of 1 mg/ml. The vials were tightly sealed and derivatized at 70^0C for 1.5 to 2 hours. Calibration standards were prepared with unlabeled compound concentration equal to 200, 100, and 50 pg/ul in similar manner, and each then spiked with labeled 8-OHG at 200 pg/ul. The standards were added to GC injector vials and analyzed with instrument conditions as described under "instrument parameters". Labeled compounds used as internal standard were stored at -80^0C after derivatization for additional experiments, but discarded after 7 days.

Sample preparation.

Aliquots of 50 ug DNA were added to duplicate 2 ml gold seal vacules (Fisher, Houston TX), and lyophilized to dryness. The samples were hydrolyzed under nitrogen vacuum in 60% formic acid at 140^{0}C for 30 minutes. After cooling to room temperature, they were transferred to 1.0 ml Reacti-vials and blown to dryness under nitrogen gas. BSTFA:acetonitrile (80 ul of a 4:1 mixture) was added to each vial in addition to 20 ul of the labeled internal 8-OHG (prepared previously and stored until use as described above). The spiked samples were then sealed in Teflon capped vials and derivatized in a 140^{0}C oven, transferred to GC injector vials, and analyzed under instrument conditions as described for standards.

Instrument parameters.

The instrumentation used was a Hewlett Packard (HP) model 6890 gas chromatograph interfaced with an HP6890 mass spectral detector. A 25-meter HP ultra 1 (fused silica, cross-linked methylsiloxane) capillary column was used with 0.2 mm diameter and 0.33 um film thickness. The carrier gas was helium with a constant pressure of 15 psi. Oven temperature was initially 120^{0}C for two minutes then ramped 10^{0}C per minute with a final temperature of 250^{0}C for 5 minutes. Inlet temperature was at 250^{0}C and transfer line temperature was kept at 280^{0}C. Chem Station software was used for data analysis under the "calibration" and "quantification menus". Parameters for identification of 8-OHG were set with a retention time window of +/- 0.5 seconds and target ions of m/z=440 for the unlabeled and m/z=443 for the labeled 8-OHG. Qualifier ion parameters were m/z=455 and m/z=456 for unlabeled and m/z=458 and 459 respectively for the labeled counterparts. An error window was set at +/- 30% of

standard target to qualifier ion ratio. Manual target tune was used to maximize sensitivity at m/z=502 and electron multiplier offset voltage was set at EM=106.

Stable isotope dilution analysis of 8-OHG.

Isotope dilution is an analytic procedure that utilizes the common chemistry of a compound and its stable labeled isotope (reviewed [147]). Since the compounds are chemically identical except for mass, an isotope added at the beginning of a procedure can be used to accurately adjust target compound changes occurring throughout the analysis. In this manner, the full strength of mass spectroscopy may be utilized since the mass spectral detector separates the otherwise identical chemicals by their atomic mass. With regard to these considerations, an isotope dilution GC-MS method modified from previously reported procedures for pesticide analysis [147] and DNA base adducts [153] was developed and evaluated.

Preparation of standards.

Unlabeled 8-hydroxy 2-deoxyguanosine (8-OHdG) was purchased from BEA (Chelmsford MA) and dissolved in double deionized water at a concentration equivalent to 1 nM 8-OHG. The 8-OHdG standard was reported by the manufacturer to be stable for at least six months refrigerated in deionized water. Labeled 8-OHG was purchased from Cambridge Isotope Laboratories inc. (Andover, MA) and dissolved in 1 molar NaOH to a 1 mg/ml concentration, then diluted to a 1 nM stock concentration with final matrix NaOH concentration of 10 mM. After preparation, the labeled stock was stored at 4^0C and used throughout the course of experiments.

Calibration curve.

Standards for calibration curves were prepared with labeled compound (Ry), unlabeled compound (Rx), or a combination (Rm). Appropriate quantities were added to

2 ml gold seal, scored vacules (Fisher) with 20, 10, 5, 2, and 1 ul of the 1 ng/ul unlabeled 8OHdG stock for Rx samples. Ry samples were prepared with 20 ul (20 ng) of labeled 8-OHG stock, and Rm samples received a combination of each 8OHdG concentration plus 20 ng labeled 8-OHG stock. Concentrations of unlabeled 8-OHG in the Rx and Rm final extracts were calculated to be 200, 100, 50, 20, 10 and 5 pg/ul. Formic acid (88%) was added to each standard to give a final concentration of 60%. The vacules were heat sealed under a nitrogen vacuum and hydrolyzed at 120^{0}C in a sand filled heat block for 30 minutes. After cooling to room temperature, the samples were transferred to 300 ul Reacti-vials, the vacules rinsed with 100 ul water, and the vials blown to dryness under a nitrogen gas flow. Derivatization was performed with 100 ul of 3:2 BSTFA:acetonitrile at 120^{0}C for 30 minutes, samples transferred to GC injector vials, and analyzed by GC-MS. All transfers of organic solvents (BSTFA) were performed with glass pipettes and disposable supplies were used where possible.

Instrument parameters.

Instrument parameters were similar to those described for the internal standard method with the following exceptions. In addition to the 25 meter HP ultra 1 column, a 15 meter HP1 (Fisher) and an XTI-5 30 meter (Restek catalog #12223, Belleford PA) were found to perform adequately. Instrument dynamic target tuning (mass 502 @ 9%, mass 219 @ 38%, and mass 131 @ 38%) was employed to provide optimum tuning without tune parameter variability between experiments. Abundance at mass 502 was routinely greater than 75,000 and 10% relative abundance.

Data analysis.

Data analysis was performed with the EPA algorithm for isotope dilution analysis of pollutant residues described in Federal Register EPA guidelines [147]. Briefly, 8-OHG

chromatographic peaks were positively identified by retention time and mass ion spectrum as well as visually evaluated for irregularities associated with poor column performance. Next, abundance ratios of either chromatographic peak height or peak area for the labeled and unlabeled target ions were calculated from the "extract ion" menu of the Chem Station software. The ratios were then used in the quantification algorithm with terms (Rx, Ry, and Rm) defined as follows. Rx was calculated as the ratio (i.e. m/z 440/mz 443) of the pure unlabeled standard at each concentration used. Ry was the ratio (m/z 440/mz 443) for the pure labeled compound at the 200 pg/ul concentration, and Rm was the ratio (m/z 440/mz 443) of labeled 200 pg/ul and unlabeled mixture at each concentration. A calibration curve was constructed from the relative response at each concentration (on the Y-axis) and the standard concentration (on the X-axis). The following formula defines this relationship:

$$RR_{standard}=(Ry-Rm)(Rx+1)/(Rm-Rx)(Ry+1)$$

The relative response for each sample was calculated as the ratio of (m/z 440 divided by m/z 443) and concentration calculated from the regression equation of the standard curve (concentrations vs. $RR_{standard}$). The mathematical power of this algorithm is two-fold. First, it is reliant upon the ratio of the target and labeled compounds, and thereby eliminates error from fluctuation in absolute abundance due to column degeneration. Secondly, the algorithm is designed to compensate for the percentage of unlabeled standard in the labeled 8-OHG, and for the natural label background in the unlabeled product. Calculations for the algorithm were programmed into a Microsoft Excel spreadsheet to provide rapid and efficient analysis of data.

RESULTS.

DNA extraction methods.

Three methods of DNA extraction were compared for ease of use, purity, and yield. Table 4.1 demonstrates comparison data for extraction time, A260/280 ratio, repeatability, and technical skills required for each procedure. The results of all three methods were nearly identical for average purity (i.e. A260/280), and for repeatability (standard deviation of the A260/280). The DNAzol procedure was the quickest and required the least technical ability, but required a basic solution (8 mM NaOH) for complete solubility of the extracted DNA. On the other hand, the chloroform method was technically more difficult and qualitatively gave the poorest recovery, but the DNA was readily dissolved in water or buffer. In comparison, the high salt extraction technique required minimal laboratory skill and intermediate time for extraction with qualitatively excellent yields of DNA. Since all of the three methods were suitable for 8-OHG DNA extraction, laboratory preference dictated the use of the high salt technique for the experiments described herein.

Table 4. 1 Comparison of DNA extraction methods.

	High salt extraction n=5	**DNAzol n=13**	**Chloroform isoamyl alcohol n=4**
Average A260/280	1.9223	1.9222	1.9401
Standard deviation of A260/280	0.0511	0.073	0.032
Time for extraction	Overnight (two days)	10 to 30 minutes	overnight (two days)
Difficulty of extraction	Some laboratory skills required	Procedurally simple	Laboratory skills required

Internal standard method for analysis of 8-OHG.

Stability of derivatized 8-OHG.

An internal standard in analytic chemistry is added prior to instrument analysis as a "yardstick" to measure repeatability and consistency between experiments [154]. A necessary requirement, therefore, is stability of the compound. The calibration curves in figure 4.1 describe the results of an experiment designed to test the stability of the derivatized labeled 8-OHG. Briefly, standards (both labeled and unlabeled) were prepared on June 1st for the calibration curve shown by blue squares. The labeled 8-OHG was stored at -80^{0}C and re-used as an internal standard on June 3rd as described in

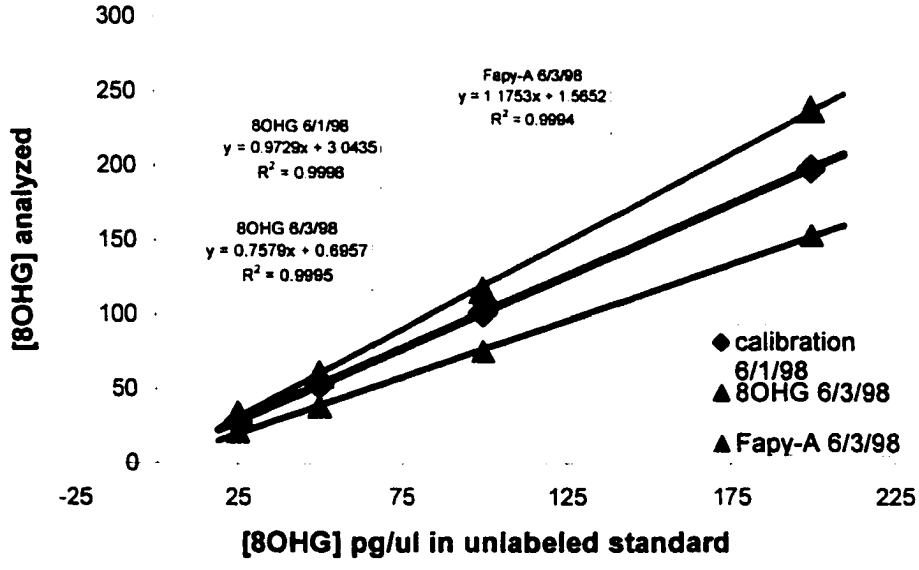

Figure 4. 1 Stability of derivatized internal standard.

Calibration curves were prepared on June 1st as shown. On June 3rd, fresh calibration standards of the same concentrations were spiked with the labeled internal from June 1st and analyzed. The decrease of 8-OHG and increase of Fapy-A indicate that the stored internal standard was not stable, and suggests that the concentration of labeled 8-OHG labeled spike increased while Fapy-A decreased in storage.

methods. Fresh unlabeled standards were prepared and used with the June 1st labeled standard from storage. The second curve (pink triangles) showed an average but consistent decline of each concentration of 8-OHG by 25%. The June 3rd curves retained the linearity of the June 1st data and indicated systematic changes at all concentrations. Interestingly, the Fapy-A values increased by the same percentage as the 8-OHG decreased (green triangles). Since the values were calculated by ratio to the labeled internal standard, this suggested that labeled 8-OHG increased in storage, and the labeled Fapy-A decreased. A probable explanation of the variation was that the Fapy-A standard was auto-oxidized to 8-OHG.

Precision of the data.

Repeatability of data with the internal standard analysis was of concern both within and between experiments. To characterize precision of the method, the relative deviation (standard deviation divided by mean) was calculated for duplicate DNA samples from three sets of analyses (21 samples in June-July 1998). The variation of values (intra-assay variability) ranges from 5.4% to 140% (average=62.2% with SEM=50.0%). Further analysis was undertaken to determine the inter-assay variability and accuracy using the 200 pg/ul standard. Briefly, three fresh 200 pg/ul 8-OHG standards spiked with labeled 8-OHG internal standard were prepared in August 1998. They were quantified using Chem Station software and a concurrent calibration curve as well as calibration curve data from June 1, 1998. The calculated concentrations with the June curve were 85.4, 52.4, and 65.8 pg/ul giving a 33% percent recovery compared to that calculated with the August curve. The conclusions of these experiments, therefore, were first that the derivatized internal standard may undergo oxidative change in storage at -80^{0}C, and furthermore, that analysis appeared not to be repeatable between sets of data.

Data from internal standard GC-MS analysis.

Analysis of 8-OHG adducts in MCF-7 cells was performed following treatment of the cells with dioxin, vehicle control, α-naphthoflavone, 4-hydroxyestradiol, 2-hydroxy estradiol, or combinations of the above. Figure 4.2 shows the analytic data of the experiment. Error bars represent standard deviation of duplicate means for triplicate samples. Unfortunately, duplicate averaging of samples prior to statistical analysis did not adequately decrease intra-assay variation. The hypothesized results were therefore inconclusive due to the large error inherent in the GC-MS internal standard analysis.

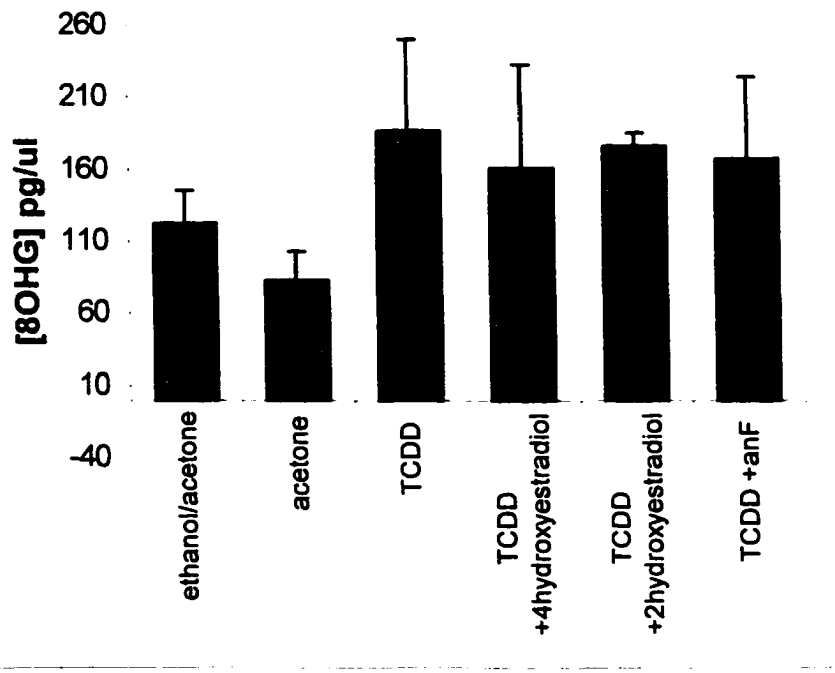

Figure 4. 2 Experimental data with GC MS.

MCF-7 cells treated with vehicle, TCDD, 2 or 4 hydroxyestradiol, or α-napthaflavone were analyzed for 8-OHG using derivatized 8-OHG as an internal standard. All data points are the average of duplicate analyses and all treatments were done in triplicate. No significant associations were shown, and large standard errors are present for each set of treatments in spite of duplicate averaging.

Isotope dilution analysis of 8-OHG.

Identification of 8-OHG by GC-MS.

Positive identification of 8-OHG by GC-MS was achieved first by chromatographic retention time (RT) and secondly by the characteristic ion spectra (review [142]). The RT of 8-OHG was rarely different from the pure standard by more than 0.05 seconds and was highly specific for the compound. Figure 4.3 demonstrates a peak with RT of 14.125 minutes identified as 8-OHG in a 150 pg/ul pure 8-OHG standard.

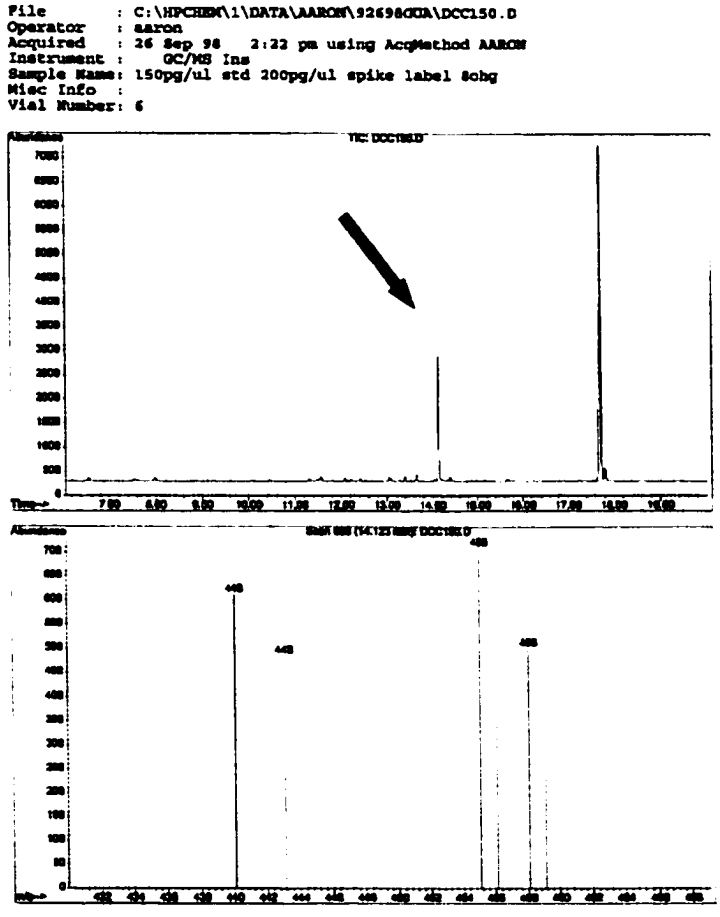

Figure 4. 3 Chromatogram and ion spectra of 8-OHG pure standard.

Identification of the peak was achieved by the retention time of the compound (upper) and its characteristic ion spectra (lower). The 150 pg/ul standard peak is indicated by arrow. The larger peak at 17.89 minutes was due to column bleed from the derivatizing agent.

Further confirmation of 8-OHG was evident from the m/z 440, 455, and 456 peaks and the plus-three AMU labeled isotope peaks (Figure 4.3). Quantity of 8-OHG was calculated from the ratios of label and unlabeled compound in the extracted ion chromatograms as shown in figure 4.4. A relative response equal to the ratio of m/z 440 divided by m/z 443 was converted to a concentration value from the standard curve (as described in methods).

Area Percent Report -- Sorted by Signal

Information from Data File:
File : C:\HPCHEM\1\DATA\AARON\92698GUA\DCC150.D
Operator : aaron
Acquired : 26 Sep 98 2:22 pm using AcqMethod AARON
Sample Name: 150pg/ul std 200pg/ul spike label 8ohg
Misc Info :
Vial Number: 6
CurrentMeth: C:\HPCHEM\1\METHODS\AARON.M

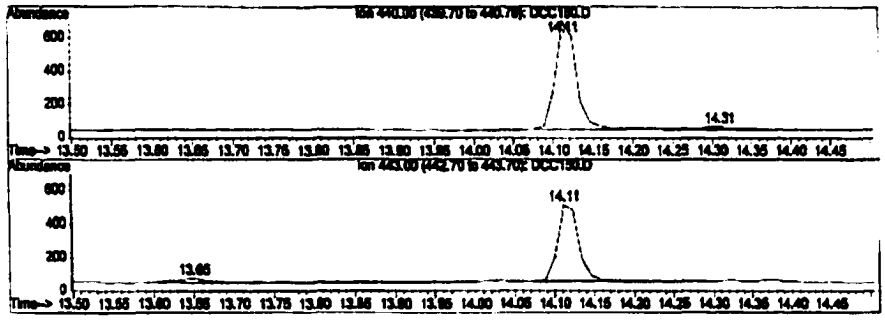

Retention Time	Area	Area %	Ratio %
440.00 amu			
14.111	1188	93.691	100.000
14.308	80	6.309	6.734
443.00 amu			
13.648	53	5.699	6.043
14.111	877	94.301	100.000

Figure 4. 4 Extracted ion chromatogram from figure 4.3

Quantification of 8-OHG for this chromatogram would be calculated from its relative response (RR). For example, the ratio, m/z 440 divided by m/z 443 equals the relative response (1188/877=1.355=RR), which was then read from the linear regression equation of the standard curve prepared as described in methods.

Stability and storage of ring labeled 8-OHG in 10 mM NaOH.

To utilize the power of isotope dilution analysis, a stable surrogate compound (N^{15}-C^{13} ring labeled 8-OHG) was spiked into the sample at the beginning of the analytic procedure. Thereafter, changes in the target compound were proportionately reflected by changes in the surrogate, and could be adjusted mathematically by the relative response algorithm (described in methods).

The labeled 8-OHG was dissolved in 10 mM NaOH, stored at 4^0C, and added to samples or standards prior to hydrolysis. In order to validate stability of the surrogate, five calibration curves were prepared over the course of one month. Fresh external standard (unlabeled 8OHdG) for each experiment was quantified relative to the mass spectral data from the stored surrogate (label compound) and the EPA algorithm (as described in methods). Figure 4.5 shows a calibration curve prepared with data from the five experiments and demonstrates the standard error of the data sets. If the surrogate were not stable, the five calibration curves would show distinct deviation from the linear average shown. Conclusions from these experiments were first, that the stored surrogate was stable for at least thirty days. Secondly, calibration data for experiments were repeatable over at least that amount of time. And thirdly, the linear analytic range was at least 10 pg/ul through 200 pg/ul. Finally, since the calibration curves were repeatable, a daily calibration control verifying the data could run with each set of experimental samples in place of the full calibration curve.

A percentage of acceptable error for the daily calibration control (DCC) should be established prior to a given set of experiments. For example, the EPA method guidelines for pollutant isotope dilution (40 CFR part 136 [147]) suggest that a daily calibration

standard should fall within 20% of the calibration curve value. Data in figure 4.3 indicated this as a suitable value for the 8-OHG method as well.

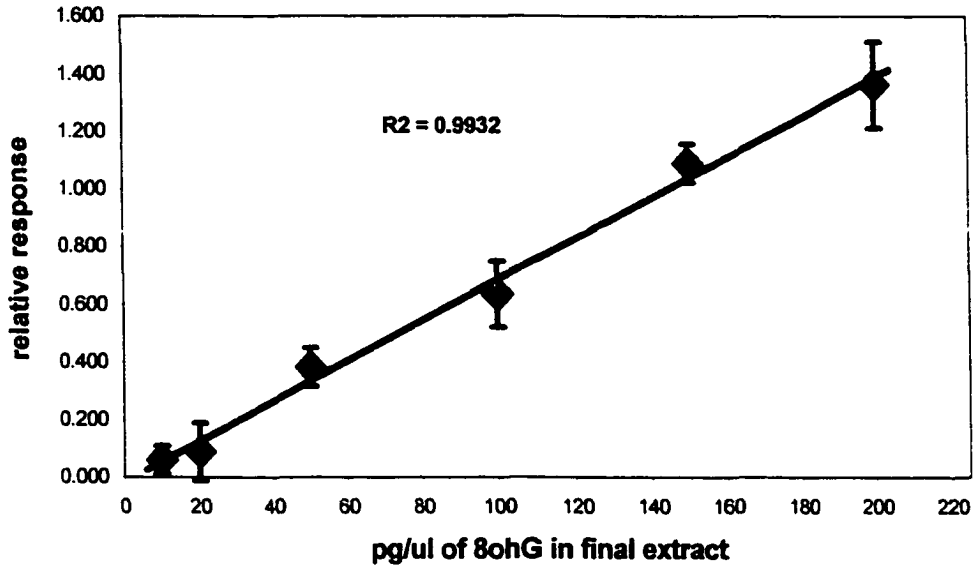

Figure 4. 5 Combination of calibration data over four weeks.

This calibration curve was prepared with combined data from five separate experiments over four weeks. Each experiment used a common ring labeled 8-OHG internal surrogate dissolved and stored between experiments in 10 mM NaOH at 4^0C. The coefficient of determination of the line was greater than 0.99 indicating good derivatization efficiency and linear range of analysis. Standard error bars represent data from the five experiments and indicate that the standard was stable, and furthermore, provided repeatable data for at least 30 days. The instrument detection limit (sensitivity) for this set of experiments was 20 picograms of 8-OHG.

Precision and accuracy of isotope method.

To determine the intra-assay variability (precision) of the isotope dilution method, seven replicates of 100 pg/ul 8-OHG were prepared with 200 pg/ul of labeled surrogate that had been stored in 10 mM NaOH for two weeks. Data shown in table 4.2 for the replicate analysis identified a relative deviation of 6.9% with a percent recovery of 99.7%. These data demonstrated the value of isotope dilution to accurately adjust

recovery of the target analyte for changes during analysis. They further established the stability of the surrogate, since any instability of the stored 8-OHG would change the analyzed quantity of the 100 pg/ul target compound. Thus, the isotope dilution analysis provided a very reliable and reproducible means of 8-OHG pure standard analysis.

Table 4. 2 Precision of isotope dilution replicates.

Replicate	Concentration of 8-OHG pg/ul
1	**103.59**
2	**91.57**
3	**96.2**
4	**92.0**
5	**100.8**
6	**103.5**
7	**110.41**
Average	**99.74**
Standard deviation	**6.897**

Seven samples of 8-OHdG were prepared to test the recovery and precision of analysis. A final concentration of 100 pg/ul 8-OHG was spiked with 200 pg/ul of labeled internal surrogate prior to hydrolysis and derivatization. Analysis with isotopic dilution provided the results shown above. The precision measured by relative deviation (standard deviation/average) was 6.9%, and the accuracy (percent recovery) was 99.7%. (Note: these samples were prepared with pure compounds containing no guanine.)

Detection limit.

Instrument sensitivity was calculated from the lowest mass of a standard with a peak greater than three times the noise. Table 4.3 is a 440 m/z scan of a 10 pg injection of 8-OHG standard in selected ion monitoring mode showing a tabular signal-to-noise ratio of

ten-to-one for this concentration. By defining instrument detection limit (IDL) as a three-to-one signal-to-noise ratio, this estimates the IDL to be approximately three picograms (20 femptomoles) of 8-OHG.

Table 4. 3 Signal to noise ratio of GC-MS 8-OHG analysis.

Peak number	Retention time (R.T.)	Peak height
1	11.090	2
2	11.136	2
3	11.240	3
4	11.298	2
5	11.390	4
6	11.483	2
7	11.622	2
8	11.772	21
9	11.864	1

Figure 4.6 displays a chromatogram from a different experiment with 10 pg/ul 8-OHG in the final extract and a 2 ul injection volume (20 pg on the column). The peak was approximately twenty times greater than noise and again suggested an IDL of about three picograms (20 femptomole).

It was apparent that GC-MS analysis of 8-OHG is extremely sensitive (low femptomolar concentrations) and provided definitive identification of the compound through retention time as well as the characteristic mass ion spectrum. On the other hand, two sources of error were characterized in the course of the isotope dilution method development and evaluation. First, oxidation of guanine to 8-OHG during DNA sample derivatization has been suggested by others [143;145] and was a cause of high levels of

8-OHG artifact (figure 4.7). Secondly, observations from the current studies described reactive breakdown of the polysiloxane columns, which affected peak identification and resolution and therefore, analytic results. To address these error sources, the following sets of experiments were designed to reduce, control, or characterize the magnitude of guanine oxidation and column degenerative effects on experimental data.

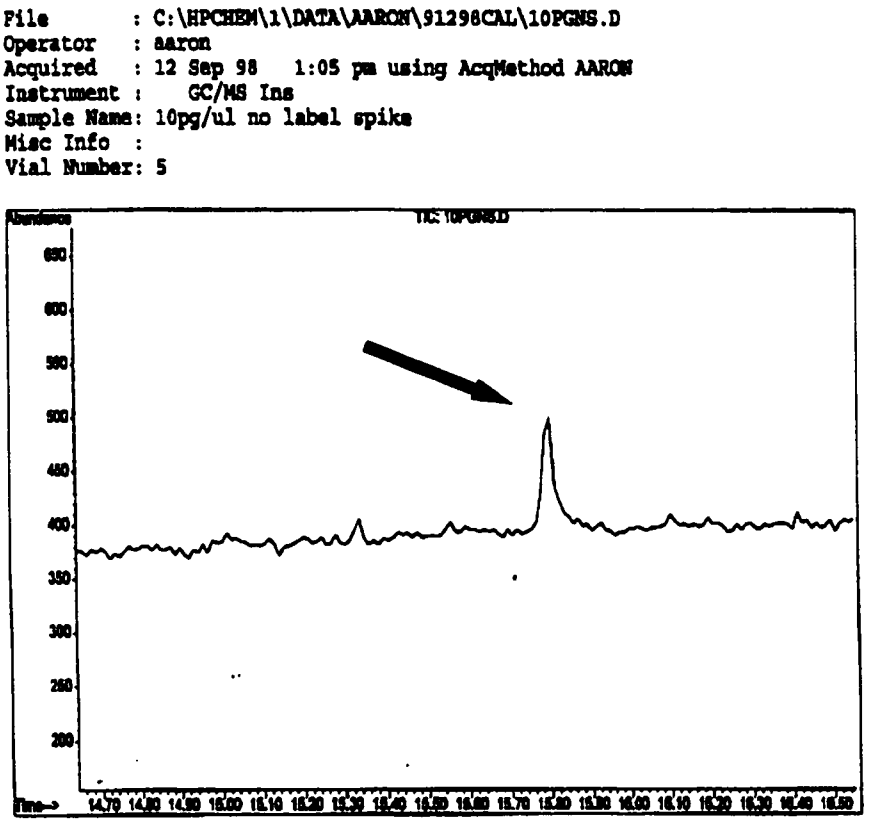

Figure 4. 6 Chromatogram of a peak from the 10 pg/ul standard.

The peak at retention time 11.772 minutes was identified as 8-OHG by both RT and ion spectrum. The peak height was ten to twenty times greater than noise. The instrument detection limit with signal to noise ratio of 3:1 from this chromatogram was estimated at 2 to 4 picograms (13 to 26 femptomole).

Although isotope dilution provided sensitive and accurate analysis of 8-OHG, the potential for artifact error remained due to DNA guanine oxidation. To explore this source of error, experiments were conducted to measure the relative deviation of replicate DNA samples. Figure 4.7 shows the results from two experiments using calf thymus DNA and MCF-7 human breast carcinoma cell DNA. The relative deviations of 8-OHG adducts were 22% and 23% indicating that substantial variation is introduced in the

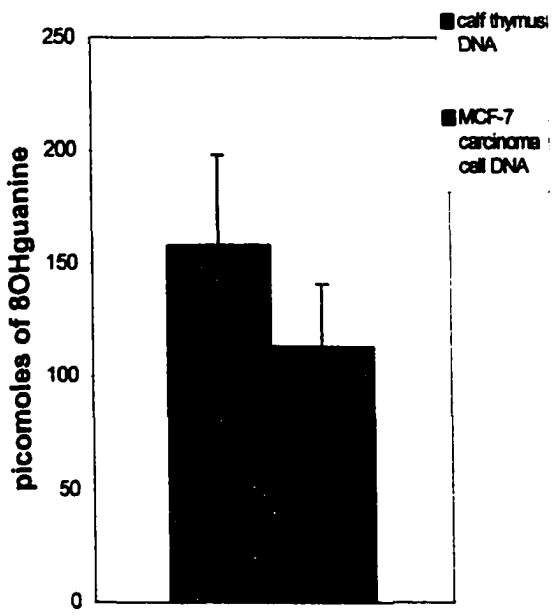

Figure 4. 7 Precision of DNA replicates.

Five untreated calf thymus and three MCF-7 human breast carcinoma cell DNA samples were analyzed for 8-OHG adducts by isotope dilution. Mean levels of adduct were 158 and 113 picomoles/50ug DNA with a relative deviation of 22% and 23% respectively.

analysis of DNA compared to the 8-hydroxydeoxyguanosine standard. The source of the variation could be inherent to the heterogeneous nature of DNA, although oxidation of guanine bases was a more likely explanation. To quantify the oxidation artifact of guanine, 50 ug of HPLC purified guanine was prepared to give a final extract concentration of 500 pg/ul as described for standards. Analysis with isotope dilution

revealed 3.37 picomoles of 8-OHG produced from the initial 301 picomoles (50 ug) of guanine. Figure 4.8 demonstrates that approximately 1.1% of guanine was oxidized, which was one hundred to one thousand fold greater than background estimates of 8-OHG [143;145]. Thus, it was evident that oxidation artifact of guanine was a factor of great concern in GC-MS DNA analysis using BSTFA derivatization procedures.

Figure 4. 8 Oxidation artifact of derivatized guanine.

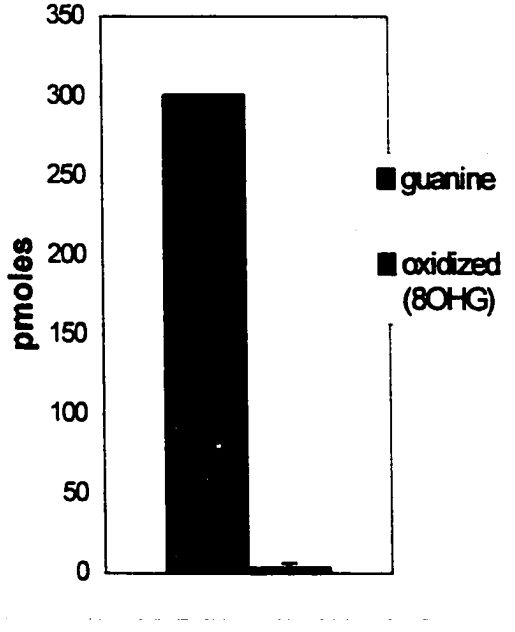

HPLC purified guanine (50 ug = 301 picomole) was prepared in final extract volume of 100 ul to a concentration of 500 pg/ul as described for standards. Analysis by isotope dilution identified 3.37 picomoles of oxidized adduct (8-OHG) from the 301 picomole of guanine (1.1%).

Evaluation of methods to reduce artifact from guanine oxidation.

Further studies were conducted to explore methods for reduction of DNA guanine oxidation. The hypotheses were tested that room temperature derivatization or addition of 5% ethane thiol would reduce oxidation artifact in the procedure. Experiments were designed using guanosine in two thousand molar excess of the 8OHdG as a surrogate for

DNA guanine. The analysis was otherwise performed as described in methods including hydrolysis of the guanosine. Endpoint parameters measured included precision (coefficient of variation), percent recovery, and method detection limit defined as Students T critical value at 99% confidence times replicate sample standard deviation. Data in table 4.4 suggested that room temperature derivatization may be valuable to reduce artifact from guanine oxidation. Surprisingly, and contrary to previously published data [155], ethane thiol increased oxidized guanine to 316%. The explanation of this may reside in the use of purified standard rather than the calf thymus DNA used in the previous study. If so, an intriguing interaction between DNA bases and the antioxidant waits to be explored.

Table 4. 4 Analysis of 8-OHG at room temperature and with the antioxidant, ethane thiol

	Precision of 7 replicates (C.V.)	Percent recovery of 8-OHG	*Detection limit
Equimolar guanosine derivatize at 120^{0}C	6.5%	83.6%	25 pg/ul
Equimolar guanosine ethane thiol 120^{0}C	5.5%	84.0%	22 pg/ul
Equimolar guanosine derivatize at 22^{0}C	3.6%	84.1%	17 pg/ul
2000 fold excess guanosine derivatize at 120^{0}C	12.7%	208%	90 pg/ul
2000 fold excess guanosine ethane thiol 120^{0}C	15.6%	316%	162 pg/ul
2000 fold excess guanosine derivatize at 22^{0}C	9.8%	153%	55 pg/ul

*Detection limit was defined as the standard deviation of final extract concentration in seven replicates times Student's T value at 99% confidence.

Quality control and quality assurance (QC/QA) (method blanks and daily calibration controls).

Two integral factors of QC/QA in 8-OHG analysis are the appropriate incorporation of method blanks and daily calibration standards. Method blanks were added in the analytic sample set prior to the first step of wet laboratory procedure (i.e. prior to hydrolysis), and assigned a blinded identification number. In every other way, their analysis was identical to the samples, and detected contaminant DNA or sources of peripherally introduced 8-OHG. The significance of an appropriate blank was emphasized by the femptomolar detection limit in the isotope dilution validation studies (figure 4.6 and table 4.3). Residues on glassware, counter-tops, or ungloved fingers could contribute substantial error to this small amount of 8-OHG. Thus, in addition to avoidance of contamination with disposable supplies, gloves, and meticulous laboratory technique, a method blank ensured that contaminant error was recognized if present.

The daily calibration control (DCC) standard was chosen as an 8OHdG standard from the mid-region of the calibration curve to verify that the analytic procedure was capable of accurately and precisely identifying the analyte, 8-OHG. In the current studies, a 100 pg/ul or 150 pg/ul DCC standard was included with each set of ten samples. The DCC provides two reassurances. First, it validated the integrity of the column and method to identify 8-OHG within each set of samples, and further indicated the need for replacement of the column due to degradation (see figures 4.9 and 4.10). Secondly, it precluded the need to run a complete calibration curve with every set of samples. Data in figure 4.4 demonstrated the inter-assay variation of calibration curves over four weeks, and validated the reliable use of a DCC with experiments. The DCC criteria used in the current studies was a value within 15% of the linear regression

average defined by the calibration curve. If the DCC did not meet the 15% requirement, construction of a new calibration curve was indicated to compensate for changes in analytic conditions.

Evaluation of column degeneration effects on GC-MS data.

The derivatization agent, BSTFA, appeared to severely compromise the integrity of the polymethylsiloxane columns used in the analyses described herein. It was notable that each chromatogram analyzed during the 8-OHG studies produced a large peak unrelated to sample or treatment type (figure 4.3, peak at 17.89 minutes). This large and consistently present peak was hypothesized to be composed of degenerative column products. To test this hypothesis, a method blank (chromatogram showing only the lone SIM peak at 17.89 minutes) containing the derivatizing agent, BSTFA:acetonitrile, was analyzed in scan mode to identify all component peaks. Figure 4.9 is a full scan chromatogram of the blank with numerous peaks present. An ion spectra shown below the chromatogram with the m/z 207 ion in most abundance is characteristic of column-associated polysiloxane bleeding [144]. The magnitude of column degeneration was evident by the comparison of the polysiloxane peak to that of a 300 pg peak from the standard in figure 4.3. The impact of column degeneration on data analysis is two-fold, and reflects on both resolution and abundance of the target analyte. Figure 4.9 displays a chromatogram from a degenerating column with an ion spectrum (SIM mode) giving positive identification of 8-OHG. Of note were the poor resolution, tailing, and low abundance of the peak at 14.196 minutes. Data from this experiment would poor sensitivity, and further column degeneration would prevent identification of 8-OHG entirely. Surprisingly, although this column was severely compromised for resolution of 8-OHG, it produced excellently resolved peaks of a pesticide standard (DDT). Hence,

two conclusions were evident from this data. First, visual observation of peak resolution in the DCC will gave warning of column decline and indicated a need for replacement. Secondly, column failure to resolve 8-OHG was not detectable by other test compounds such as organic pesticide standards.

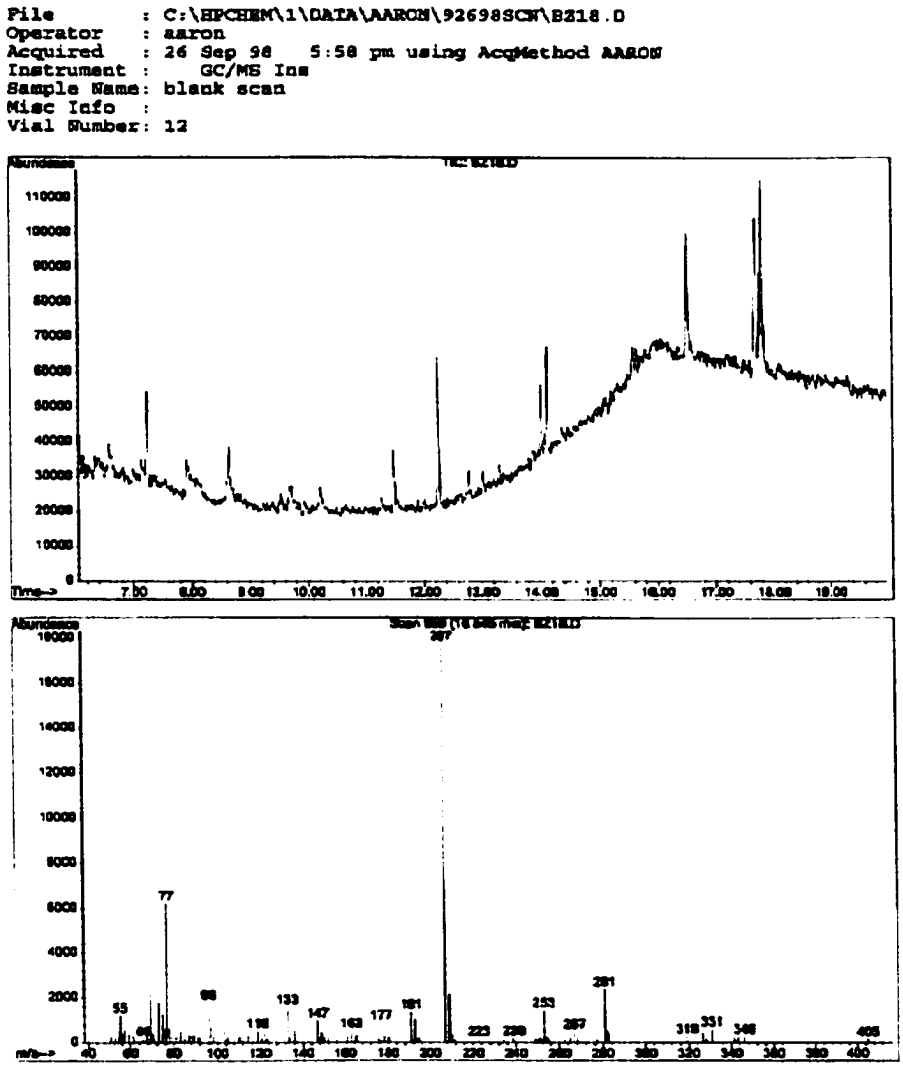

Figure 4. 9 Chromatogram in scan mode of method blank.

The ion spectra of this 16.545 minute chromatogram peak demonstrated an extreme abundance of the m/z 207 peak characteristic of column degeneration. Total ion chromatogram scans for other peaks (not shown) had similar m/z 207 abundance and suggested multiple degenerative products from column bleed. The method blank contained only the BSTFA:acetonitrile derivatizing agent.

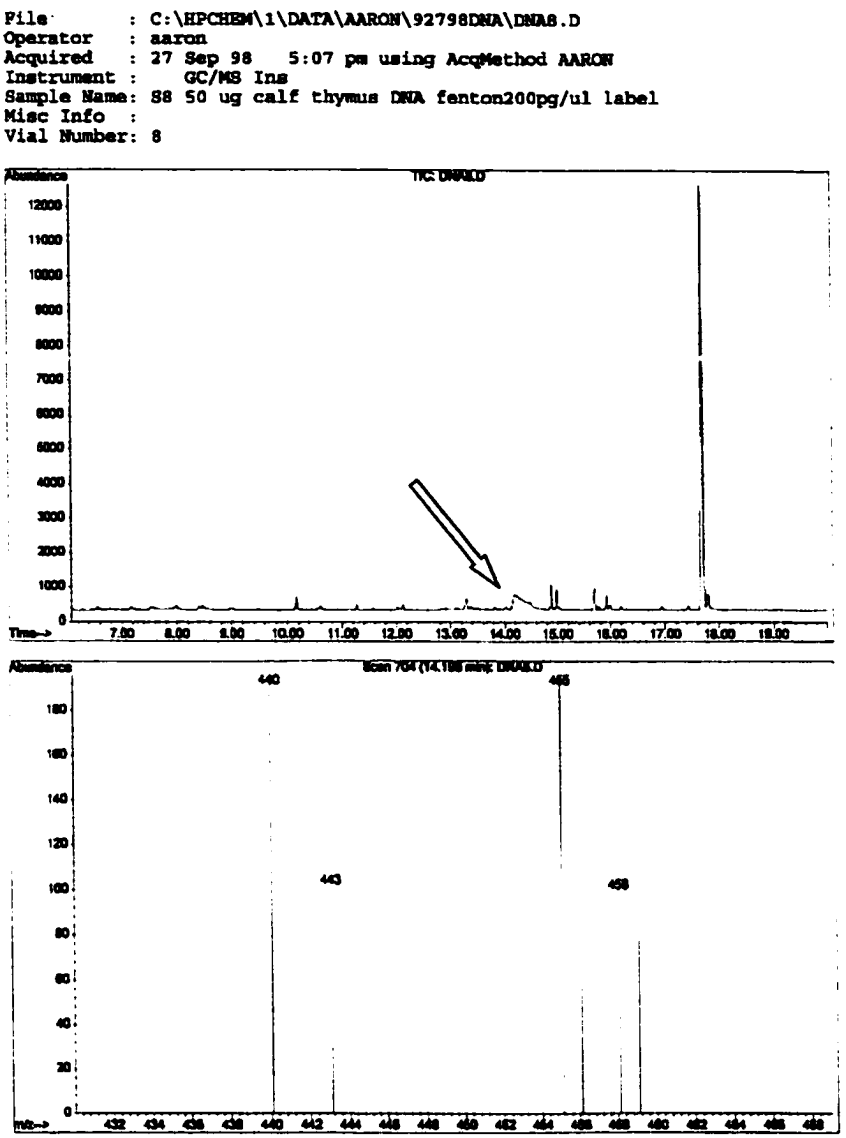

Figure 4. 10 Chromatogram of a degenerating column.

The chromatogram above was from a Restek XTI-5 dimethyl polysiloxane column after approximately 75 injections of BSTFA. The 8-OHG peak at RT=14.195 minutes (arrow) had low abundance and poor resolution evident by the wide poorly shaped peak. The peak was positively identified as 8-OHG by the ion spectra (lower). Sensitivity (IDL) was decreased, but quantification was still possible with the EPA algorithm described in methods

Experimental data from isotope dilution analysis of 8-OHG.

To further evaluate the use of isotope dilution analysis of 8-OHG, an experiment was conducted to analyze the adducts in melatonin treated MCF-7 cells. Briefly, the cells were grown in DMEM containing 10% FBS and culture conditions as described in Chapter 1. After 72 hours, the cells were trypsin harvested, DNA extracted by the high salt procedure described in methods, and analyzed with the isotope dilution method as described. The treatments were done in triplicate of either 100 nM melatonin or 0.00005% ethanol. Analysis was not done with duplicate averages as described for the internal standard method. Data shown in figure 4.11 did not show a significant difference

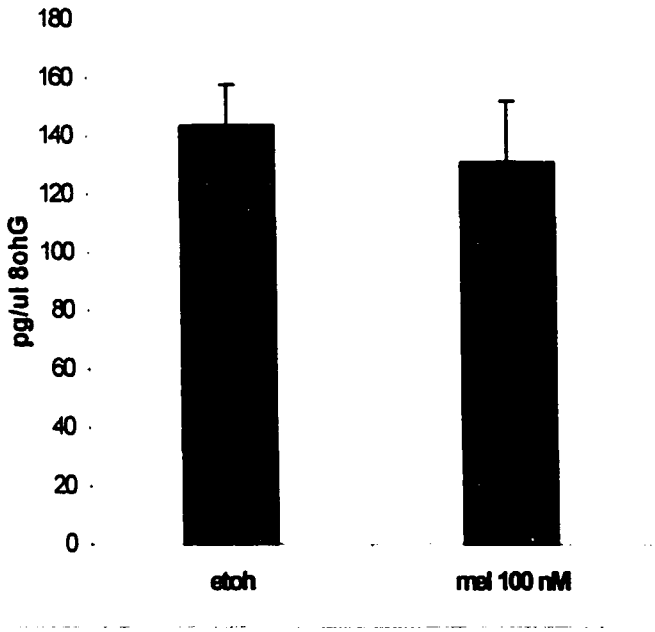

Figure 4. 11 Isotope dilution analysis of 8-OHG in melatonin treated MCF-7 cells. MCF-7 cells were treated with either 100 nM melatonin or 0.00005% ethanol (vehicle) and analyzed for 8-OHG as described in methods. Treatments were done in triplicate and analyses done singly without averaging duplicates. Relative deviations were 10% and 16% respectively for control and treatments. Similar relative deviations are present in triplicate biological analyses from other MCF-7 cell experiments shown in section I.

in treatments versus control, but did demonstrate low relative deviations (10% and 16%) of the control and treatment replicates. This relative deviation was comparable to other general MCF-7 cell biology assays (see data in section I for a variety of analyses and endpoints).

DISCUSSION.

Two methods for 8-OHG analysis by gas chromatography mass spectroscopy were evaluated.

Two methods of 8-OHG analysis by gas chromatography mass spectroscopy were evaluated in the current studies with specific emphasis on validity of data and method quality assurance. Specifically, the three main considerations for validation and quality control of the analytic procedures were data precision and accuracy, error identification, and description of the error magnitude. Since initial data suggested that isotope dilution was a preferred approach to 8-OHG analysis, further examination of this method was undertaken. In addition to precision, accuracy, detection limit, and evaluation of oxidation artifact, quality assurance parameters from method blanks, daily calibration controls, and evaluation of column degeneration were established. The criteria described by the data herein were therefore a comprehensive evaluation of both strengths and weaknesses of the GC-MS analysis of 8-OHG, including applicable modifications of isotope dilution analysis for 8-OHG.

DNA extractions were evaluated for 8-OHG studies.

Analysis of 8-OHG required the extraction of DNA from cells or tissue. Three extraction techniques were evaluated for ease of use, DNA purity, and recovery of adequate sample. Table 4.1 summarizes the comparison of methods. There was no difference in purity of DNA measured by A260/280 ratios, and recovery of sample was

adequate with each technique. Assessment of guanine oxidation during extraction was not done, but because of a low potential for artifact, the high salt extraction method was chosen to perform studies herein.

Data from the internal standard method was not repeatable.

Data validation first requires a repeatability (precision) assessment both within and between analyses. The repeatability (measured by relative deviation) of data with the analytic method using derivatized labeled 8-OHG as an internal standard was consistent neither within nor between analyses. Although, averaging duplicates of each sample reduced the intra-assay error; unfortunately, the relative deviation within duplicates was as high as 140% with an average of 60% $\pm$ SEM =50%. A further detriment to data validity was the inter-assay variability, which resulted in a recovery for 200 pg/ul 8-OHG equal to 33% (66 pg/ul) when quantified from a calibration curve constructed two months earlier. This variation was likely due to instability and storage degradation of the derivatized labeled 8-OHG. The data shown in figure 4.1 suggested that an internal standard mixture containing 8-OHG and Fapy-A underwent auto-oxidation and resulted in increased amounts of 8-OHG and decreased Fapy-A. These alterations of the labeled internal standard concentrations therefore, may have elevated the analyzed concentration of sample Fapy-A and decreased the 8-OHG systematically relative to storage time.

A second source of error with this type of analysis is the lack of control for compound quantification related to column degeneration. Chromatograms in Figures 4.3 and 4.10 demonstrated the severity of column bleed with the BSTFA derivatization and the peak size variation between a nearly new and used column. Clearly, this magnitude

of variation in analytic conditions cannot be controlled or compensated without a stable internal standard or surrogate compound.

An isotope dilution method was developed and evaluated.

Storage of surrogate.

Because of the inherent error within the internal standard protocol, an isotope dilution method was patterned with modification of a procedure described by Dizdariglu et al. [153]. A series of quality control experiments was undertaken to evaluate the method repeatability and reliability. The first requirement for validation of the isotope method was preparation and storage of isotopically labeled 8-OHG in 10 mM NaOH. The sets of experiments described in figure 4.5 established the stability for standard storage throughout one month of analysis. Further evaluation however, of the stored 8-OHG suggested that it noticeably degenerated after nine-months (data not shown). The data in figure 4.5 also defined linearity for derivatization efficiency and analysis over the 10 pg/ul to 200 pg/ul range as shown. Finally, the repeatability present in the calibration curves validated the use of daily calibration control standards in place of a complete standard curve, thus providing daily controls and decreasing the required time for analysis of experimental data (figure 4.5).

Positive identification of 8-OHG by RT and mass ion spectrum.

A second requirement for validity of the analytic method was positive identification of the target compound. The preceding paragraphs describe the identification of 8-OHG both by its characteristic mass ion spectra and by chromatographic retention time. In the current studies, confirmation of 8-OHG was evaluated first by a retention time ± 0.05 second of the pure standard, secondly by the characteristic mass ion spectrum, and thirdly by visual evaluation of the chromatographic peak. Furthermore, elimination of

computerized quantification algorithms necessitated the analyst to carefully evaluate chromatograhic information provided by peak shape, size, and shoulders. For example, the chromatogram in figure 4.9 would immediately alert the analyst to the need for column replacement, while a computer algorithm would continue to calculate data until the peak was non-existent and subsequent data lost or recorded in error.

Isotope dilution precision of analysis and daily calibration control.

Precision of 8-OHG quantification by isotope dilution was shown to be repeatable both within and between assays from standard calibration curves and the 1984 EPA pesticide algorithm for isotope dilution [147]. In the absence of exogenous guanine, the 8-OHG coefficient of variation for replicate DNA samples was 6.9% (table 4.2). Additional validation of the method precision was apparent in figure 4.5 data showing small inter-assay variability with data from five independent calibrations plotted on a single regression line. The inter-assay coefficients of variation for standards in the five calibrations ranged from 6% to 18%. Moreover, the inter-assay validation shown in figure 4.5 established criteria for the use of a daily calibration control standard (DCC). The DCC was a chosen 8-OHG concentration analyzed in conjunction with each set of ten samples. Its value was two-fold; first it eliminated the need to reproduce a standard curve (one day of laboratory time) with each data set. A second and more important value of the DCC was the continuous monitoring of column integrity and thus data validity. In this regard, the DCC served the function of a positive control with a known amount of 8-OHG, and a guarantee of column integrity.

Accuracy of isotope dilution.

Finally, target compound adjustment by spiking an isotopically labeled surrogate analyte at the earliest stage of analysis was shown to provide nearly 100% accuracy in 8-OHG recovery (table 4.2). The accuracy experiments also validated the stability and storage of the labeled surrogate 8-OHG used in the analyses since surrogate degradation would result in inaccurate quantification of the 100 pg/ul target compound.

Data from GC-MS analysis of 8-OHG.

Data in figure 4.2 (internal standard method, averages of duplicate analysis, triplicate samples) suggested a definite increase in adducts associated with the dioxin cell treatments. Unfortunately, a lack of statistical significance and unusable data was the result of the large error bars shown on the charted results. On the other hand, the greater precision and accuracy provided by isotope dilution substantially decreased the variation in analysis. For instance, figure 4.11 demonstrates data from an experiment with melatonin treated cell DNA analyzed for 8-OHG by isotope dilution. The error bars are in the magnitude of replicate DNA analysis (figure 4.7), and further, were of similar error magnitude generally seen with other types of MCF-7 cell biochemical analysis (e.g. see Chapters 1, 2, and 3). Never the less, derivatization with BSTFA clearly resulted in oxidation of guanine to 8-OHG (figure 4.8 and table 4.4). Thus, isotope dilution was concluded to provide precise and accurate recovery of 8-OHG, but did not prevent artifact from oxidative changes in matrices that contain guanine.

Artifactual oxidation of guanine.

Experiments were conducted to characterize the extent of guanine oxidation and to explore means of decreasing artifact. Figure 4.8 demonstrated that as much as 1.1% of guanine in a sample could undergo oxidation to 8-OHG under the conditions used for

derivatization. This was an excessive quantity compared to the estimated background levels of natural 8-OHG in physiologic systems [143;145]. Because others had reported lower levels of oxidation in samples derivatized at room temperature or with added anti-oxidants, these parameters were evaluated with isotope dilution. Table 4.4 summarizes a set of studies done using these analytical conditions in addition to low and high guanine concentrations in the preparations. The results showed, as predicted, that room temperature derivatization substantially lowered the artifact (i.e. percent recovery of 8-OHG minus 100%) from 108% to 53% in the presence of 2000-fold molar excess guanine (table 4.4). Interestingly however, the addition of the anti-oxidant, ethane thiol, increased artifact from 108% to 216%. This apparent contradiction to previous findings [155] may represent the use of purified standards in present studies as opposed to calf thymus DNA previously. This explanation would imply that chemical interactions between the derivatizing agent and other constituents of DNA (e.g. bases, sugars, phosphates, or trace proteins) were present. Thus, the hypothesis arises that ethane thiol could decrease oxidation in DNA samples at the expense of other bases. Until this hypothesis is further tested, use of ethane thiol to decrease artifact in base oxidation studies is not warranted.

Isotope dilution for 8-OHG analysis in urine biomarker studies.

Although artifact was present in analyses with 2000-fold excess guanine, there was none identified in samples containing equimolar concentrations of guanine and 8-OHG (table 4.4). The intriguing suggestion of this finding was that the isotope method could be of great value to analyze matrices with minimal guanine such as urine or serum. GC-MS isotopic dilution analysis provided excellent sensitivity (low femptomoles), good

precision (6.9%), excellent accuracy (99.7%), and time efficiency (approximately 5 hours per sample set). Furthermore, the cost of analytic supplies (including a column replacement) per 100 samples was between $5.00 and $6.00. Thus, while application of the isotope dilution for analysis of DNA samples resulted 22% precision for replicate analyses, biomarker studies of urine or serum could be developed to utilize the full potential of the method without interference by guanine oxidation artifact.

CONCLUSIONS.

In conclusion.

The current studies described two methods of 8-OHG analysis by gas chromatography with mass selective detection. Only isotope dilution utilized the full power of the mass spectrometer by allowing accurate adjustment of analytic losses relative to a chemically identical surrogate. Thus, the surrogate added at the initiation of analysis performed a dual function as internal standard and surrogate spike compound, and was only differentiated from the target analyte by the mass selective detector. The major values of the method were precision, accuracy, sensitivity, and a rapid analysis at moderate expense. The primary weakness was guanine oxidation artifact, and therefore, suggested that the method may have best applicability in biomarker studies of analytic matrices not containing excess guanine (such as urine or serum).

Summary of the study findings:

1) Labeled 8-OHG surrogate dissolved in 10 mM NaOH and stored at 4^0C was stable for at least 30 days.
2) Because of the stable surrogate, a daily calibration control was used as a positive control, to monitor column degeneration, and in lieu of repeated calibrations.

3) Isotope dilution provided accurate and precise recovery of 8-OHG in compounds that did not contain extraneous guanine (CV=6.9% and recovery =99.7%).
4) The sensitivity was very low; approximately 20 femptomoles
5) Oxidation artifact of guanine was present in levels as high as 1.1% of total guanine but was reduced substantially by room temperature derivatization.
6) Precision of DNA replicates was approximately 22%.
7) Degeneration of bonded and crosslinked polymethyl siloxane columns was observed and could critically affect data.
8) Addition of ethane thiol as an anti-oxidant increased guanine oxidation artifact in a pure standard system, and suggested a possibility of yet undefined interference with DNA bases other than 8-OHG.
9) The full potential of isotope dilution could benefit biomarker studies in a matrix containing low levels of guanine in urine or serum.

Application of 8-OHG GC-MS analysis in oxidative stress or cancer risk studies may be a valuable tool to elucidate the effects of environmental exposures in study populations. However, reliable and repeatable analytic methodology is needed for useful interpretation of the epidemiological data from the populations. The experimental results presented herein validated and defined the quality assurance parameters for use of an isotopic dilution method of 8-OHG analysis. Furthermore, the definition of analytic error source and the degree of error expected within the data are of utmost importance. Thus, the researcher contemplating GC-MS analysis may apply the QC/QA parameters described in this dissertation to validate 8-OHG study results.

Reference List

1) Rubin,E. and Farber,J.L. (1994) *Pathology*. J.B. Lippincott Company.

2) King,S.E., Schottenfeld,D., and Searle,J.G. (1996) The "epidemic" of breast cancer in the U.S.- determinining the factors. *Oncology*, **10**, 453-462.

3) Russo,J., Calaf,G., Sohi,N., Tahin,Q., Zhang,P.L., Alvarado,M.E., Estrada,S., and Russo,I.H. (1993) Critical steps in breast carcinogenesis. *Ann.N.Y.Acad.Sci.*, **698**, 1-20.

4) Contributors (1997) *The Melatonin Hypothesis: Breast Cancer and the use of Electricity*. Batelle Press.

5) Blask,D. (1993) Melatonin in Oncology. In Yu,H.-S. and Reiter,R. (eds.) *Melatonin: Biosynthesis, Physiological Effects, and Clinical Applications*. CRC press, Ann Arbor, pp 447-74.

6) Viljoen,P.A. (1997) The validity of melatonin as an oncostatic agent. *J.Pineal Res.*, **22**, 184-202.

7) Vanacek,J. (98 A.D.) Cellular mechanisms of melatonin action. *Physiol.Rev.*, **78**, 687-721.

8) Arendt,J. and Deacon,S. (1997) Treatment of circadian rhythm disorders--melatonin. *Chronobiol.Int.*, **14**, 185-204.

9) Brezezinski,A. (1997) Melatonin in humans. *N.Engl.J.Med.*, **336**, 186-195.

10) Cos,S. and Sanchez-Barcelo,E.J. (1994) Differences between pulsatile or continuous exposure to melatonin on MCF-7 human breast cancer cell proliferation. *Cancer Lett.*, **85**, 105-109.

11) Molis,T., Spriggs,L.L., Jupiter,Y., and Hill,S. (1997) Melatonin modulation of estrogen regulated proteins, growth factors, and proto-oncogenes in human breast cancer. *J.Pineal Res.*, **18**, 93-103.

12) Hill,S., Spriggs,L.L., Simon,M., Muraoka,H., and Blask,D. (1992) The growth inhibitory action of melatonin on human breast cancer cells is linked to the estrogen response system. *Cancer Lett.*, **64**, 249-256.

13) Eck,K.M., Yuan,L., Duffy,L., Ram,P.T., Ayettey,S., Chen,I., Cohn,C.S., Reed,J.C., and Hill,S.M. (1998) A sequential treatment regimen with melatonin and all-trans retinoic acid induces apoptosis in MCF-7 tumour cells. *Br.J.Cancer*, **77**, 2129-2137.

14) Molis,T.M., Spriggs,L.L., and Hill,S.M. (1994) Modulation of estrogen receptor mRNA expression by melatonin in MCF-7 human breast cancer cells. *Mol.Endocrinol.*, **8**, 1681-1690.

15) Saarela,S. and Reiter,R.J. (1994) Function of melatonin in thermoregulatory processes. *Life Sci.*, **54**, 295-311.

16) Hill,S. and Blask,D. (1988) Effects of the pineal hormone melatonin on the proliferation and morphological characteristics of human breast cancer cells (MCF-7) in culture. *Cancer Res.*, **46**, 6121-6126.

17) Cavalli,L.R., Varella-Garcia,M., and Liang,B.C. (1997) Diminished tumorigenic phenotype after depletion of mitochondrial DNA. *Cell Growth Differ.*, **8**, 1189-1198.

18) Lemus-Wilson,A.M., Kelly,P.A., and Blask,D. (1995) Melatonin blocks the stimulatory effects of prolactin on human breast cancer cell growth. *Br.J.Cancer*, **72**, 1435-1440.

19) Morgan,P.J., Barrett,P., Howell,H.E., and Helliwell,R. (1994) Melatonin receptors: localization, molecular pharmacology and physiological significance. *Neurochem.Int.*, **24**, 101-146.

20) Dubocovich,M.L. (1995) Melatonin receptors: are there multiple subtypes? *Trends Pharmacol.Sci.*, **16**, 50-56.

21) Becker-Andre,M., Wiesenberg,I., Schaeren-Wiemers,N., Andre,E., Missbach,M., Saurat,J.H., and Carlberg,C. (1994) Pineal gland hormone melatonin binds and activates an orphan of the nuclear receptor superfamily [published erratum appears in J Biol Chem 1997 Jun 27;272(26):16707]. *J.Biol.Chem.*, **269**, 28531-28534.

22) Poeggler,B., Saarela,S., Reiter,R., Tan,D., Chen,L., Manchester,L.C., and Barlow-Walden,L.R. (1994) Melatonin-- A highly Potent Endogenous Radical Scavenger and Electron Donor: New Aspects of the Oxidation Chemistry of this Indole Accessed *in vitro*. *Ann.N.Y.Acad.Sci.*, **738**, 419-420.

23) Poeggler,B., Reiter,R., Hardeland,R., Sewerynek,E., Melchiorri,D., and Barlow-Walden,L.R. (1995) Melatonin, a mediator of electron transfer and repair reactions, acts synergistically with the chain-breaking antioxidants ascorbate, trolox, and glutathione. *Neuroendocrinol Lett*, **17**, 87-92.

24) Contributors (1997) *Antioxidants in Disease Mechanisms and Therapy*. Academic Press, San Diego.

25) Ruddon,R. (1995) *Cancer Biology*. Oxford University Press, New York.

26) Dorward,A., Sweet,S., Moorehead,R., and Singh,G. (1997) Mitochondrial contributions to cancer cell physiology: redox balance, cell cycle, and drug resistance. *J.Bioenerg.Biomembr.*, **29**, 385-392.

27) Sen,C.K. and Packer,L. (1996) Antioxidant and redox regulation of gene transcription [see comments]. *FASEB J.*, **10**, 709-720.

28) Sun,Y. and Oberley,L.W. (1996) Redox regulation of transcriptional activators. *Free Radic.Biol.Med.*, **21**, 335-348.

29) Williams,J. (1998) *Williams Textbook of Endocrinology*. W.B. Saunders.

30) Contributors (1991) *The Breast: Comprehensive Management of Benign and Malignant Diseases*. W.B. Saunders, Philadelphia.

31) Rollag,M.D. and Niswender,G.D. (1976) Radioimmunoassay of Serum Concentrations of Melatonin in Sheep Exposed to Different Lighting Regimens. *Endocrinology*, **98**, 482-489.

32) Higami,Y., Shimokawa,I., Okimoto,T., and Ikeda,T. (1994) An age-related increase in the basal level of DNA damage and DNA vulnerability to oxygen radicals in the individual hepatocytes of male F344 rats. *Mutat.Res.*, **316**, 59-67.

33) Olive,P., Durand,W., and Banath,J. (1992) Factors Influencing DNA Migration from Individual cells subjected to Gel Electrophoresis. *Exp.Cell.Res.*, **198**, 259-267.

34) Hellman,B., Vaghef,H., and Bostrom,B. (1995) The concepts of tail moment and tail inertia in the single cell gel electrophoresis assay. *Mutat.Res.*, **336**, 123-131.

35) Vandeputte,C., Guizon,I., Genestie-Denis,I., Vannier,B., and Lorezon,G. (1994) A microtiter plate assay for total glutathione and glutathione disulfide contents in cultured/isolated cells: performance study of a new miniaturized protocol. *Cell Biol.and Tox.*, **10**, 415-421.

36) Birch-Machin, M., Jackson, S., Kler, R. S., and Turnbull, D. M. Mitochondrial Dysfunction. Lash, L. H. and Jones, D. P. 1(2), 51-69. 1993. USA, Academic Press inc. Methods in Toxicology. tyson, C. A. and Witschi, H.

37) Turnbull,D.M., Chrzanowski-Lighttowlers,Z.M.A., and Lightowlers,R.N. (1993) A microtiter plate assay for cytochrome C oxidase in permeabilized whole cells. *Anal.Biochem.*, **214**, 45-49.

38) Ahmed,S.A., Gogal,R.M.J., and Walsh,J.E. (1994) A new rapid and simple non-radioactive assay to monitor and determine the proliferation of lymphocytes: an alternative to [3H]thymidine incorporation assay. *J.Immunol.Methods*, **170**, 211-224.

39) Mosmann,T. (1983) Rapid colorimetric assay for cellular growth and survival: application to proliferation and cytotoxicity assays. *J.Immunol.Methods*, **65**, 55-63.

40) Kleinbaum,D.G., Kupper,L.L., Muller,K.E., and Nizam,A. (1998) *Applied Regression Analysis and Multivariate Methods*. Duxbury Press, Pacific Grove CA.

41) Contributors. Cell Death. Schwartz, L. M. and Osborne, B. A. (46). 1995. San Diego, Academic Press. Methods in Cell Biology. Wilson, L. and Matsudaira, P.

42) Blask,D., Wilson,S.T., and Zalatan,F. (1997) Physiologic Melatonin Inhibition of Human Breast Cancer Cell Growth *In Vitro*: Evidence for a Glutathione Mediated Pathway. *Cancer Res.*, **57**, 1909-1914.

43) Bartsch,C., Bartsch,H., and Lippert,T.H. (1992) The pineal gland and cancer: facts, hypotheses and perspectives. *The Cancer Journal*, **5**, 194-199.

44) Ronco,A.L. and Halberg,F. (1996) The pineal gland and cancer. *Anticancer Res.*, **16**, 2033-2039.

45) Uehara,J., Nazario,A.C., Rodrigues,d.L., Simoes,M.J., Juliano,Y., and Gebrim,L.H. (1998) Effects of tamoxifen on the breast in the luteal phase of the menstrual cycle. *Int.J.Gynaecol.Obstet.*, **62**, 77-82.

46) Alberts,B., Bray,D., Lewis,J., Raff,M., Roberts,K., and Watson,J.D. (1994) *Molecular Biology of The Cell*. Garland Publishing Inc., New York.

47) Lizard,G., Miguet,C., Gueldry,S., Monier,S., and Gambert,P. (1997) [Flow cytometry measurement of DNA fragmentation in the course of cell death via apoptosis. New techniques for evaluation of DNA status for the pathologist]. *Ann.Pathol.*, **17**, 61-66.

48) Warburg,O., Wind,E., and Negelein,E. (1926) Uber den Stoffwechsel von Tumoren in Korper. *Klin.Woch.*, **5**, 829-832.

49) Lodish,H., Baltimore,D., Berk,A., Zipursky,S.L., Matsudaira,P., and Darnell,J. (1995) *Molecular Cell Biology*. Scientific American Books, New York.

50) Baggetto,L.G. (1992) Role of mitochondria in carcinogenesis. *Eur.J.Cancer*, **29A**, 156-159.

51) Golshani-Hebroni,S.G. and Bessman,S.P. (1997) Hexokinase binding to mitochondria: a basis for proliferative energy metabolism. *J.Bioenerg.Biomembr.*, **29**, 331-338.

52) Cavalli,L.R. and Liang,B.C. (1998) Mutagenesis, tumorigenicity, and apoptosis: are the mitochondria involved? *Mutat.Res*, **398**, 19-26.

53) Amarante-Mendes,G.P., Naekyung,K.C., Liu,L., Huang,Y., Perkins,C.L., Green,D.R., and Bhalla,K. (1998) Bcr-Abl exerts its antiapoptotic effect against diverse apoptotic stimuli through blockage of mitochondrial release of cytochrome C and activation of caspase-3. *Blood*, **91**, 1700-1705.

54) Vistica,D.T., Kenney,S., Hursey,M., and Boyd,M.R. (1996) Role of membrane potential in the accumulation of quaternized ellipticines by human tumor cell lines. *J.Pharmacol.Exp.Ther.*, **279**, 1018-1025.

55) Dorward,A.M. and Singh,G. (1996) Energetic characteristics of cisplatin resistant ovarian carcinoma cells. *Anticancer Res.*, **16**, 443-447.

56) Nadakavukaren,K.K., Nadakavukaren,J.J., and Chen,L.B. (1985) Increased rhodamine 123 uptake by carcinoma cells. *Cancer Res.*, **45**, 6093-6099.

57) Vayssiere,J.L., Berthelot,F., Gros,F., and Croizat,B. (1984) Is the induction of neuroblastoma differentiation by CCA mediated by its effects on the electrochemical gradient? *FEBS Lett.*, **173**, 19-22.

58) Levenson,R., Macara,I.G., Smith,R.L., Cantley,L., and Housman,D. (1982) Role of mitochondrial membrane potential in the regulation of murine erythroleukemia cell differentiation. *Cell*, **28**, 855-863.

59) Bustamante,E. and Pedersen,P.L. (1977) High aerobic glycolysis of rat hepatoma cells in culture: role of mitochondrial hexokinase. *Proc.Natl.Acad.Sci.U.S.A*, **74**, 3735-3739.

60) Arora,K.K. and Pedersen,P.L. (1988) Functional significance of mitochondrial bound hexokinase in tumor cell metabolism. Evidence for preferential phosphorylation of glucose by intramitochondrially generated ATP. *J.Biol.Chem.*, **263**, 17422-17428.

61) Kikuchi,Y., Sato,S., and Sugimura,T. (1972) Hexokinase isozyme patterns of human uterine tumors. *Cancer*, **30**, 444-447.

62) Nakashima,R.A., Paggi,M.G., Scott,L.J., and Pedersen,P.L. (1988) Purification and characterization of a bindable form of mitochondrial bound hexokinase from the highly glycolytic AS-30D rat hepatoma cell line. *Cancer Res.*, **48**, 913-919.

63) Thelen,A.P. and Wilson,J.E. (1991) Complete amino acid sequence of the type II isozyme of rat hexokinase, deduced from the cloned cDNA: comparison with a hexokinase from novikoff ascites tumor. *Arch.Biochem.Biophys.*, **286**, 645-651.

64) Rempel,A., Bannasch,P., and Mayer,D. (1994) Differences in expression and intracellular distribution of hexokinase isoenzymes in rat liver cells of different transformation stages. *Biochim.Biophys.Acta*, **1219**, 660-668.

65) Mathupala,S.P., Rempel,A., and Pedersen,P.L. (1995) Glucose catabolism in cancer cells. Isolation, sequence, and activity of the promoter for type II hexokinase. *J.Biol.Chem.*, **270**, 16918-16925.

66) Mathupala,S.P., Rempel,A., and Pedersen,P.L. (1997) Aberrant glycolytic metabolism of cancer cells: a remarkable coordination of genetic, transcriptional, post-translational, and mutational events that lead to a critical role for type II hexokinase. *J.Bioenerg.Biomembr.*, **29**, 339-343.

67) Parry,D.M. and Pedersen,P.L. (1983) Intracellular localization and properties of particulate hexokinase in the Novikoff ascites tumor. Evidence for an outer mitochondrial membrane location. *J.Biol.Chem.*, **258**, 10904-10912.

68) Miller,D.S. and Sykes,D.B. (1991) Stimulation of protein synthesis by internalized insulin. *J.Cell Physiol*, **147**, 487-494.

69) Dubocovich,M.L. (1988) Luzindole (N-0774): A novel melatonin receptor antagonist. *J.Pharmacol.Exp.Ther.*, **246**, 902-910.

70) Papa,S., Guerrieri,F., and Capitanio,N. (1997) A Possible Role of Slips in Cytochrome C Oxidase in the Antioxygen Defense System of the Cell. *Bioscience Reports*, **17**, 23-31.

71) Molis,T.M., Walters,M.R., and Hill,S.M. (1993) Melatonin Modulation of Estrogen Receptor Expression in MCF-7 Human Breast Cancer Cells. *Int.J.Oncol.*, **3**, 687-694.

72) Dang,C.V., Lewis,B.C., Dolde,C., Dang,G., and Shim,H. (1997) Oncogenes in tumor metabolism, tumorigenesis, and apoptosis. *J.Bioenerg.Biomembr.*, **29**, 345-354.

73) Demonacos,C.V., Karayanni,N., Hatzoglou,E., Tsiriyiotis,C., Spandidos,A., and Sekeris,C.E. (1996) Mitochondrial Genes as Sites of Primary Action of Steroid Hormones. *Steroids*, **61**, 226-232.

74) Kadowaki,T. and Kitagawa,J. (1988) Enhanced Transcription of Mitochondrial Genes after Growth Stimulation and Glucocorticoid Treatment of Reuber Hepatoma H35 cells. *FEBS Lett.*, **233**, 51-56.

75) Van Itallie,C.M. (1990) Thyroid Hormone and Dexamethasone Increase the Levels of a Messenger Ribonucleic Acid for a Mitochondrially Encoded Subunit but not for a Nuclear Encoded Subunit of Cytochrome C Oxidase. *Endocrinology*, **127**, 55-62.

76) Van Itallie,C.M. and Dannies,P.S. (1988) Estrogen Induces Accumulation of the Mitochondrial Ribonucleic Acid for Subunit II of Cytochrome Oxidase in Pituitary tumor Cells. *Mol.Endocrinol.*, **2**, 332-337.

77) Lehninger,A.L., Nelson,D.L., and Cox,M.M. (1997) *Principles of Biochemistry*. Worth Publishers, New York.

78) Arnold,S. and Kadenbach,B. (1997) Cell respiration is controlled by ATP, an allosteric inhibitor of cytochrome-c oxidase. *Eur.J.Biochem.*, **249**, 350-354.

79) Yokoyama,T., Shirono,H., Yamada,N., Kato,N., and Koga,J. (1998) Utilization of changes in the metabolic rate of melatonin receptor- expressing cells to quantify melatonin. *Anal.Biochem.*, **255**, 159-161.

80) Schuchard,M., Landers,J.P., Sandhu,N.P., and Spelsberg,T.C. (1993) Steroid hormone regulation of nuclear proto-oncogenes. *Endocrine Reviews*, **14**, 659-669.

81) Shim,H., Dolde,C., Lewis,B.C., Wu,C.S., Dang,G., Jungmann,R.A., Dalla-Favera,R., and Dang,C.V. (1997) c-Myc transactivation of LDH-A: implications for tumor metabolism and growth. *Proc.Natl.Acad.Sci.U.S.A*, **94**, 6658-6663.

82) Maestroni,J.M. and Conti,A. (1996) Melatonin in human breast cancer tissue:Assocication with nuclear grade and estrogen receptor status. *Lab.Invest.*, **75**, 557-561.

83) Blask,D. and Hill,S. (1986) Effects of Melatonin on Cancer: Studies on MCF-7 Heman Breast Cancer Cells in Culture. *J.Neural Transm.(suppl)*, **21**, 443-449.

84) Stalheim-Smith,A. and Fitch,G. (1993) *Understanding Human Anatomy and Physiology*. West Publishing Company, St. Paul.

85) Crespo,D., Fernandez-Viadero,R., Verduga,R., Ovejero,V., and Cos,S. (1997) Interaction between melatonin and estradiol on morphological and morphometric features of MCF-7 human breast cancer cells. *J.Pineal Res.*, **16**, 215-222.

86) Cooper,G.M. (1997) *The Cell A Molecular Approach*. ASM Press, Washington D.C.

87) Netteheim,P., Smits,H.L., George,M.A., Gray,T., and Jetten,A.M. (1989) Squamous differentiation in normal and transformed rat trachael epithelial cells. *Carcinogenesis*, **10**, 743-748.

88) Sun,T. and Green,H. (1976) Differentiation of the Epidermal Keratinocyte in Cell Culture: Formation of the Cornified Envelope. *Cell*, **9**, 511-521.

89) Cosma,G.N., Marchok,A.C., and Garte,S.J. (1989) Oncogene expression in cell lines derived from rat tracheal implants exposed in vivo to 7,12-dimethylbenz[a]anthracene. *Mol.Carcinog.*, **2**, 268-273.

90) Nettesheim,P., Smits,H.L., George,M.A., Gray,T., and Jetten,A.M. (1989) Squamous differentiation in normal and transformed rat trachael epithelial cells. *Carcinogenesis*, **10**, 743-748.

91) Lai,L.C., Coldham,N.G., Islam,S., Reed,M.J., Ghilchik,M.W., and James,V.H. (1990) Effect of breast cyst fluid on oestrogen 17-oxidoreductase activity in MCF-7 breast cancer cells. *Cancer Lett.*, **55**, 165-169.

92) Erbas,H., Lennard,T.W., and Lai,L.C. (1996) Effect of breast cyst fluid on oestrone sulphatase activity in MCF-7 breast cancer cells. *Anticancer Res.*, **16**, 833-836.

93) Lai,L.C., Ghilchik,M.W., Shaikh,N.A., Reed,M.J., and James,V.H. (1989) Realtionship between epidermal growth factor and dehydroepiandrosterone and its sulphate in breast cyst fluid. *Br.J.Cancer*, **60**, 320-323.

94) Lai,L.C., Dunkley,S.A., Reed,M.J., Ghilchik,M.W., Shaikh,N.A., and James,H.T. (1990) Epidermal growth factor and oestradiol in human breast cyst fluid. *Eur.J.Cancer*, **26**, 481-484.

95) Cassoni,P., Sapino,A., Haagensen,D.E., Naldoni,C., and Bussolati,G. (1995) Mitogen effect of the 15-kDa gross cystic disease fluid protein (GCDFP-15) on breast cell lines and on immortal mammary cells. *Int.J.Cancer*, **60**, 216-220.

96) Levitz,M., Raju,U., Boccardo,F., Arcuri,F., and Castagnetta,L. (1992) Steroid and cation correlations in human breast cyst fluid: Preliminary findings. *Cancer Detect.Prev.*, **16**, 57-59.

97) Angeli,A., Caraci,P., Puligheddu,B., Torta,M., and Orlandi,F. (1992) Categorization of cysts and steroid levels in breast cyst fluid. *Cancer Detect.Prev.*, **16**, 53-56.

98) Torrisi,R., Zanardi,S., Valenti,G., De Franchis,V., Nicolo,G., Barreca,A., Minuto,F., and Boccardo,F. (1995) Epidermal growth factor content of breast cyst fluids from women with breast cnacer or proliferative disease. *Breast Cancer Res.Treat.*, **33**, 219-224.

99) Tapper,D., Gajdusek,C., Moe,R., and Ness,J. (1990) Identification of a unique biological tumor marker in human breast cyst fluid and breast cancer tissue. *Am.J.Surg.*, **159**, 473-478.

100) Bruzzi,P., Dogliotti,L., Naldoni,C., bucchi,L., Costantini,M., Cicognani,A., Torta,M., Buzzi,G.F., and Angeli,A. (1997) Cohort study of association of risk of breast cancer with cyst type in women with gross cystic disease of the breast. *Br.Med.J.*, **314**, 925-928.

101) Lai,L.C., Siraj,A.K., Erbas,H., and Lennard,T.W. (1995) Relationship between basic fibroblast growth factor and transforming growth factor-beta2 in breast cyst fluid. *J.Clin.Endocrinol.Metab.*, **80**, 711-714.

102) Vorherr,H. (1986) Fibrocystic breast disease: pathophysiology, pathomorphology, clinical picture, and management. *Am.J.Obstet.Gynecol.*, **154**, 161-179.

103) Wellings,S.R., Jenson,H.M., and Marcum,R.G. (1975) An Atlas of Subgross Pathology of the Human Breast with Special Reference to Possible Precancerous Lesions. *J Natl.Cancer Inst.*, **55**, 231-243.

104) Petrakis,N.L., Wrensch,M.R., Ernster,V.L., Miike,R., Murai,J., Simberg,N., and Siiteri,P.K. (1987) Influence of pregnancy and lactation on serum and breast fluid estrogen levels: implications for breast cancer risk. *Int.J.Cancer*, **40**, 587-591.

105) Lai,L.C., Kadory,S., Siraj,A.K., and Lennard,T.W. (1994) Oncostatin M, interleukin 2, interleukin 6 and interleukin 8 in breast cyst fluid. *Int.J.Cancer*, **59**, 369-372.

106) Petrakis,N.L. (1993) Nipple aspirate fluid in epidemiologic studies of breast disease. *Epidemiol.Rev.*, **15**, 188-195.

107) Rose,D.P., Lahti,H., Laakso,K., Kettunen,K., and Wynder,E.L. (1986) Serum and breast duct fluid prolactin and estrogen levels in healthy Finnish and American women and patients with fibrocystic disease. *Cancer*, **57**, 1550-1554.

108) Wrensch,M.R., Petrakis,N.L., King,E.B., Miike,R., Mason,L., Chew,K.L., Lee,M.M., Ernster,V.L., Hilton,J.F., Schweitzer,R., Goodson III,W.H., and Hunt,T.K. (1991) Breast cancer incidence in women with abnormal cytology in nipple aspirates of breast fluid. *Am.J.Epidemiol.*, **135**, 130-141.

109) Haagensen,C.D., Bodian,C., and Haagensen,D.E. (1981) *Breast Carcinoma, Risk and Detection*. W.B.Saunders, Philadelphia.

110) Gann,P., Chatterton,R., Volgelsong,K., Dupuis,J., and Ellman,A. (1997) Mitogenic growth factors in breast fluid obtained from healthy women: Evaluation of biological and extraneous sources of variability. *Cancer Epidemiol.Biomarkers.Prev.*, **6**, 421-428.

111) Sauter,E.R., Ross,E., Daly,M., Klein-Szanto,A., Engstrom,P.F., Sorling,A., Malick,J., and Ehya,H. (1997) Nipple aspirate fluid: a promising non-invasive method to identify cellular markers of breast cancer risk. *Br.J.Cancer*, **76**, 494-501.

112) Wynder,E.L., Lahti,H., Laakso,K., Cheng,S.L., DeBevoise,S., and Rose,D.P. (1985) Nipple aspirates of breast fluid and the epidemiology of breast disease. *Cancer*, **56**, 1473-1478.

113) Frame,K.L., Patton,K., Reed,M.J., Ghilchik,M.W., and Parish,D.C. (1996) Angiotensin-converting enzyme and enkephalinase in human breast cyst fluid. *Br.J.Cancer*, **74**, 807-813.

114) Dixon,J.M., McDonald,C., Elton,R.A., and Miller,W.R. (1997) Breast Cancer Risk with Cyst type in Cystic Disease of the Breast. *Br.Med.J.*, **315**, 545-546.

115) Rose,D.P., Berke,B., Cohen,L.A., and Lahti,H. (1987) A comparison of serum and breast duct fluid-immunoassayable prolactin and growth hormone with bioassayable lactogenic hormones in healthy women and patients with cystic breast disease. *Cancer*, **60** , 2761-2765.

116) Lai,L.C., Ghatei,M.A., Takahashi,K., Patel,K.V., Schrey,M.P., Ghilchik,M.W., Bloom,S.R., and James,V.H. (1990) Mitogenic peptides in breast cyst fluid: relationship with intracystic electrolyte ratios. *Int.J.Cancer*, **46**, 1014-1016.

117) Cos,S. and Blask,D. (1994) Melatonin modulates growth factor activity in MCF-7 human breast cancer cells. *J.Pineal Res.*, **17**, 25-32.

118) Robson,H., Anderson,E., James,R.D., and Schofield,P.F. (1996) Transforming growth factor β1 expression in human colorectal tumours: an independent prognostic marker in a subgroup of poor prognosis patients. *Br.J.Cancer*, **74**, 753-758.

119) Gorsch,S.M., Memoli,V.A., Gold,L.I., and Arrick,B.A. (1992) Immunohistochemical staining for TGFβ1 asscociates with disease progression in human breast cancer. *Cancer Res.*, **52**, 6949-6952.

120) Pilichowska,M., Kimura,N., Fujiwara,H., and Nagura,H. (1997) Immunohistochemical study of TGF-alpha, TGF-beta1, EGFR, and IGF-1 expression in human breast carcinoma. *Mod.Path.*, **10**, 969-975.

121) Cos,S. and Sanchez-Barcelo,E.J. (1995) Melatonin inhibition of MCF-7 human breast cancer cells growth: influence of cell proliferation rate. *Cancer Lett.*, **93**, 207-212.

122) Cos,S., Recio,J., and Sanchez-Barcelo,E.J. (1996) Modulation of the length of the cell cycle time of MCF-7 human breast cancer cells by melatonin. *Life Sci.*, **58**, 811-816.

123) Cos,S., Fernandez,F., and Sanchez-Barcelo.E.J. (1996) Melatonin inhibits DNA synthesis in MCF-7 human breast cancer cells in vitro. *Life Sci.*, **58**, 2447-2453.

124) Wilson,S.T., Blask,D., and Lemus-Wilson,A.M. (1992) Melatonin augments the sensitivity of MCF-7 human breast cancer cells to tamoxifen in vitro. *J.Clin.Endocrinol.Metab.*, **75**, 669-670.

125) Levenson,A.S. and Jordan,V.C. (97 A.D.) MCF-7: the first Hormone-Responsive Breast Cancer Cell Line. *Cancer Res.*, **57**, 3071-3078.

126) Elstner,E., Muller,C., Koshizuka,K., Williamson,E.A., Park,D., Asou,H., Shintaku,P., Said,J.W., Heber,D., and Koeffler,H.P. (1998) Ligands for peroxisome proliferator-activated receptorgamma and retinoic acid receptor inhibit growth and induce apoptosis of human breast cancer cells in vitro and in BNX mice. *Proc.Natl.Acad.Sci.U.S.A.*, **95**, 8806-8811.

127) Koli,K.M., Ramsey,T.T., Ko,Y., Dugger,T.C., Brattain,M.G., and Arteaga,C.L. (1997) Blockade of transforming growth factor-beta signaling does not abrogate antiestrogen-induced growth inhibition of human breast carcinoma cells. *J.Biol.Chem.*, **272**, 8296-8302.

128) Malins,D.C. (1993) Identification of hydroxyl radical-induced lesions in DNA base structure: biomarkers with a putative link to cancer development. *J Toxicol.Environ.Health*, **40**, 247-261.

129) Malins,D.C. and Haimanot,R. (1990) 4,6-Diamino-5-formamidopyrimidine, 8-hydroxyguanine and 8- hydroxyadenine in DNA from neoplastic liver of English sole exposed to carcinogens [published erratum appears in Biochem Biophys Res Commun 1991 Feb 28;175(1):359]. *Biochem.Biophys.Res.Commun.*, **173**, 614-619.

130) Floyd,R.A. (1990) The role of 8-hydroxyguanine in carcinogenesis. *Carcinogenesis*, **11**, 1447-1450.

131) Malins,D.C., Holmes,E.H., Polissar,N.L., and Gunselman,S.J. (1993) The etiology of breast cancer. Characteristic alteration in hydroxyl radical-induced DNA base lesions during oncogenesis with potential for evaluating incidence risk. *Cancer*, **71**, 3036-3043.

132) Malins,D.C. and Haimanot,R. (1991) Major alterations in the nucleotide structure of DNA in cancer of the female breast. *Cancer Res.*, **51**, 5430-5432.

133) Musarrat,J., Arezina-Wilson,J., and Wani,A.A. (1996) Prognostic and aetiological relevance of 8-hydroxyguanosine in human breast carcinogenesis. *Eur.J.Cancer*, **32A**, 1209-1214.

134) Contributors (1996) *Casarett & Doull's Toxicology; the Basic Science of Poisons*. McGraw-Hill, New York.

135) Loft,S. and Poulsen,H.E. (1996) Cancer risk and oxidative DNA damage in man [published erratum appears in J Mol Med 1997 Jan;75(1):67-8]. *J.Mol.Med.*, **74**, 297-312.

136) Stillwell,W.G., Xu,H.X., Adkins,J.A., Wishnok,J.S., and Tannenbaum,S.R. (1989) Analysis of methylated and oxidized purines in urine by capillary gas chromatography-mass spectrometry. *Chem.Res.Toxicol.*, **2**, 94-99.

137) Camhi,S.L., Lee,P., and Choi,A.M. (1995) The oxidative stress response. *New Horiz.*, **3**, 170-182.

138) Lloyd,D.R., Carmichael,P.L., and Phillips,D.H. (1998) Comparison of the formation of 8-hydroxy-2'-deoxyguanosine and single- and double-strand breaks in DNA mediated by fenton reactions. *Chem.Res.Toxicol.*, **11**, 420-427.

139) Malins,D.C., Polissar,N.L., and Gunselman,S.J. (1996) Progression of human breast cancers to the metastatic state is linked to hydroxyl radical-induced DNA damage. *Proc.Natl.Acad.Sci.U.S.A*, **93**, 2557-2563.

140) Kasai,H. (1997) Analysis of a form of oxidative DNA damage, 8-hydroxy-2'-deoxyguanosine, as a marker of cellular oxidative stress during carcinogenesis. *Mutat.Res.*, **387**, 147-163.

141) Floyd,R., Watson,J.D., Wong,P.K., Altmiller,D.H., and Rickard,R.C. (1985) Hydroxyl Free Radical Adduct of Deoxyguanosine: Sensitive Detection and Mechanisms of Formation. *Free Rad.Res.Comms.*, **1**, 163-172.

142) Dizdaroglu,M. (1991) Chemical determination of free radical-induced damage to DNA. *Free Radic.Biol.Med.*, **10**, 225-242.

143) Cadet,J., Douki,T., and Ravanat,J.L. (1997) Artifacts associated with the measurement of oxidized DNA bases. *Environ.Health Perspect.*, **105**, 1034-1039.

144) Hewlett Packard (1995) *Hewlett Packard Hardware Reference Manual for HP5972A and 6890 series MSD.*

145) Ravanat,J.L., Turesky,R.J., Gremaud,E., Trudel,L.J., and Stadler,R.H. (1995) Determination of 8-oxoguanine in DNA by gas chromatography--mass spectrometry and HPLC--electrochemical detection: overestimation of the background level of the oxidized base by the gas chromatography--mass spectrometry assay. *Chem.Res.Toxicol.*, **8**, 1039-1045.

146) Dizdaroglu,M. and Bergtold,D.S. (1986) Characterization of free radical-induced base damage in DNA at biologically relevant levels. *Anal.Biochem.*, **156**, 182-188.

147) EPA (1984) Guidelines Establishing Test Procedures for the Analysis of Plooutants Under the Clean Water Act; Final Rule and Interim Final Rule and Proposed Rule. *Federal Register*, **49**, 185-197.

148) Ally,A. and Chromozynski,P. (1997) DNAzol Reagent for Rapid and Efficient Purification of Genomic DNA. *Life Technologies Focus*, **17**, 70-72.

149) Ausubel,F.M., Brent,R., Kingston,R.E., Moore,D.D., Seidman,J.G., and Struhl,K. (1990) *Current Protocols in Molecular Biology*. John Wiley and Sons, inc., New York.

150) Sauer,P. and kang,J. (1998) Quantitation of DNA. *Qiagen News*,23-26.

151) Miller,S.A., Dykes,D.D., and Polesky,H.F. (1988) A simple salting out procedure for extracting DNA from human nucleated cells. *Nucleic.Acids.Res.*, **16**, 1215.

152) Marmur,J. (1961) A Procedure for the Isolation of Deoxyribonucleic Acid from Micro-Organisms. *J.Mol.Biol.*, **3**, 208-218.

153) Dizdaroglu,M. (1993) Quantitative determination of oxidative base damage in DNA by stable isotope-dilution mass spectrometry. *FEBS Lett.*, **315**, 1-6.

154) Vogel,A.I. (1989) *Textbook of Quantitative Chemical Analysis*. Wiley, New York.

155) Jenner,A., England,T.G., Aruoma,O.I., and Halliwell,B. (1998) Measurement of oxidative DNA damage by gas chromatography-mass spectrometry: ethanethiol prevents artifactual generation of oxidized DNA bases. *Biochem.J.*, **331 (Pt 2)**, 365-369.